



2017

# SIMULATION OF HORSE-FENCE CONTACT AND INTERACTION AFFECTING ROTATIONAL FALLS IN THE SPORT OF EVENTING

Gregorio Robles Vega

University of Kentucky, gro226@g.uky.edu

Digital Object Identifier: <https://doi.org/10.13023/ETD.2017.386>

**[Click here to let us know how access to this document benefits you.](#)**

---

## Recommended Citation

Vega, Gregorio Robles, "SIMULATION OF HORSE-FENCE CONTACT AND INTERACTION AFFECTING ROTATIONAL FALLS IN THE SPORT OF EVENTING" (2017). *Theses and Dissertations--Mechanical Engineering*. 98.  
[https://uknowledge.uky.edu/me\\_etds/98](https://uknowledge.uky.edu/me_etds/98)

This Master's Thesis is brought to you for free and open access by the Mechanical Engineering at UKnowledge. It has been accepted for inclusion in Theses and Dissertations--Mechanical Engineering by an authorized administrator of UKnowledge. For more information, please contact [UKnowledge@lsv.uky.edu](mailto:UKnowledge@lsv.uky.edu).

**STUDENT AGREEMENT:**

I represent that my thesis or dissertation and abstract are my original work. Proper attribution has been given to all outside sources. I understand that I am solely responsible for obtaining any needed copyright permissions. I have obtained needed written permission statement(s) from the owner(s) of each third-party copyrighted matter to be included in my work, allowing electronic distribution (if such use is not permitted by the fair use doctrine) which will be submitted to UKnowledge as Additional File.

I hereby grant to The University of Kentucky and its agents the irrevocable, non-exclusive, and royalty-free license to archive and make accessible my work in whole or in part in all forms of media, now or hereafter known. I agree that the document mentioned above may be made available immediately for worldwide access unless an embargo applies.

I retain all other ownership rights to the copyright of my work. I also retain the right to use in future works (such as articles or books) all or part of my work. I understand that I am free to register the copyright to my work.

**REVIEW, APPROVAL AND ACCEPTANCE**

The document mentioned above has been reviewed and accepted by the student's advisor, on behalf of the advisory committee, and by the Director of Graduate Studies (DGS), on behalf of the program; we verify that this is the final, approved version of the student's thesis including all changes required by the advisory committee. The undersigned agree to abide by the statements above.

Gregorio Robles Vega, Student

Dr. Suzanne Weaver Smith, Major Professor

Dr. Haluk E. Karaca, Director of Graduate Studies

---

SIMULATION OF HORSE-FENCE CONTACT  
AND INTERACTION AFFECTING ROTATIONAL FALLS IN THE SPORT OF  
EVENTING

---

THESIS

---

A thesis submitted in partial fulfillment of the  
requirements for the degree of Master of Science in Mechanical Engineering in the  
College of Engineering  
at the University of Kentucky

By

Gregorio Robles Vega

Lexington, Kentucky

Director: Dr. Suzanne Weaver Smith, Professor of Mechanical Engineering

Lexington, Kentucky

2017

Copyright 2017 © Gregorio Robles Vega

## ABSTRACT OF THESIS

### SIMULATION OF HORSE-FENCE CONTACT AND INTERACTION AFFECTING ROTATIONAL FALLS IN THE SPORT OF EVENTING

Rotational falls, or somersault falls, have led to serious and fatal injuries during the cross-country phase of Eventing competitions. Research to improve the safety of the sport began in 2000 after five fatal injuries occurred in the 1999 Eventing season. These efforts led to safety devices such as air jackets, improved helmets, and frangible/deformable fences. The focus of this thesis is to develop a more complete understanding of the horse-fence interaction as the approach motion transitions to a rotational fall. To achieve this, a large distribution of inertial properties was compiled through the development of a cylinder-based inertia approximation and a citizen science effort to gather equine geometrical measurements through a survey distributed by the United States Eventing Association (USEA). Furthermore, fundamental kinematic properties of the horse and rider were gathered from the literature. These distributions were used to conduct a Monte Carlo analysis to examine if the approach conditions of the horse and rider would result in a transition to a rotational fall upon horse-fence contact. Through the analysis the sensitivity of the main control parameters was explored to determine the dominant variables in the transition.

**KEYWORDS:** Rotational Falls, Somersault Falls, Eventing, Equestrian, Cross-Country Eventing, Equine Inertia

Gregorio Robles Vega

---

June 30, 2017

---

SIMULATION OF HORSE-FENCE CONTACT AND INTERACTION  
AFFECTING ROTATIONAL FALLS IN THE SPORT OF EVENTING

By

Gregorio Robles Vega

Suzanne Weaver Smith, Ph. D.

Director of Thesis

Haluk Karaca, Ph. D.

Director of Graduate Studies

June 30, 2017

Dedicated to my family and friends who are always there to encourage me as I strive to accomplish my dreams.

## ACKNOWLEDGMENTS

Thanks to God I was given this great privilege to contribute to the efforts to make this sport safer for all the participants who are passionate about Eventing. I would like to thank my academic advisor, Dr. Suzanne Smith, for not only the opportunity to be part of this effort but also for her guidance throughout the process. Dr. Smith was also very supportive in helping me graduate in time to pursue my service in the Peace Corps. I would also like to thank Lange Ledbetter, Christina Heilman, and Shannon Wood for all their hard work on this project. Lange Ledbetter, and Christina Heilman conducted undergraduate research in this project and were a fantastic help in conducting the data analysis of the Goodyear and British Eventing Safety Fences. Shannon Wood was a huge help to this effort, not only for her knowledge of Eventing, but also her work with the USEA survey was fabulous. I am very excited she will be continuing her studies and coming to the University of Kentucky to work on this effort.

I would also like to thank my parents, Agustin Robles Paz and Maria Vega, as well as my siblings, Cielo Rosas Robles and Agustin Robles Vega for all their support and motivation. I would also like to thank my close friends, Colton Roach, Sarah Edrington, and Alan Varughese, who endured several difficult classes with me. I would like to thank my friends, Caterine Meza, Matthew Jehnke, and Ezra McNichols, for all their motivation. I would also like to thank all my brothers and sisters in Christ who helped encourage me.

I would like to thank Dr. Suzanne Weaver Smith, Dr. Martha Grady, Dr. John Baker and Dr. Mark Hanson for their willingness to be committee members. I would like to thank all my professors at the University of Kentucky for their great job in teaching my fellow classmates and I the tools that we needed for our careers. I would like to thank the professors at the University of Kentucky Paducah Campus, Dr. Vincent Capece, Dr. William Murphy, Dr. John Baker, and Dr. Charles Lu along with all my other professors for their encouragement.

Last but not least, I would like to thank the United States Eventing Association (USEA) for providing the funding for this project and giving us the opportunity to help contribute to their sport. I would also like to thank the University of Kentucky Graduate School for allowing me to be a Teaching Assistant.

# TABLE OF CONTENTS

ACKNOWLEDGMENTS.....	iii
LIST OF TABLES.....	vi
LIST OF FIGURES.....	vii
Chapter 1: Introduction.....	1
1.1 Goals and Objectives .....	2
1.2 Thesis Outline .....	3
Chapter 2: Background and Literature Review .....	4
2.1 Introduction.....	4
2.2 Timeline of Safety Efforts .....	5
2.3 Inertial Properties.....	16
2.4 Kinetic properties of horses while jumping .....	19
2.5 Summary of Available Data.....	29
Chapter 3: Inertia Approximation.....	32
3.1 Introduction.....	32
3.2 Standing Inertia Models.....	32
3.2.1 Dutch Warmblood (DWB) Standing Inertia Model.....	33
3.2.2 Three Cylinder Model (TCM) of Standing Inertia .....	39
3.2.3 Inertia Approximation for the Rider .....	52
3.3 United States Eventing Association (USEA) Survey .....	55
3.4 Results from the USEA Survey .....	58
Chapter 4: Phenomenological Study.....	65
4.1 Fundamental Mechanics of Rotational Falls.....	66
4.2 Mechanisms Principles .....	68
4.3 Overview of the Geometric Cases .....	69
4.3 Case I .....	70
4.3.1 Case 1a Results .....	72
4.3.2 Case 1b Results .....	74
4.3.3 Case 1c Results .....	76
4.4 Case 2.....	78
4.4.1 Initial Conditions for Variables .....	78
4.4.2 Case 2a Results .....	83
4.4.3 Case 2b Results .....	84
4.4.4 Case 2c.....	85



4.4.5 Case 2d.....	86
4.5 Case 3.....	87
4.5.1 Case 3a Results .....	88
4.5.2 Case 3b Results .....	89
Chapter 5: Sensitivity Analysis.....	90
5.1 Sensitivity Analysis .....	91
5.1.1 Convergence .....	91
5.1.2 Alpha.....	92
5.1.3 Beta .....	93
5.1.4. Phi .....	94
5.1.5. Nu.....	95
5.1.6. Lambda .....	96
5.1.7 Contact Velocity Percent .....	97
5.1.8 ABL Percentage.....	98
5.1.9 Psi.....	99
5.1.10 Npass Sensitivity Results.....	100
Chapter 6: Conclusion and Future Work .....	101
6.1 Conclusion .....	101
6.2 Future Work .....	102
APPENDIX A .....	103
REFERENCES .....	112
VITA.....	114

## LIST OF TABLES

Table 2.1 Summary of available data.....	31
Table 3.1 Segment center of mass, segment mass, and segment reference length for Horse 3 provided by Buchner, 2016 [4] .....	34
Table 3.2 Inertia tensor measurements of Horse 3 provided by Buchner, 2016 [4].....	35
Table 3.3 angle from global X-axis to segment local x-axis.....	36
Table 3.4 First comparison method for inertias of segments of the DWB.....	42
Table 3.5 Second comparison method for inertias of the segments of the DWB.....	43
Table 3.6 Evaluation of the significance of a Thigh element.....	45
Table 3.7 Original set of measurements used to test segment mass approximation.....	50
Table 3.8 Percent error of the Izz component on the inertia of the DWB model and the three methods of estimating segments mass.....	51
Table 3.9 List of parameters requested on the USEA survey.....	55
Table 3.10 List of mean and standard deviation of geometric and cylinder-based inertia approximations of USEA survey.....	58
Table 4.1 Geometric illustration of the three cases explored.....	68
Table 4.2 Description of conditions for various cases.....	69
Table 4.3 Description of parameter settings on various conditions.....	69
Table 4.4 Subcases for Case 2.....	77
Table 5.1 Control variables and ranges used in sensitivity study.....	89

## LIST OF FIGURES

Figure 2.1 Image of NED, a horse simulator impact tester created by TRL [1] .....	8
Figure 2.2 Image of BESS during an impact test.....	10
Figure 2.3 Timeline of Eventing safety efforts.....	15
Figure 2.4 Aerial sketch of Obstacle 15 called the “Dog Kennel” or the “Hundgarden” [27].....	20
Figure 2.5 Velocities of 60 horses during the approach phase.....	21
Figure 2.6 2008 Goodyear Safety Research Fence [11].....	26
Figure 2.7 British Eventing Safety Research Fence [11].....	26
Figure 2.8 Rose plots of the contact angles measured using the 2008 Goodyear Safety Research Fence. The rose plot on the left is all provided front leg contacts of the 60, while the plot on the right is all provided rear leg contacts.....	27
Figure 2.9 Rose plots of the 2009 British Eventing Safety Research Fence. The rose plots are divided up into four categories. Starting from the top left and going clockwise the plots represent the categories FLFR, FLRR, BLRR, and BLFR.....	28
Figure 3.1 Location of dissections for the 26 segments of the six Dutch Warmblood horses that were measured for inertial properties [5].....	33
Figure 3.2 An illustration of the distances used for the evaluation method for the segment contributions. The distance $d$ used in the evaluation is highlighted by the red arrows. The rider element is excluded in this image but was used in the analysis.....	41
Figure 3.3 An illustration of TCM plus the Rider elements.....	46
Figure 3.4 Illustrations of the measurements used to create the horse segment.....	47
Figure 3.5 Illustration of the body position defined as sitting back erect, seat $90^\circ$ to back, legs $50^\circ$ to thighs and both hands on overhead control [36].....	53
Figure 3.6 Illustration of the measurements that were requested in the USEA survey....	54
Figure 3.7 Partial image of the USEA survey.....	56
Figure 3.8 Histogram of Body Length (a) and a randomly generated distribution replicating the Body Length (b). The (c) plot the histogram of the Body Radius and the randomly generated distribution replicating the Body Radius (d).....	59
Figure 3.9 Histogram of Neck Length (a) and a randomly generated distribution replicating the Neck Length (b) The (c) plots the histogram of the Neck Radius and the randomly generated distribution replicating the Neck Radius (d).....	60
Figure 3.10 Histogram of Head Length (a) and a randomly generated distribution replicating the Head Length (b). The (c) plots the histogram of the Head Radius and the randomly generated distribution replicating the Head Radius (d).....	61

Figure 3.11 Histograms of moment of inertia about the sagittal plane of motion. Histogram (a) is the IZZ about the TCM COM calculated from USEA survey data. (b) is the approximation of the histogram on the left using normal-distribution from random generation function in MATLABTM. (c) is the translation of (b) to the contact point located at mid antebrachium.....	63
Figure 4.1 Illustration of the iterations of Case 1 at the time of contact and at a moment n seconds later.....	70
Figure 4.2 block ratio range from 0.1 to 3 with block length held constant.....	72
Figure 4.3 Block ratio varied from 0.1 to 3 with block length held constant. Block velocity ranged from 0 m/s to 10 m/s.....	73
Figure 4.4 Block ratio ranged form 0 to 3 with block length held constant. Velocity varied from 0 m/s to 10 m/s.....	74
Figure 4.5 Block ratio ranged from 0 to 3 with block length held contant at 1. The velocity ranged from 0 m/s to 10 m/s. Alpha ranged from -45° to 45°.....	75
Figure 4.6 Gamma vs $\omega_{\text{contact}}$ vs Alpha.....	76
Figure 4.7 Illustration of Case 2 geometric parameters.....	78
Figure 4.8 Parameter map of variables used in Case 2.....	81
Figure 4.9 Case 2a scatter plot of Gamma (angle from x-axis to TCM COM), contact velocity, and Alpha.....	82
Figure 4.10 Case 2b scatter plot of Gamma, contact angular velocity, and Alpha.....	83
Figure 4.11 Case 2c scatter plot of Gamma, contact angular velocity, and Alpha.....	84
Figure 4.12 Case 2d scatter plot of Gamma, contact angular velocity, and Alpha.....	85
Figure 4.13 Case 3a scatter plot of Gamma, contact angular velocity, and Alpha.....	87
Figure 4.14 Case 3b scatter plot of Gamma, contact angular velocity, and Alpha.....	88
Figure 5.1 Convergence study of Case 3a.....	90
Figure 5.2 Sensitivity Analysis of Case 3a with Alpha set as the control variable.....	91
Figure 5.3 Sensitivity Analysis of Case3a with Beta set as the control variable.....	92
Figure 5.4 Sensitivity Analysis of Case3a with Phi set as the control variable.....	93
Figure 5.5 Sensitivity Analysis of Case 3a with Nu as the control variable.....	94
Figure 5.6 Sensitivity Study of Case 3a with Lambda as the control variable.....	95
Figure 5.7 Sensitivity analysis of Case 3a with Contact Velocity Magnitude as the control variable.....	96
Figure 5.8 Sensitivity analysis of Case 3a with ABL percentage as the control variable.....	97
Figure 5.9 Sensitivity analysis of Case 3a with Psi as the control variable.....	98

## Chapter 1: Introduction

The origins of the sport of Eventing date back to 1902 when the first Eventing competition that resembled the current sport took place at the Championnat du Cheval d'Armes in France [42]. Ten years later Eventing was brought to the Olympics when Count Clarence von Rosen, Master of the Horse to the King of Sweden, planned the event at the 1912 Summer Olympic Games. The objective of the competition was to test military officers and horses on any challenge that could occur on and off duty. Originally, competitions were limited to military officers but the restriction was lifted in 1951 in time to allow women to compete in the 1952 Helsinki Olympic games [25]. The most recent change to the sport was the implementation of the short format for all Three-Day Events that took place in 2004 and 2005. The short format shortened the Cross-Country Test by removing the Roads and Tracks, and Steeplechase phases [13].

In recent years the sport has focused major efforts on combating high-risk injuries through rule changes and safety devices. One major cause for serious and fatal injuries for both the rider and horse is a rotational fall. A rotational fall is defined as a horse fall in which the horse somersaulted before landing [30]. Rotational falls are rare and have been steadily decreasing over the past decade, likely as a result of the safety efforts. According to the Fédération Equestre Internationale (FEI) 2005-2016 Statistics Report the percentage of starters that suffered a rotational fall in 2015 was 0.19% [17]. In comparison, in 2005 the percentage of starters that suffered a rotational fall was 0.45%.

Even though rotational falls are rare they can be deadly. A study funded by Rural Industries Research & Development Corporation (RIRDC) and the Equestrian Federation of Australia (EFA) found that during the time span between May 1997 and September 2007 25 rider deaths occurred around the world in the sport of Eventing. Of the 25 rider fatalities, 18 were a result of rotational falls [32]. To date, introduction of safety measures such as collapsible fences [27] and air jackets [7] have been undertaken to decrease the risk of rotational falls. However, a foundational analysis of the motion during rotational falls has yet to be undertaken and therefore is the focus of this thesis.

## 1.1 Goals and Objectives

The United States Eventing Association (USEA) initiated an effort in 2015 focused on developing a more complete understanding of the motion and forces related to the horse-fence interaction as approach motion transitions to a rotational fall. This knowledge would explain proper use of existing frangible devices, provide understanding of benefits of geometric safety designs, and allow new deformable and resettable fence designs to be developed. The effort was divided into five tasks:

- 1) Phased development of validated horse-fence interaction analyses to define key parameters for rotational motion prevention
- 2) Revisit British Eventing (BE) on-course contact data analysis to complete publication of the initial results and extract more detailed information of contact angle and force for Task 1

- 3) Video analysis of rotational fall videos to extract motion information for use in validating the analyses of Task 1
- 4) Expand previous literature review conducted by Katie Kahmann in 2009-2010 for all information available on motion for validation of analyses of Task 1
- 5) Review annual safety statistics in comparison with original published statistics to evaluate performance effectiveness of currently available designs to see if a gap exists indicating the potential for implementation improvements with the results of this project

## 1.2 Thesis Outline

In this thesis, Chapter 2 presents not only a timeline of the major safety efforts to date, but also an overview of research with key significance to understanding the underlying mechanisms that occur in a rotational fall. Chapter 3 reports on the development of the cylinder-based mass moment of inertia approximation and its implementation to create a large database of geometric and inertial parameters. Chapter 4 outlines the phenomenological model designed to capture the fundamental mechanics of the horse-fence interactions. Chapter 5 summarizes the results from the sensitivity study to determine the dominant control variables of the motion that occurs in rotational falls. Lastly, Chapter 6 recaps the efforts of this thesis, providing the major conclusions of this safety effort along with future work.

## Chapter 2: Background and Literature Review

### 2.1 Introduction

Research regarding rotational falls in the sport of Eventing primarily dates from 1999 with the deaths of five riders in the United Kingdom during the cross-country phase of Eventing competitions [30]. As a reaction to the deaths, the first International Eventing Safety Committee was established to review the sport and make recommendations [39]. Prompted by the recommendations and the desire by the Eventing community to provide a safer sport environment several projects were undertaken. During the same period, several studies in the literature also focused on horses jumping obstacles. Internal forces such as moments and mechanical energy were examined focused on the hind limbs [12, 3]. Measurement of kinematic quantities such as horse strides prior to jumps, jumping form, rider effects, and time characteristics have also received attention over the last two decades [8, 29, 34, 35].

Other published studies focus on quantifying key parameters such as equine inertial properties [43, 5, 31]. Human inertial properties were measured in studies performed for the aerospace field [6, 38]. In addition to providing a general timeline of safety efforts related to rotational falls in the sport of Eventing, this chapter highlights results of prior research that significantly contribute to this thesis.



## 2.2 Timeline of Safety Efforts

Even though the sport of Eventing dates back to 1902, focused policy and research efforts on rotational falls did not commence until the year 2000. These efforts were driven by the deaths of five eventers in the cross-country phase of Eventing competitions held in the United Kingdom. In April 2000 as a response to the deaths, the British Horse Trials Association (BHTA) and the Fédération Equestre Internationale (FEI) jointly convened the 1<sup>st</sup> International Eventing Safety Committee. The Committee later released The International Eventing Safety Committee Report in April 2000 [39] also referred to as the “Hartington Report”. In the report the Committee outlined recommendations to the FEI and the BHTA, including the establishment of an FEI Annual Report to cover at least the following seven areas: 1) Medical, 2) Veterinary, 3) Training of Riders and Horses, 4) Cross Country Course Design, 5) Training and Appraisal of Officials, 6) Rules and Tests, and 7) Statistics. Furthermore, specific recommendations were made in the following eight areas: 1) Statistics, 2) Riders, 3) Training and Qualifications, 4) Officials, 5) Medical, 6) Equipment, 7) Veterinary, and 8) Cross Country.

Among the recommendations was the formation of a worldwide statistical database regarding injuries to riders and horses along with any relevant details of the cross-country phase. The statistics were to be reviewed and published annually by the FEI with necessary actions taken to mediate any trends.

Another recommendation was an immediate investigation into helmets to establish the highest possible international specification for the sport. The Committee also requested an International Standard for Body Protectors. These recommendations along with others outlined by the Committee provided a direction for the sport to start addressing the safety of Eventing.

A study that commenced prior to the 1<sup>st</sup> International Eventing Safety Committee and was mentioned in the Statistics section of the report was the study performed by Jane Katherine Murray at the University of Liverpool. The focus of this study was to conduct an epidemiological analysis of the risk factors associated with falls, both equine and rider, in the sport of Eventing [30]. The study collected data for 180 jumping efforts that resulted in a fall of the horse during the cross-country phase of Eventing competitions in the United Kingdom during 2001 and 2002. In Murray's dissertation, which was published in 2004, two variable sets associated with increased risk were identified in two or more multivariable models. The first multivariable set was associated with the competitive nature of a rider. The variables included in this set were the rider's knowledge of their position, previous refusals on the cross-country course, and cross-country tuition (instruction or coaching) received by the rider. The second multivariable set was related to the fence and ground: 1) fences with a take-off or landing in water, 2) non-angled fences with a spread of two meters or greater, 3) angled fences and fences with a drop landing.

A study that ran concurrently with Jane Murray's was conducted by the Transport Research Laboratory (TRL) based in the United Kingdom [40]. The TRL focused on the use of "Frangible Fence" technology as a method of improving safety in Eventing competitions. In their initial safety study, Incident Report Forms were distributed to allow the reporting of falls in the year 2000. Out of 45,000 cross-country starters, 853 forms revealed rider injuries to be 1 fatal, 20 serious, 134 slight, 597 uninjured, and 101 unknown. TRL also conducted video analysis of falls to determine the nature of the fall related to rider injury. From this video analysis they determined two main findings that led to significant risk: 1) a landing angle (defined as the angle between the ground and the longitudinal axis running through the horse) greater than 90° and 2) if the location of the horse-fence contact occurred in the forearm (antebrachium) of the horse between its knee and elbow. If the contact was below the antebrachium the horse was able to safely go over the fence, and if it was higher the horse would remain behind the fence.

Additionally, TRL designed and built a horse simulator impact tester (shown in Figure 2.1). The 475-kg tester was named New Equestrian Dummy (NED). NED was designed based on measurements taken at the University of Liverpool of mass, geometry, and center of mass (COM) from a post-mortem equine specimen. A rail system was designed to provide the designated approach velocity and NED-fence contact point. The approach velocity was fixed at 6 m/s for all tests. The contact point was fixed at 150 mm below the elbow joint [1]. NED was then used to investigate four variables: critical vertical load, critical horizontal load, rail mass, and energy absorption.



Figure 2.1 Image of NED, a horse simulator impact tester created by TRL [1]

The critical vertical and horizontal loads were found to be 30 kN and 3.7 kN, respectively. A safety factor of two was then applied to the critical loads resulting in vertical and horizontal load limits of 15 kN and 1.85 kN, respectively. The rail mass was also explored in a freely supported post and rail fence. It was found that the maximum

rail mass before NED overturned was 300 kg. The last variable was energy absorption and it was found that this variable did not prevent rotational falls.

Subsequently, TRL constructed and tested frangible pins that were designed to fail at the critical loads that were determined by the NED horse simulator impact tester under sponsorship of British Eventing. The frangible pins were trialed through the 2002 season at 13 British Eventing competitions, and 14 FEI events across three continents [37]. The pins broke twice in the 2002 season at Weston Park Prelim and at the Boekolo CCI\*\*\*. Frangible pins are still in use.

In 2007, the FEI created the Safety Sub-Committee, which met in June in London, England [26]. The Committee's mission was defined by four tasks: 1) identify all areas of concern, 2) investigate or trigger specific investigations, 3) manage all issues related to Eventing safety by recommending rule updates and policy changes in the sport, and 4) communicate on all findings.

The following year, the FEI took two major steps. First, the World Safety Summit was held at Copenhagen, Denmark on January 26, 2008. Second, as part of the FEI Eventing Safety Program, national federations appointed Eventing Safety Officers who met for the first time on January 24<sup>th</sup> and 25<sup>th</sup> in Hartpury, England.

Also in 2007, a new effort began at the University of Bristol. The objective of the effort was to gain a better understanding of loads applied to the obstacles along with the dynamic behavior of the horse at collision. The Bristol student team designed and built

the Bristol Equine Safety Subject (BESS) to model the horse's body and front leg. The geometry was formed using 50 mm mild steel box sections and designed to be one third of the horse mass. The muscle stiffness of the horse was approximated by using a covering for the leg composed of a combination of fabric and foam. The material combination was selected because it matched the horse muscle stiffness measured by a myotonometer. The Bristol team measured a horse muscle stiffness of 4 N/mm while conducting measurement on horses available at the University of Bristol Veterinary department. A frame from the video recordings of the BESS impact test can be seen in Figure 2.2.

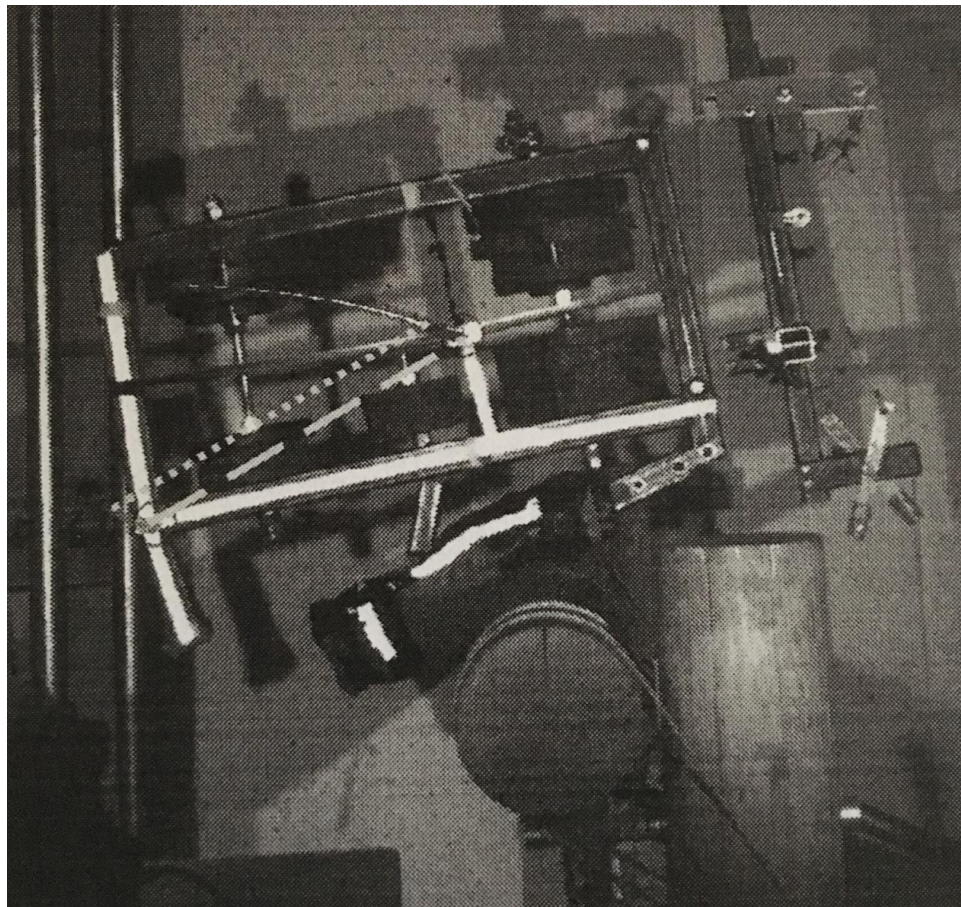


Figure 2.2 Image of BESS during an impact test [24]

Approach conditions for the testing performed with BESS were as follows: approach speed equal to 2.5 m/s, mass held constant at 150 kg, BESS-fence contact point fixed at 150 mm below the elbow, and synthetic muscle stiffness set at 2 N/mm. A high speed camera that could measure 500 frames per second was used to record the tests [24]. The tests were conducted using BESS to strike different fence setups at the prescribed conditions. From the tests it was found that the rail configuration that reduced the initial angular rotation the greatest was the reverse pin setup with the rail on the opposite side of the posts from the direction BESS was approaching.

The Bristol team also conducted field testing using fence load cells. The load cells were placed on two post and rail fences at the Belton Horse Trials. Along with the Force measurements, the Bristol team also took high-speed video of the attempts. Out of the 120 horses that completed the course there were no horse falls or rider falls. The team did measure forces from minor contacts.

The Bristol Study continued in 2008, with further impact testing. BESS was used to conduct tests on both solid and frangible fences at three different velocities (2.2 m/s, 2.8 m/s, 3.3 m/s). From the findings it was hypothesized that the frictional force was a significant component of the measured horizontal force. To test the hypothesis a rotating rail was designed with a single steel shaft spanning its length and brackets on the posts. The rotating fence was tested in three configurations: 1) rotating fence on frangible

pins, 2) rotating fence on solid pins, and 3) rotating fence on solid pins that were constrained to prevent rotation. The three configurations were tested at two different approach velocities: 2.2 m/s and 3.3 m/s. In the tests of the rotational fence with frangible pins it was found that no critical rotations occurred. After the frangible pins failed from the impact the rail began to rotate, reducing the frictional component of the horizontal force and thus the angular velocity. However, the Bristol team was not able to decouple the effects of the reduced stiffness of the rotating rail and the decrease of friction.

That same year (2008) a sports engineering consultant company named Competitive Measure Sports Engineering constructed a fence to take impact measurements during actual Eventing competitions [9, 10, 11]. The fence was sponsored by Goodyear and therefore named the Goodyear Safety Research Fence. The project continued in 2009 under the sponsorship of British Eventing. The British Eventing Safety Research Fence varied in geometry from the 2008 Goodyear Safety Research Fence. The results from this study were directly used for this thesis and are further explained in Section 2.4.

In 2008 an effort was also conducted at the University of Kentucky under sponsorship of the United States Equestrian Federation (USEF) and the United States Eventing Association (USEA) [27]. The main goal of the project was the evaluation of Eventing safety designs. Furthermore, the project had four sub-objectives: 1) to survey the current state of research and available safety design within the sport, 2) to create a safety design evaluation and validation process, 3) to apply the evaluation process to



existing designs, and 4) to determine the process's applicability to the wide range of safety designs within the sport. As part of the evaluation of frangible and deformable safety fence devices the University of Kentucky team conducted Monte Carlo computer simulations to study variable interactions on a hinged gate. Then a full-size hinged gate was build and tested. Also a scale-model resettable collapsible table jump was developed and constructed.

In 2012, FEI released the standard for frangible devices [19] that was developed in 2011 with advice from academic and private industry leaders. The standards for frangible/deformable obstacles were implemented on January 01, 2013 for international competitions [18]. Six devices were approved for use: 1) MIM NewERA system MIM Clip, 2) MIM NewERA Safety MIM Pin, 3) BE Frangible Pin – Short, 4) BE Frangible Pin – Long, 5) MIM NewERA system MIM Wall Kit (not approved for Ponies), and 6) MIM NewERA system MIM Table Kit (not approved for ponies).

Later, the 2015 FEI Eventing Risk Management Seminar took place in Madrid, Spain [16]. In the FEI report from the seminar it was announced that statistics reports from 2015 forward would include a 10 year period. Also in the report were statistical results that made evaluation of the effectiveness of air jackets difficult. The results showed that in 2013, 30% of serious injuries occurred even though the rider used an air jackets while in 2014 the number rose to 71%.

On the 26<sup>th</sup> of July 2016, a report prepared by Charles Barnett for the FEI was released [2]. The report dealt with the collection of data, safety, riders and their qualifications, and the appeal of the sport and its future. Included in the report was a study titled “Analysis of horse falls related to jumping efforts during the cross country test of FEI Eventing competitions” and was prepared by Dr. Nia Huws, Dr. Jane Murray, and Dr. Ellen Singer. The study analyzed data from 2008-2014 for variables that either increased or decreased the risk of horse falls. There were five findings from this study. One key finding was that frangible fences had an increased risk. In the study, it was found that for 94% (118/125) of horse falls at frangible fences the frangible device had not activated. The team was not able to obtain comparative data relating to the number of frangible devices that were activated in the absence of a horse fall or unseated rider. Therefore, it was not possible to explore whether frangible fences had prevented any horse falls.

To further illustrate the safety efforts in Eventing a timeline was created in Figure 2.3. The figure does not include all the events, but tries to create a concise picture for the reader.

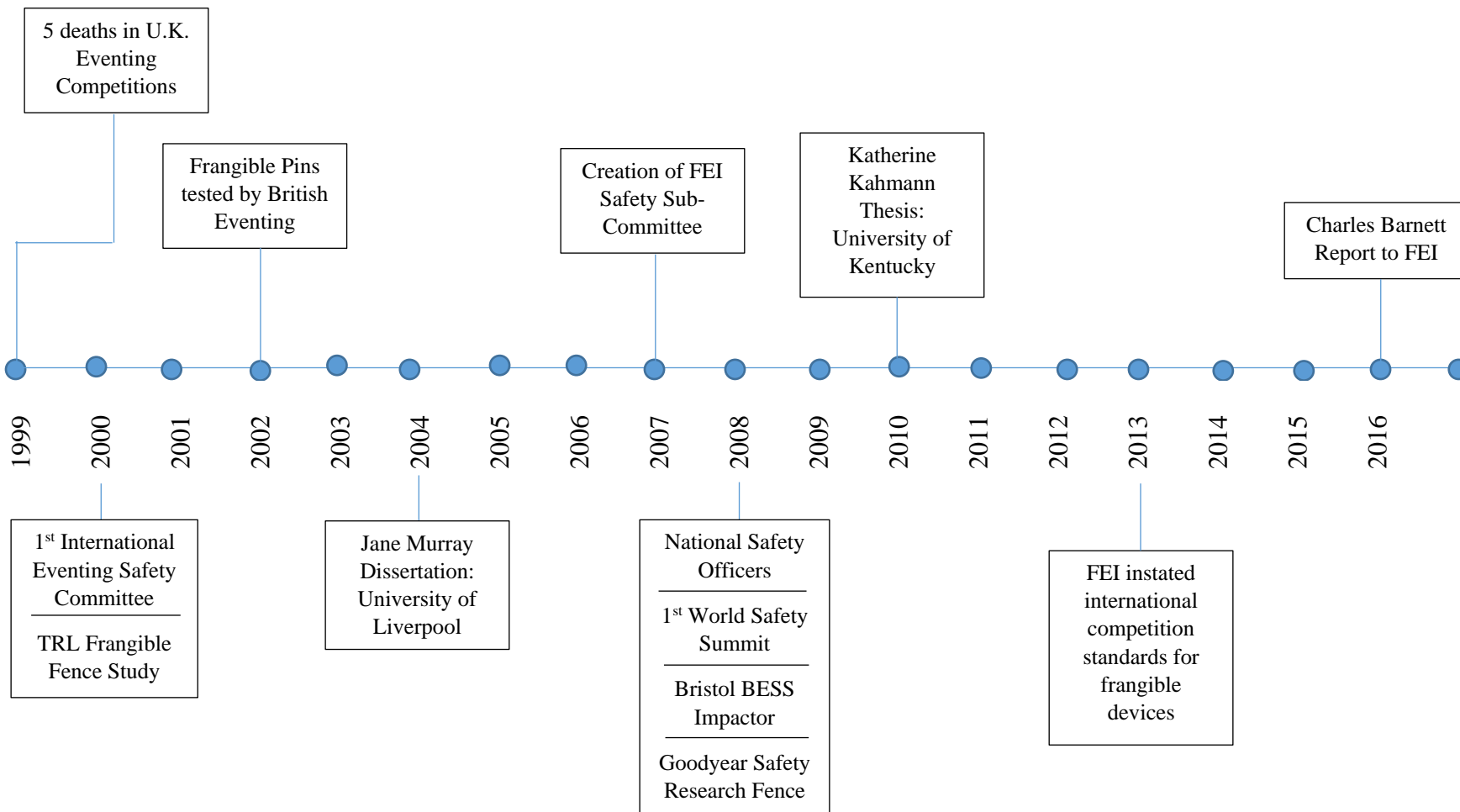


Figure 2.3 Timeline of Eventing safety efforts

### 2.3 Inertial Properties

Inertial quantities for horses and riders include mass and density, and combinations of these with geometry to produce center of mass (COM) and moment of inertia (MOI). For rotational motion, a key property among these is the moment of inertia. This property can either be calculated as a composite body, measured, or determined via a combination of measurement and composite-body calculations. Due to the complex composition and geometry of both the horse and the rider, both empirical measurements and calculations alone are extremely difficult to perform. Therefore, a combination of experimental measurements and composite-body methods has been the optimal way to obtain moment of inertia.

Three prior studies determined equine inertial properties [43 31, 5]. All three used horse cadavers that were divided into a specified set of segments. Two of the three studies were performed at Utrecht University. The earlier of the two was performed on ponies as part of a computer model of equine locomotion [43]. The second study used Dutch Warmblood cadavers [5]. The final was performed on limb segments of various breeds [31]. Cadaver segment mass, density and volume was also measured by Kubo et al in a fourth study [28]. All four will be discussed in the following paragraphs arranged by the order of importance to the current thesis.

The most complete study of horse inertial properties is the *Inertial Properties of Dutch Warmblood Horses* [5]. Six Dutch Warmblood cadavers were each dissected into 26 segments. Average values for mass, density, segment COM, and the inertia tensor

were determined. In addition, regression equations were provided for selected properties of specific segments. Additionally, measurements for each of the six horses were obtained directly from the author for this thesis, but only three of the horses had full measurements available [4].

Both experimental measurements and geometrical approximations of inertial properties were determined for five ponies [43]. Each of the five ponies were dissected into 25 segments. The average segment CG, segment mass moment of inertia about the sagittal plane of motion, and segment mass were tabulated in the dissertation. Regression equations for the moment of inertia for some segments were also provided. Resulting regression equations are functions of a reference length and segment mass. Additionally, photographs of the horses enabled a geometrical approximation via digitized photographs to calculate segment volume, volume moment of inertia, and volume center. These volume inertial parameters were transformed to their mass counterparts through the use of multiplication factors that were optimized using measurements from the cadavers.

The researchers of the most recent study adopted a different approach [31]. Rather than selecting a specific breed of horse the researchers measured the inertial properties of various breeds. Furthermore the researchers did not measure inertial properties for the entire horse, but focused only on the limbs. Segment mass, segment COM, and mass moment of inertia were measured for 38 horses of different breeds and sizes. Various breeds were classified by their morphotype and temperament (cold-blooded, hot-blooded, and warm-blooded horses). Key findings are that the mass distribution of the limbs was

constant with size for animals under 600 kg. Also, no direct correlations exist between the inertial properties and a specific morphotype. The authors believed that differences observed in previous studies regarding inertial properties were based on segmentation technique rather than on body type and size.

In the final of these, the researchers did not measure mass moment of inertia, but did measure segment mass, segment volume, and segment density [28]. The researchers conducted measurements on three frozen thoroughbreds that were dissected into 20 segments. Researchers did provide both the individual measurements and average values for the three horses.

Studies of human inertial properties are typically more abundant in the literature [15]. In March 1975 the Aerospace Medical Research Laboratory focused on measuring mass, COM, principal moments of inertia, and volume of six cadavers [6]. The Federal Aviation Agency effort focused on determining the COM of a man in various positions [38].

The more useful study concerning human inertial properties was the *Investigation of Inertial Properties of the Human Body* that was conducted by researchers at the Aerospace Medical Research Laboratory [6]. The researchers focused on providing inertial properties for humans for use in the design and testing of impact protective systems. The researchers took measurements of six male cadavers. Cadaver weights, COMs, and moments of inertia were measured prior to dissection. Cadavers were then

each segmented into fourteen segments and segment mass, COM, moment of inertia and volume were measured for each.

The second study for the Federal Aviation Agency focused on determining the CG of an adult male in various body positions [38]. The researchers took measurements of five men in 67 different positions. The subjects varied greatly in height and weight. The position that was selected as being the most similar to that of riders in equestrian events was that of a pilot operating controls with back erect, seat 90° to back, legs 50° to thighs, and both hands on overhead control. It should be noted that the COM of males does vary from females. However, no study was available to provide measurement of female COM in a position similar to that measured in the study.

#### 2.4 Kinetic properties of horses while jumping

Kinetic properties that the competitors (horse and rider) exhibit during jumps will be key to conducting any analysis. Researchers used a 16 mm motion picture camera to record Obstacle 15 at the 1990 Stockholm World Equestrian Games Three-Day Event [29]. An aerial sketch illustrates the shape of the obstacle that was the focus of the study and is reproduced as Figure 2.4. The Obstacle referred to as the “Dog Kennel” or “Hundgarden” required a jump of 0.96m downward from a 3.12 m wide face across a 1.98 m wide open space. The main purpose of the analysis was to characterize the variables for leads and temporal patterns of ground contact variables. Furthermore, as part of the study velocities at the approach stage were determined for 60 horses. A distribution of these measurements can be seen in the histogram in Figure 2.5 which was

constructed from the reported data. The range of velocities recorded was 4.59 m/s – 6.92 m/s. It should be noted that the velocity used for the TRL NED impact tester (6 m/s) occurs within this range.

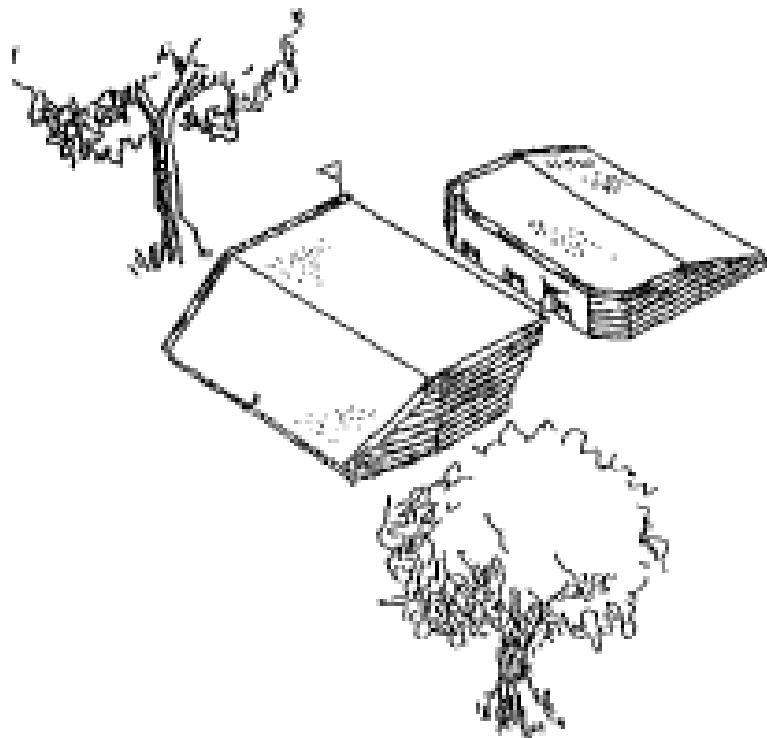


Figure 2.4 Aerial sketch of Obstacle 15 called the “Dog Kennel” or the “Hundgarten” [29]



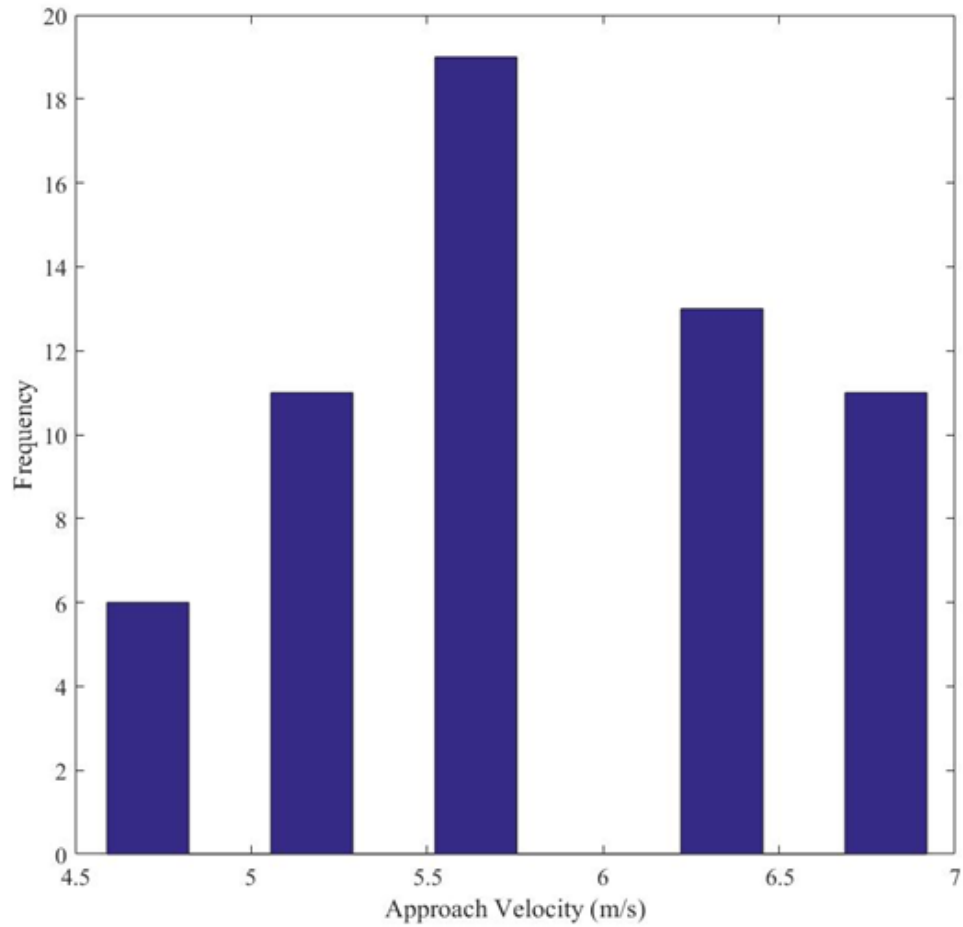


Figure 2.5 Velocities of 60 horses during the approach phase using data form [29])

Another measured quantity was the airborne time. The researchers found that airborne times during the jumps were shorter for the higher placed horses. The top quartile of competitors had an airborne time of  $0.282 \pm 0.019$  seconds. Conversely, the bottom quartile had an airborne time of  $0.355 \pm 0.020$  seconds.

Time motion characteristics for different competition levels in show jumping were also researched in a separate study. Videographic recordings measured both the airborne time and time between fences. It was found that even though speed did not vary between levels the time was progressively decreased from preliminary (80.8 seconds), intermediate (75.0 seconds), and open (67.5 seconds) [8]. One key observation of this study was the difference in airborne times between this study that focused on the sport of show jumping, compared to the study performed on the cross-country phase in the sport of Eventing [27].

Equine jumping form and the effects of riders were studied with a focus on the techniques used by untrained horses during loose jumping. The study consisted of Super-VHS (Super Video Home System) video recordings of 31 untrained horses. The horses jumped a 1 m high by 0.5 m wide fence. Using qualitative evaluation, the horses were divided into two groups: good and poor. The good group consisted of 18 horses while the poor group consisted of 13 horses. After analyzing 20 kinematic variables significant variations were found between the two groups. The main differences were in the horizontal velocity at the last approach stride (Good:  $5.7 \pm 0.80$  m/s; Poor:  $6.42 \pm 0.95$  m/s), relative carpal angles at take off, height of the COM over the center of the fence, horizontal velocity at landing (Good:  $5.26 \pm 0.92$  m/s; Poor:  $6.27 \pm 0.84$  m/s), and angle of the COM to the ground at landing [34].

The authors also considered effects of the rider on the jumping horse. This study took SVHS video recordings of eight horses jumping a vertical 1 m high fence in two conditions, loose and ridden. Loose riding was defined as the horse jumping the obstacle without the rider. Furthermore, once the videos were digitized, the rider's digitized data was removed to provide a new condition of just the horse to be analyzed. Results from this study showed that the effect of the riders are primarily due to behavioral changes in the horses motion rather than inertial changes [35].

Similarly, equine kinematic properties were considered for horses jumping the wall at an international Puissance competition. Sagittal plane SVHS video recording (50 Hz frame rate) were used to measure six kinematic variables at take-off. Nine horses attempted the first fence in the competition at a fence height of 1.8 m. Two horses attempted the final round with a fence height at 2.27 m. The results of the study indicated that the body position at take-off was the most important aspect when jumping high fences [33].

Contact forces on the fence were measured during the cross-country phase of multiple Eventing competitions using adjustable transportable instrumented fences. No rotational falls were measured in the study. In 2008, featuring a single instrumented rail the Goodyear Safety Research Fence was used to measure the forces as shown in Figure 2.6. In 2009, the British Eventing fence included two instrumented rails in an oxer configuration as seen in Figure 2.7. Forces were measured using load cells oriented both

horizontally and vertically at each end of the rails. Furthermore, all jump attempts were recorded using a high-speed camera.

Competitive Measure, who constructed the fences and conducted the testing, provided the top 60 impacts in the 2008 data set and the top 229 impacts in the 2009 data set for further analysis. The contacts for the 2008 data set were separated into two categories using notes accompanying the experimental records: front leg contacts, and back leg contacts, resulting in only four front leg impacts in the data set. These results can be seen in Figure 2.8 plotted as a rose plot. The rose plot combines the number of occurrence and the contact vector direction. The frequency of occurrence is plotted in the radial direction with the center of the rose plot being set to zero. Along the circumferential direction the contact angle is plotted with  $0^\circ$  being set at the intersection of Quadrant IV and Quadrant I. The angles were defined in a counter-clockwise motion. Also for all the contacts the horse approached from the right.

There are two key findings to observe from Figure 2.8. First is the greater frequency of rear leg contacts. 90.7% (39/43) of the contacts measured were rear leg contacts. Also the wide variation in the front leg contacts which spanned from  $-13^\circ$  to  $93^\circ$ .

The 2009 data set was similarly divided into four categories: front leg-front rail (FLFR, 35 contacts), front leg-rear rail (FLRR, 27 contacts), back leg-front rail (BLFR, 98 contacts), and back leg-rear rail (BLRR, 61 contacts). Rose plots from the 2009 British Eventing Safety Research fence are shown in Figure 2.9. The plots are divided

into four categories starting from the top left plot and going clockwise: FLFR, FLRR, BLRR, BLFR. The difference between front leg and back leg contacts can be clearly seen by the distribution of the number of occurrences per angle. This difference is important because safety devices have to be designed not to activate when experiencing these incidental contact forces. Therefore understanding both the contact force magnitude and its direction are necessary for the safety device design. As was previously mentioned, none of these contacts resulted in a rotational fall, however these results still provide some insight into what happens in a jump. For example the contacts beyond 90° were found to be mostly hoof strikes. For each of the contacts, the angle, duration, maximum force, and impulse were calculated among other quantities of interest.



Figure 2.6 2008 Goodyear Safety Research Fence [11]



Figure 2.7 British Eventing Safety Research Fence [11]

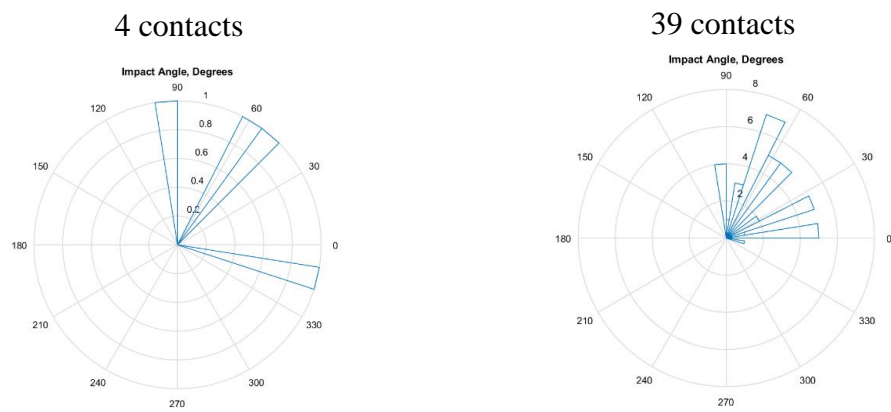


Figure 2.8 Rose plots of the contact angles measured using the 2008 Goodyear Safety Research Fence. The rose plot on the left is all provided front leg contacts of the 60, while the plot on the right is all provided rear leg contacts

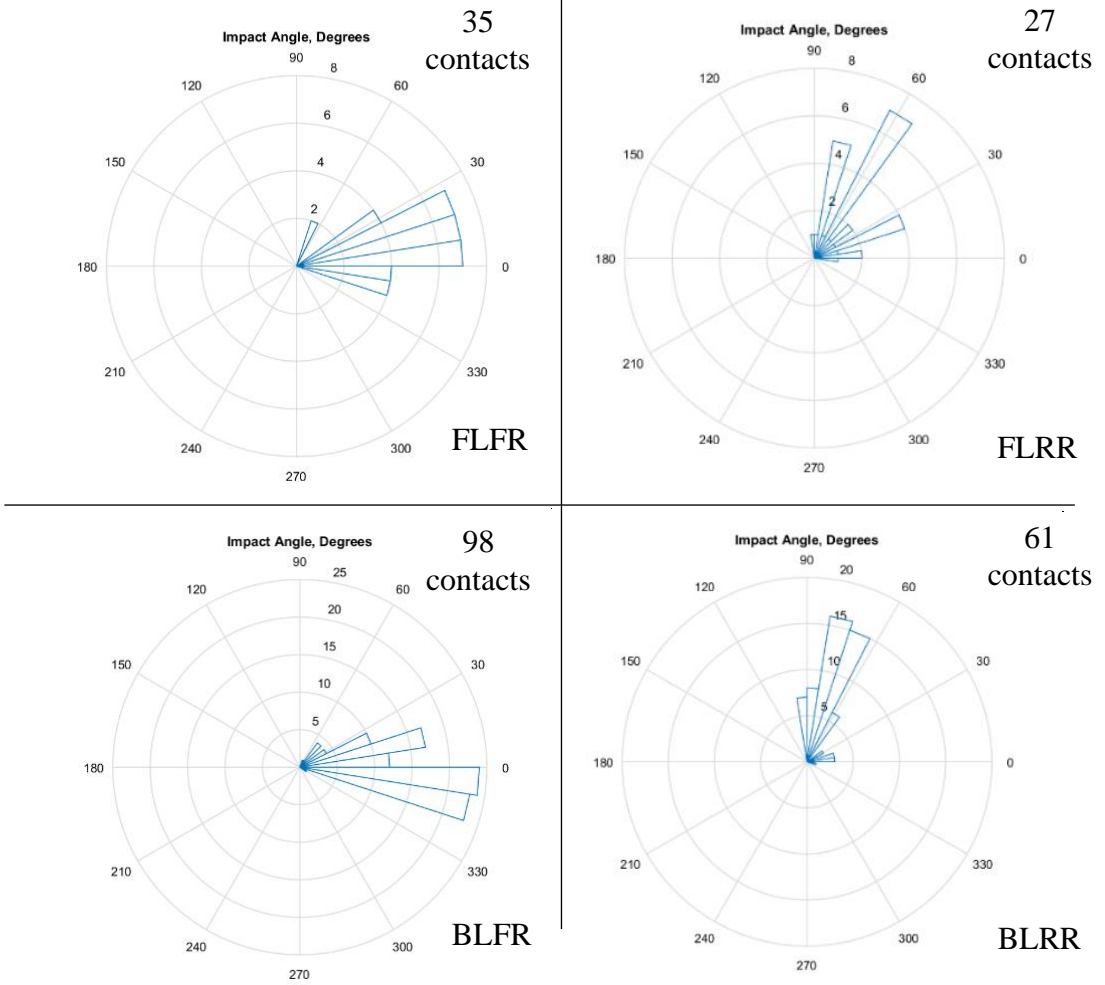


Figure 2.9 Rose plots of the 2009 British Eventing Safety Research Fence. The rose plots are divided up into four categories. Starting from the top left and going clockwise the plots represent the categories FLFR, FLRR, BLRR, and BLFR



## 2.5 Summary of Available Data

To better understand the available data for use in this effort, Table 2.1 summarizes the current state. Eleven key parameters for the current effort were identified and are as follows: 1) contact velocity magnitude, 2) contact velocity direction, 3) take-off velocity, 4) airborne time, 5) contact force magnitude, 6) contact force direction, 7) horse inertia, 8) rider inertia, 9) rider CG, 10) horse geometry, and 11) rider geometry. In the list of parameters contact velocity magnitude refers to the magnitude of the contact velocity at the instant just before the contact between the horse and the fence. Similarly, the contact velocity direction is the direction of the competitor (horse and rider) velocity vector at the instant before contact. Take-off velocity is different from the contact velocity because it takes place at the moment of time that the horse and rider first start the jumping trajectory. Airborne time is defined as the time that elapses from the take-off of the competitor to the moment the competitor lands. Contact force magnitude is defined as the amount of force that is applied by the horse on the fence. Similarly, the contact force direction is the elevation angle of the horse-fence contact. Both the horse inertia and the rider inertia are defined as the overall moment of inertia about axes perpendicular to the sagittal plane of motion. The last two parameters referred to the geometrical properties of both the horse and the rider.

The parameters were divided into three categories for which Eventing research data is available. The categories were rotational fall, jumping, and standing. The rotational fall category lists the available research that was measured for each of the parameters during a rotational fall. The jumping category lists the data that is available

for jumps that either had no contacts or had slight contacts but did not lead to a rotational fall. The last category lists research that was measured for a horse in the standing position.

A key factor to note from Table 2.1 is simply the lack of measured data that can be obtained from past Eventing research. Especially the rotational fall category has only one parameter with any available data. Moreover, the data that is available, 6 videos, was obtained from amateur videos and not a scientific study. Part of the lack of quantifiable data is simply due to how infrequently rotational falls occur. According to the FEI, in 2015 the percentage of rotational falls was 0.19% which is 1 rotational horse fall every 536 starters [17]. In 2015 the FEI statistics recorded 20,351 starters. Furthermore, there would be multiple fences per competition per starter. If this averaged 30, then there would be one rotational fall per 16,080 jump attempts. To fill the information gaps for rotational falls, available data can be used as a basis to appropriately approximate the correct physics. Chapter 3 presents a closer look at horse and rider inertia.

Table 2.1 Summary of available data

Parameter	Eventing Research		
	Rotational Fall	Jumping	Standing
Contact Velocity Magnitude	Not Available	Not Available	
Contact Velocity Direction	Not Available	Not Available	
Take-off Velocity	Not Available	60 Jump Attempts [29]	
Airborne Time	6 videos	60 Jump Attempts [29]	
Contact Force Magnitude	Not Available	62 Front Leg Contacts [9, 10, 11]	
Contact Force Direction	Not Available	62 Front Leg Contacts [9, 10, 11]	
Horse Inertia			5 Pony Cadavers [43] 6 Dutch Warmblood Cadavers [5] 38 Fore and Hind Limbs only [31]
Rider Inertia			6 Human Cadavers [6]
Rider CG			1 Person [38]
Horse Geometry	Not Available	Not Available	
Rider Geometry	Not Available	Not Available	

## Chapter 3: Inertia Approximation

### 3.1 Introduction

In order to model a rotational fall as it occurs in the sport of Eventing, inertial properties of the starter (horse and rider) are required. However, with only six horses, there is not a sufficient basis of inertial values from available data to be confident of breadth of applicability. Regression equations derived in two of the previous efforts were considered as a possible approach to expand the available data. However, not all the cadaver segments had regression equations determined for the moment of inertia about the sagittal plane. In addition, several segments that did have regression equations did not have sufficient information to calculate the segment mass required to use the moment of inertia regression equation. Breed differences in the sport further complicate the situation. Therefore, developing a simple geometric model as an inertia phenomena model was adopted as the approach. Available data from published studies serves as a metric to evaluate the validity and accuracy of the developed geometric model.

### 3.2 Standing Inertia Models

*Inertial Properties of Dutchwarmblood Horse* presented the most comprehensive information of the prior inertia studies. Properties of a standing inertia model referred to as DWB were calculated from the available data. The DWB inertia was then used to optimize a simplified geometrical model based on three cylinders representing the head, neck, and body (remainder) and referred to as TCM. Both the DWB and the TCM were oriented in a standing configuration as shown in Figure 3.1.

### 3.2.1 Dutch Warmblood (DWB) Standing Inertia Model

The DWB inertia model was developed using measured data obtained by Dr. Buchner and his team for Horse 3, a Dutch Warmblood breed dissected into 26 segments. The segmentation of the horse is depicted in Figure 3.1. The local segment data recoded in the study is provided in Table 3.1 and Table 3.2. Note that the Tail segment was not included as it did not qualify as a rigid body and could not be measured using the pendulum method. Furthermore, differences between the left and right segments of the limbs were observed to be caused due to differences in segmentation and possible mass loss. Horse 3 was selected from the three available complete measurement sets because it was of similar height and weight to a living horse available for use to develop the approach of this thesis.

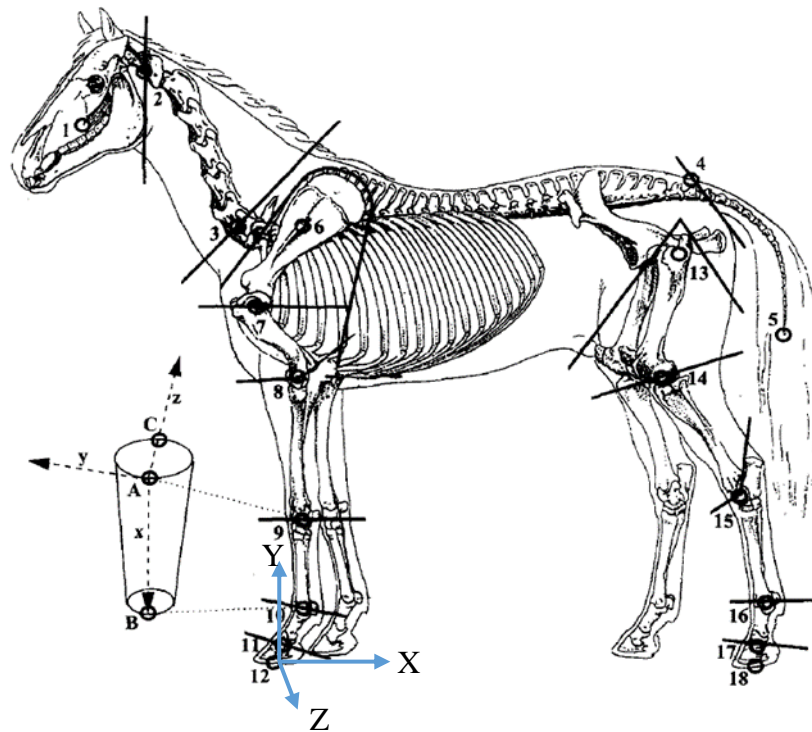


Figure 3.1 Location of dissections for the 26 segments of the six Dutch Warmblood horses that were measured for inertial properties [5]

Table 3.1 Segment center of mass, segment mass, and segment reference length for Horse 3  
 Provided by Buchner, 2016 [4]

Segment	CG absolute (m)						Segment		Reference	
	X		Y		Z		Mass (kg)		Length (m)	
<b>Trunk</b>	0.6837		-0.1753		0.2400		353.0		1.6	
<b>Head</b>	0.2136		-0.0217		0.0896		21.6		0.3	
<b>Neck</b>	0.2382		0.1007		0.0422		28.4		0.5	
<b>Scapula</b>	0.0827	0.0852	-0.0463	-0.0461	0.0532	0.0583	12.0	12.2	0.3	0.3
<b>Brachium</b>	0.1246	0.1442	-0.0218	-0.0292	0.0769	0.0506	8.6	9.4	0.3	0.3
<b>Antebrachium</b>	0.1618	0.1466	-0.0004	0.0099	0.0551	0.0624	6.2	6.8	0.4	0.4
<b>Metacarpus</b>	0.1268	0.1346	0.0022	-0.0005	0.0425	0.0486	1.4	1.5	0.3	0.3
<b>Pastern Forelimb</b>	0.0602	0.0578	-0.0111	-0.0095	0.0410	0.0494	0.8	0.7	0.1	0.1
<b>Hoof Forelimb</b>	0.0405	0.0282	-0.0142	-0.0197	0.0575	0.0397	1.1	1.2	0.1	0.1
<b>Thigh</b>	0.2287	0.2165	-0.0230	-0.0211	0.0774	0.0681	18.1	15.6	0.4	0.4
<b>Crus</b>	0.1601	0.1770	-0.0350	-0.0205	0.0683	0.0646	7.5	7.5	0.4	0.5
<b>Metatarsus</b>	0.1121	0.1118	-0.0121	-0.0192	0.0413	0.0504	2.7	2.7	0.4	0.3
<b>Pastern Hind Limb</b>	0.0568	0.0690	-0.0145	-0.0163	0.0381	0.0406	0.9	0.8	0.1	0.1
<b>Hoof Hind Limb</b>	0.0284	0.0315	-0.0201	-0.0184	0.0489	0.0449	1.0	0.9	0.1	0.1

Table 3.2 Inertia tensor measurements of Horse 3 provided by Buchner, 2016 [4]

Segment	Inertia Tensor (kg m <sup>2</sup> )											
	I <sub>xx</sub>		I <sub>yy</sub>		I <sub>zz</sub>		P <sub>xy</sub>		P <sub>yz</sub>		P <sub>zx</sub>	
<b>Trunk</b>	30.6490		70.5660		55.6273		-2.2588		3.3251		-2.3838	
<b>Head</b>	0.3766		0.4849		0.6361		0.1517		-0.0428		0.0284	
<b>Neck</b>	0.2481		0.9339		0.9257		0.3311		0.0273		-0.1852	
<b>Scapula</b>	0.1357	0.1281	0.1658	0.1722	0.2968	0.3141	0.0006	-0.0432	0.0543	0.0657	-0.0085	0.0342
<b>Brachium</b>	0.0631	0.0732	0.0624	0.0915	0.1013	0.1326	0.0116	0.0372	-0.0035	0.0089	0.0033	-0.0025
<b>Antebrachium</b>	0.0185	0.0226	0.1167	0.1233	0.1279	0.1387	-0.0099	-0.0178	0.0036	0.0018	-0.0023	0.0031
<b>Metacarpus</b>	0.0009	0.0009	0.0118	0.0128	0.0117	0.0128	-0.0004	0.0011	0.0003	-0.0007	0.0010	-0.0012
<b>Pastern Forelimb</b>	0.0003	0.0003	0.0017	0.0012	0.0018	0.0013	-0.0001	0.0001	-0.0002	0.0000	-0.0003	0.0001
<b>Hoof Forelimb</b>	0.0018	0.0021	0.0022	0.0021	0.0018	0.0016	-0.0004	-0.0003	-0.0002	-0.0003	0.0002	0.0003
<b>Thigh</b>	0.2446	0.1485	0.2489	0.1854	0.2903	0.2743	0.0094	-0.0061	0.0297	0.0216	-0.0684	0.0492
<b>Crus</b>	0.0283	0.0274	0.1249	0.1319	0.1341	0.1358	-0.0075	-0.0140	0.0019	-0.0019	0.0112	-0.0092
<b>Metatarsus</b>	0.0037	0.0021	0.0456	0.0509	0.0490	0.0545	-0.0050	-0.0027	0.0007	-0.0027	0.0022	-0.0001
<b>Pastern Hind Limb</b>	0.0005	0.0003	0.0023	0.0016	0.0022	0.0017	-0.0001	-0.0004	-0.0002	-0.0001	-0.0002	0.0000
<b>Hoof Hind Limb</b>	0.0013	0.0012	0.0017	0.0016	0.0012	0.0011	-0.0004	-0.0004	0.0000	0.0001	0.0002	0.0003

The method used to calculate the COM of the DWB horse involved reducing the problem to two dimensions by taking the horse to be symmetric along the sagittal plane. The absolute X, Y axes were oriented horizontally and vertically with both laying in the sagittal plane as depicted in Figure 3.1, with the origin of the coordinates located at the fore hoof. Each segment had a set of local axes that can be seen depicted in Figure 3.1. Furthermore, to find the X and Y coordinates of the COM it was necessary to assume angles for the standing position of the segments. These angles were defined from the positive global X-axis counterclockwise to the individual local segment x-axis and are tabulated in Table 3.3.

Table 3.3 Angle from global X-axis to segment local x-axis

<b>Segment</b>	<b>Angle to X-axis (°)</b>
Fore Hoof	50
Pastern Forelimb	50
Metacarpus	90
Antebrachium	90
Brachium	135
Scapula	45
Neck	135
Head	225
Trunk	0
Thigh	45
Crus	135
Metarsus	90
Pastern Hindlimb	55
Hind Hoof	55

Once the segment COM coordinates were converted to the absolute coordinate frame, then Equations 3.1 and 3.2 were used to calculate the composite COM, which was found to be located at X=0.74 m and Y=1.14 m. In Equation 3.1  $X_i$ = segment x-coordinate of COM,  $m_i$ = segment mass, and  $X$ = composite x-coordinate of COM. In



Equation 3.2  $Y_i$ = segment y-coordinate of COM,  $m_i$ = segment mass, and  $Y$ = composite y-coordinate of COM.

$$\bar{X} = \frac{\sum \bar{X}_i m_i}{\sum m_i}, \text{ for } i=1, \dots, 25 \quad (3.1)$$

$$\bar{Y} = \frac{\sum \bar{Y}_i m_i}{\sum m_i}, \text{ for } i=1, \dots, 25 \quad (3.2)$$

After the DWB COM was calculated, the overall inertia tensor for the DWB had to be determined by rotating each segment inertia tensor to align with the global axes orientations before the composite body inertia is calculated. Segment rotations were conducted about the global Z-axis (perpendicular to sagittal plane) using Euler's rotation theorem as defined in *Advanced Engineering Dynamics* [20]. The transformation used for all 25 segments can be seen in Equation 3.3, where theta is an arbitrary rotation angle.

$$C = \begin{bmatrix} \cos(\theta) & \sin(\theta) & 0 \\ -\sin(\theta) & \cos(\theta) & 0 \\ 0 & 0 & 1 \end{bmatrix} \quad (3.3)$$

The rotation transformation shown in Equation 3.3 was then used to rotate the segment inertia tensor. An inertia tensor is the matrix form of  $I_{ij}$  where  $i$  and  $j$  can equal 1, 2, or 3 with 1 corresponding to the x-axis, 2 to the y-axis, and 3 to the z-axis. When  $i$  and  $j$  are equal the values are referred to as the moments of inertia and are located along the diagonal of Equation 3.3, while the others are the products of inertia. To transform

the original segment inertia tensor into the rotated frame Equation 3.3 and its transpose are used as defined in *Advanced Dynamics* [21] and can be seen in Equation 3.4.

$$I_{\text{rotated}} = [C][I_{\text{original segment}}][C]^T \quad (3.4)$$

Once all the segment inertia tensors were oriented to the equine standing position the parallel-axis theorem or transfer formula was applied to each. The parallel-axis theorem is defined in both *Advanced Mechanics of Materials and Applied Elasticity* [41] and *Engineering Mechanics: Dynamics* [23] as a method to determine moments of inertia about any parallel axis when the moment of inertia of the body about an axis passing through the body's mass center is known. The parallel-axis equation can be seen in Equation 3.5, where  $d$  is the perpendicular distance between the parallel axes.

$$I = I_G + md^2 \quad (3.5)$$

The parallel-axis theorem and the principle of superposition were used for each segment in turn to determine its inertia tensor about the horse COM. These were added to complete the composite-body inertia for the horse. The DWB inertia tensor about the COM can be seen in Equation 3.6.

$$I_{\text{DWB}} = \begin{bmatrix} 266.9 & 231.3 & 231.4 \\ 231.3 & 306.7 & 237.3 \\ 231.4 & 237.3 & 293.2 \end{bmatrix} \text{ kg m}^2 \quad (3.6)$$

### 3.2.2 Three Cylinder Model (TCM) of Standing Inertia

The TCM was developed with the main objective of allowing an effective and accurate method of estimating the moment of inertia about the axis perpendicular to the sagittal plane ( $I_{ZZ}$ ) based on minimal noninvasive measurements of a living horse. The first step in achieving this objective was to reduce the number of elements required in the cylinder-based model. This was mainly to decrease the number of measurements needed from the horse.

To determine what segments from the DWB had the greatest effect relative to a typical rotational fall contact, each segment was evaluated in two ways derived from the parallel-axis theorem. The first evaluation method used the distance,  $d$ , from a point at the midspan of the antebrachium segment to the COM of each segment. The point at the midspan of the antebrachium was used because in the literature this area had been identified as the critical area for rotational falls. An illustration of this distance for key equine segments can be seen in Figure 3.2. It should be noted that the rider was not included in this illustration but was included in the analysis. Utilizing the first evaluation method two results were obtained for each segment. The first results, referred to as  $md^2$ , took into account the individual segment mass and the distance from the segment COM to the overall DWB COM. To better understand the importance of each segment  $md^2$  term the percentage of each segment relative to the sum of the 26  $md^2$  segment values

was also calculated. Results from the first evaluation method can be seen in Table 3.4 for each of the 26 segments.

The results from the first evaluation shown in Table 3.4 highlighted that for the 26 segments, all equine segments excluding the tail segment plus rider, the highest contributors due combination of high mass and segment COM location relative to overall DWB COM were the rider, and the horse head, neck, trunk, and thigh. A key observation was the variation between the right and left thigh segments. The variation is attributed to inconsistencies in the dissection process, along with possible mass loss from segmentation.

The second method of evaluation took into account the full parallel-axis theorem contribution of each segment. Four properties were used for this evaluation:  $I_{zz}$ ,  $md^2$ ,  $I_{zz}$ -plus- $md^2$ , and the percentage of each individual segment  $I_{zz}$  plus  $md^2$  term with respect the sum of all 26  $I_{zz}$ -plus- $md^2$  segment terms. The results from the second method of evaluation can be seen in Table 3.5.

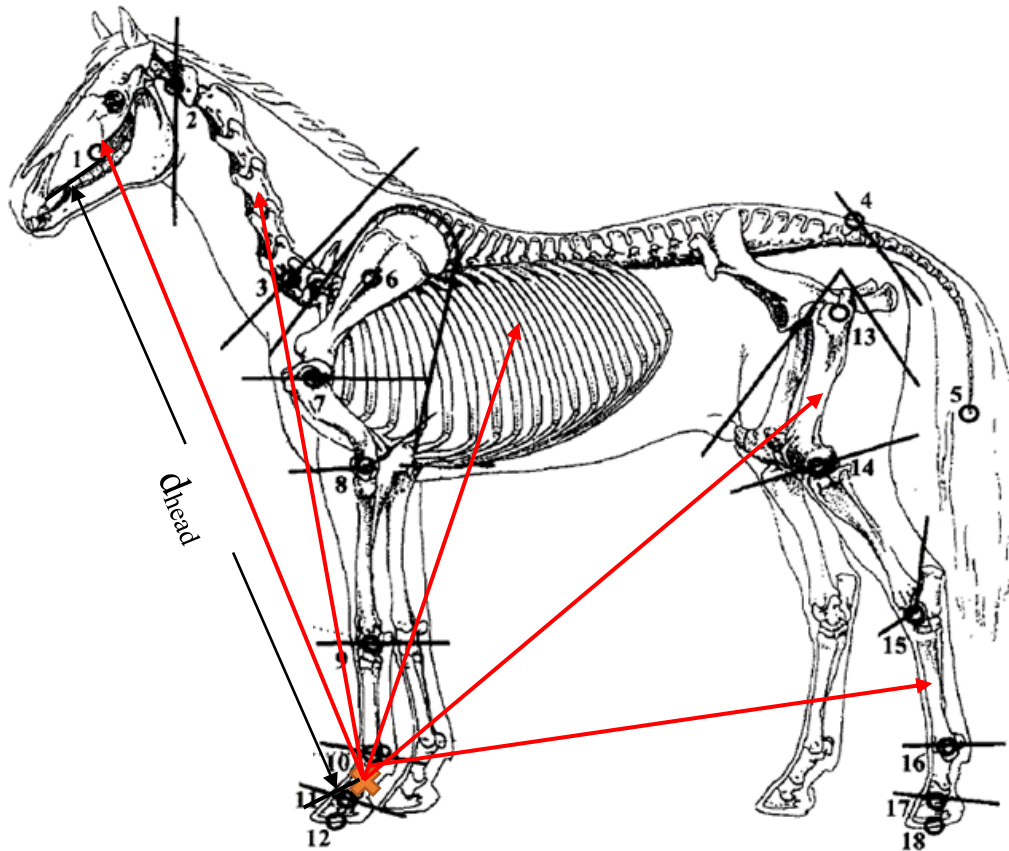


Figure 3.2 An illustration of the distances used for the evaluation method for the segment contributions. The distance  $d$  used in the evaluation is highlighted by the red arrows. The rider element is excluded in this image but was used in the analysis. The point of reference here is at the fore hoof, but later is calculated along the ante brachium between points 8 and 9 for the analysis.

Table 3.4 First comparison method for inertias of segments of the DWB

<b>Segment</b>	<b>md2 (kg m2)</b>		<b>md2 (%)</b>	
<b>Rider</b>	109.6		6.5	
<b>Trunk</b>	906.3		53.7	
<b>Head</b>	97.1		5.8	
<b>Neck</b>	82.0		4.9	
<b>Scapula</b>	19.2	16.5	1.1	1.0
<b>Brachium</b>	6.1	5.0	0.4	0.3
<b>Antebrachium</b>	2.8	2.1	0.2	0.1
<b>Metacarpus</b>	0.1	0.0	0.0	0.0
<b>Pastern Forelimb</b>	0.0	0.0	0.0	0.0
<b>Hoof Forelimb</b>	0.0	0.0	0.0	0.0
<b>Thigh</b>	185.2	107.6	11.0	6.4
<b>Crus</b>	41.4	41.8	2.5	2.5
<b>Metatarsus</b>	21.1	21.8	1.3	1.3
<b>Pastern Hind Limb</b>	5.1	5.1	0.3	0.3
<b>Hoof Hind Limb</b>	6.0	6.5	0.4	0.4

Table 3.5 Second comparison method for inertias of the segments of the DWB

Segment	Izz		md2		Izz+md2 (kg m <sup>2</sup> )		Izz+md2 (%)	
<b>Rider</b>	3.9		109.6		113.5		6.5	
<b>Trunk</b>	55.6		906.3		961.9		54.9	
<b>Head</b>	0.6		97.1		97.7		5.6	
<b>Neck</b>	0.9		82.0		83.0		4.7	
<b>Scapula</b>	0.3	0.3	19.2	16.5	19.5	16.8	1.1	1.0
<b>Brachium</b>	0.1	0.1	6.1	5.0	6.2	5.2	0.4	0.3
<b>Antebrachium</b>	0.1	0.1	2.8	2.1	2.9	2.2	0.2	0.1
<b>Metacarpus</b>	0.0	0.0	0.1	0.0	0.1	0.1	0.0	0.0
<b>Pastern Forelimb</b>	0.0	0.0	0.0	0.0	0.0	0.0	0.0	0.0
<b>Hoof Forelimb</b>	0.0	0.0	0.0	0.0	0.0	0.0	0.0	0.0
<b>Thigh</b>	0.3	0.3	185.2	107.6	185.5	107.9	10.6	6.2
<b>Crus</b>	0.1	0.1	41.4	41.8	41.6	41.9	2.4	2.4
<b>Metatarsus</b>	0.0	0.1	21.1	21.8	21.2	21.8	1.2	1.2
<b>Pastern Hind Limb</b>	0.0	0.0	5.1	5.1	5.2	5.1	0.3	0.3
<b>Hoof Hind Limb</b>	0.0	0.0	6.0	6.5	6.0	6.5	0.3	0.4
<b>Total</b>					1751.8			

The results from the second evaluation shown in Table 3.5 were consistent with the results of the first evaluation. This showed that the  $md^2$  term dominates the results. Again, the primary segments were found to be the horse trunk, neck, head, thigh and the rider. The difference was minimal between the percentage contributions in both evaluation methods for each individual segment to the overall total.

It was hypothesized that the Thigh segment along with the other segments of the forelimbs and hind limbs could be included in a body cylinder along with the trunk. To verify this hypothesis four test cases were compared. Test Case 1 was defined as the full 25 segment DWB model without any modifications and this is the reference for others which are approximations. Test Case 2 was defined as the DWB Head, Neck, Thigh, and Trunk segments only. Test Case 3 excluded the Thigh segment but kept the Head, Neck, and Trunk. Test Case 4 combined the forelimbs and hindlimbs including the thigh into a Body segment, while still keeping the Head and Neck segments. For all four cases the COM X and Y coordinates were found. The principal measure used to evaluate the four test cases was the angle Gamma defined as the angle from the positive horizontal axis to the overall COM calculated for each case. Results in Table 3.6 indicate that a Thigh segment does not need to be added separately (Case 2) due its small effect versus combining it into a Body segment (Case 4). Also shown was that the Body element performs better than simply using the Trunk segment. Therefore, the TCM can consist of



only the Head, Neck, and Body segments. This allows the TCM-plus-Rider model to consist of only Head, Neck, Body and Rider elements. An illustration of the TCM-plus-Rider can be seen in Figure 3.3.

Table 3.6 Evaluation of the significance of a Thigh element

<b>DWB COM Test Cases</b>	<b>X-Coordinate (m)</b>	<b>Y-Coordinate (m)</b>	<b><math>\gamma^*</math> (<math>^{\circ}</math>)</b>
Case 1	0.74	1.14	57.0
Case 2	0.70	1.06	56.6
Case 3	0.65	1.02	57.5
Case 4	0.70	1.04	56.1

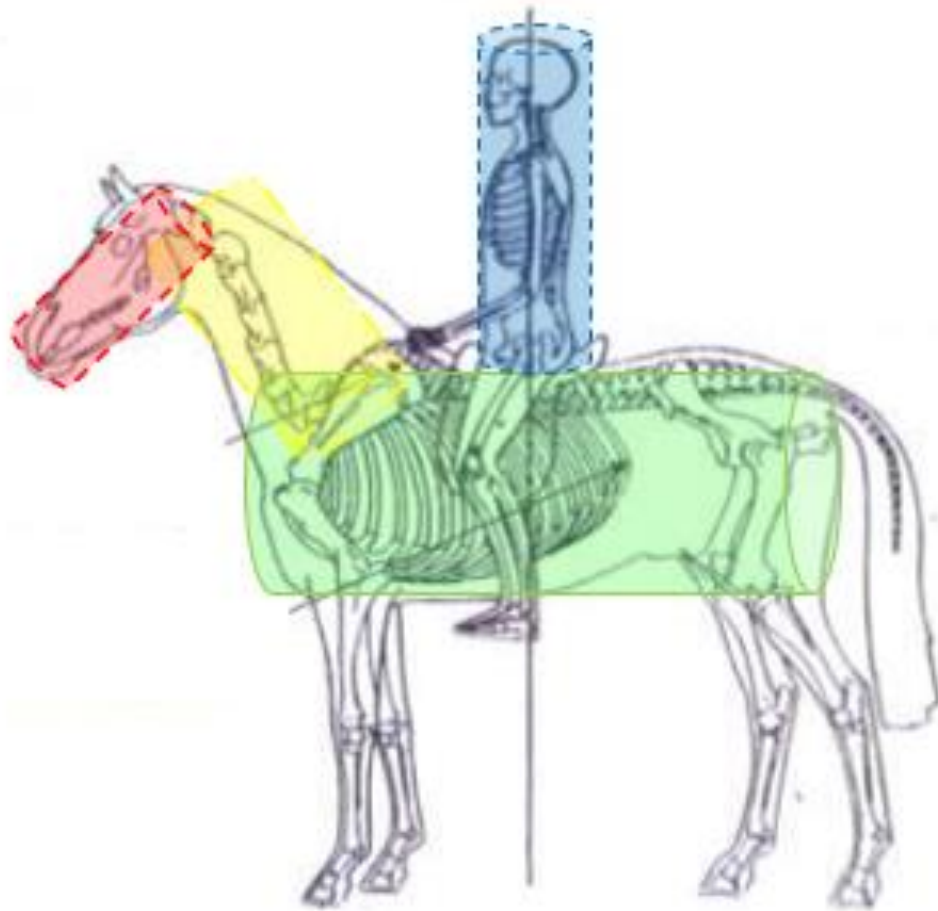


Figure 3.3 An illustration of TCM plus the Rider elements

Each of the significant body elements is represented as an equivalent cylinder. Take the Head segment for example. Two measurements that were used to create the head cylinder were the head length defined from the base of the ears to the tip of the nose and the head circumference below the cheek bone. Figure 3.4 shows the two measurements that were used for the head cylinder.

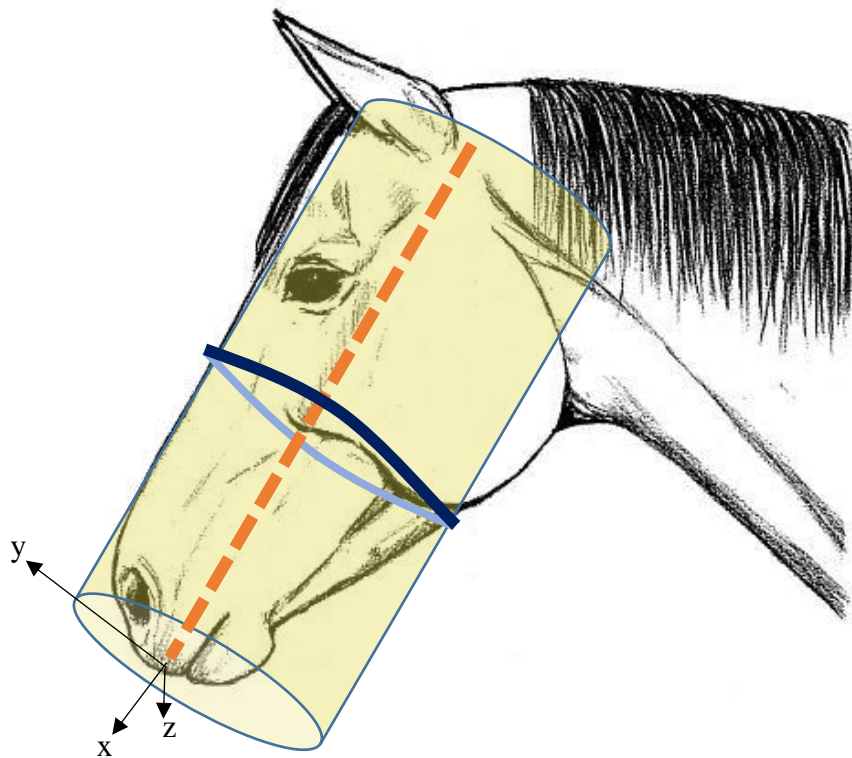


Figure 3.4 Illustrations of the measurements used to create the Head segment

The mass moment of inertia of the head cylinder about its local COM axis perpendicular to the sagittal plane can then be approximated by Equation 3.7, which was obtained from *Engineering Mechanics: Dynamics* [23].

$$I_{ZZ,H} = \frac{1}{12} m_H (3R_H^2 + L_H^2) \quad (3.7)$$

In Equation 3.7  $I_{ZZ,H}$ = mass moment of inertia of the Head,  $m_H$ = mass of Head,  $R_H$ = Head radius, and  $L_H$ =Head length. As part of using the this approach the cylinder is assumed to be homogenous. As can be seen from the Equation, the  $I_{ZZ}$  approximation requires the element mass to be known. Therefore, a method had to be developed on how to approximate the element mass. Three methods were tested and compared to determine the optimal: 1) segment percentage, 2) volumetric approximation, and 3) published densities.

The segment percentage method determined the mass of the head segment by using the percentage of the total mass that corresponded to the head. This percentage was found by taking the average head mass of the six horses that were studied in the *Inertial Properties of Dutch Warmblood Horses* and then finding its percentage with respect to the average total mass of the six horses in the study. By this method it was found that the head is approximately 4.3% of the total mass. To test this approximation the total mass of the living horse that is approximated would be multiplied by 4.3% resulting in the percentage of the horses' total mass corresponding to the head.

The volumetric approximation approach made use of an effective density. The effective density was calculated by taking the total mass of a living horse and dividing it

by the volume of the three cylinders (Head, Neck, and Body) used to construct the TCM. The effective density was then used to find the individual segment mass by multiplying the segment volume by the effective density.

The published density approach used the average densities measured in the study *Inertial Properties of Dutch Warmblood Horses*. The density for the trunk segment was modified to be the average of not only the trunk segment density but also the segments composing the forelimb and the hindlimb. This modification resulted in a new density called the body density. Another study also found the densities of Thoroughbred horses. Results from both studies are listed below with the standard deviation of the densities shown in parenthesis.

**Dutch Warmblood Horses:**

Head Density=1,081 kg/m<sup>3</sup> (0.027)

Neck Density=1,038 kg/m<sup>3</sup> (0.002)

Body Density=1,288 kg/m<sup>3</sup> (0.01)

**Thoroughbred Horses:**

Head Density=1,031 kg/m<sup>3</sup> (0.045)

Neck Density=1,019 kg/m<sup>3</sup> (0.015)

Body Density=1,193 kg/m<sup>3</sup> (0.054)

In order to test the three methods of calculating segment mass, measurements from living horses had to be obtained. Measurements were obtained for four horses available to the University of Kentucky team. The measurements can be seen in Table 3.7. Hugo was selected to evaluate the methods due to its similarities in weight and breed with Horse 3 from the DWB study. The I<sub>zz</sub> term was approximated for Hugo using all three methods and then compared to the I<sub>zz</sub> term measured in the DWB model as

reference. The percent error of each comparison can be seen in Table 3.8. From this comparison it was observed that the published density method of estimating segment mass was the most accurate.

Table 3.7 Original set of measurements used to test segment mass approximation

Horse	Breed	Horse Weight (kg)	Length of Body (m)	Heart Girth (m)	Neck length (m)	Neck Circumference (m)	Head Length (m)	Head Circumference (m)
Tyler	TB	482	1.6256	1.8796	0.7112	0.9144	0.6096	0.6350
Tulepo	TB	484	1.5494	1.9304	0.6604	0.9398	0.5842	0.5969
Hugo	Warmblood	535	1.6256	1.9939	0.8128	0.9652	0.6350	0.6604
Rocky	TB	449	1.4732	1.9050	0.7620	0.9652	0.5969	0.6223

Table 3.8 Percent error of the  $I_{zz}$  component on the inertia of the DWB model and the three methods of estimating segments mass

Method	Percent Error
Segment Percentage	20.9%
Volumetric Density	25.3%
Published Density	4.1%

Following a similar process as that of the Head segment Equations 3.8 and 3.9 were established. In Equation 3.8  $I_{ZZ,B}$ = mass moment of inertia of Body,  $m_B$ = mass of Body,  $R_B$ = Body radius, and  $L_B$ = Body length. Similarly, in Equation 3.9  $I_{ZZ,N}$ = mass moment of inertia of Neck,  $m_N$ = mass of Neck,  $R_N$ = Neck radius, and  $L_N$ = Neck length.

$$I_{ZZ,B} = \frac{1}{12} m_B (3R_B^2 + L_B^2) \quad (3.8)$$

$$I_{ZZ,N} = \frac{1}{12} m_N (3R_N^2 + L_N^2) \quad (3.9)$$

### 3.2.3 Inertia Approximation for the Rider

Once the geometric approximation for the horse was verified, then a similar approximation was needed to model the rider. Various methods have been developed to obtain inertial properties of a human [15]. These methods range from geometrical approximations, to penetrative methods that utilize x-rays. Typically, inertia approximations of a human body require several detailed measurements of the human body. In order to have a more effective inertia approximation for our purposes, a similar cylindrical approach as that was used. This approach used two principal publications of morphological properties [6,38].



Human moment of inertia measurements were documented in a study for impact protective systems in the aerospace field. During this study moments of inertia were measured for six cadavers with three in the seated position and three cadavers in the standing position [6]. Age, weight, stature, trochanterion height, CM- vertex, and principal moments of inertia were provided.

Human mass centers in various positions was also the focus of another study conducted for the Federal Aviation Agency at the Civil Aeromedical Research Institute [36]. Researchers measured the location of the center of gravity of five living men in sixty-seven positions. Of these, the body position that was selected due to its similarities with a rider position was with the subject sitting back erect, seat  $90^\circ$  to back, legs  $50^\circ$  to thighs and both hands on overhead control [38] . An illustration of the body position can be seen in Figure 3.5. The location of the average CG was measured as 9% of the height from the chair. To compensate for the variation the author of this thesis selected to use 10%.



Figure 3.5 Illustration of the body position defined as sitting back erect, seat  $90^\circ$  to back, legs  $50^\circ$  to thighs and both hands on overhead control [38]

The rider CG cylinder-based approximation lead to a new parameter being defined as  $R_{COM}$  or Rider COM. The  $R_{COM}$  was defined as the distance from the posterior body plane to the measured COM.  $R_{COM}$  was then calculated using Equation 3.10, where  $R_H$ = Rider height.

$$R_{COM}=0.1(0.5R_H) \quad (3.10)$$

Applying results from the studies and using only two measurements of eventers, height and weight, the cylindrical approximation was validated by applying correction factors derived from ratios (Equation 3.11). In Equation 3.11  $I_{ZZ,R}$ = mass moment of inertia of Rider,  $m_R$ = Rider mass, and  $R_H$ = Rider height.

$$I_{ZZ,R}=\frac{1}{12}m_R\left(3\left(\frac{0.54R_H}{2\pi}\right)^2+0.7R_H^2\right) \quad (3.11)$$

To validate the cylindrical approximation of the moment of inertia, data from cadavers in the sitting position was used. It was found that the percent difference of the approximation when compared to the measured value ranged from 0.66% to 10.1% which was deemed acceptable for our use in Monte Carlo simulation of large populations.

### 3.3 United States Eventing Association (USEA) Survey

After the geometric model was developed, a method was devised to acquire a large dataset of inertial parameters in an effective manner. To achieve this a “citizen science” effort was conducted through the USEA to distribute a survey internationally. Seven measured parameters from the survey are depicted in Figure 3.6. A summary of all survey questions along with a description of available options are included in Table 3.9. Also a partial picture of the USEA survey is shown in Figure 3.7. To increase the reliability of the citizen science measurements the survey results are validated through several accuracy checks [43].

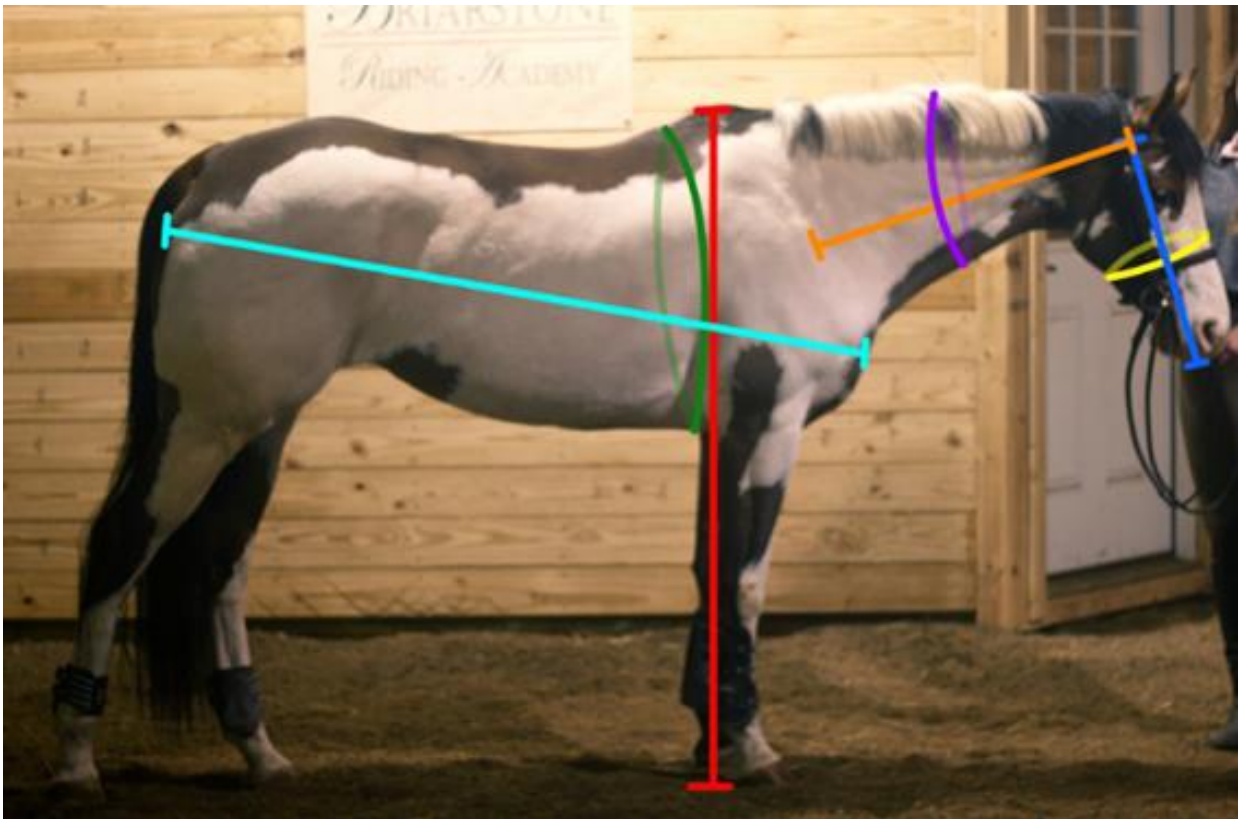


Figure 3.6 Illustration of the measurements that were requested in the USEA survey

Table 3.9 List of parameters requested on the USEA survey

<b>Parameter</b>	<b>Description</b>
<b>Breed</b>	Categories: Thoroughbred Warmblood Cross Warmblood - Light bodied Warmblood- Heavy bodied (weight above 635 kg) Other
<b>Competition Level</b>	Categories: BN (0.80m) Novice (0.90m) Training (1.00m) Preliminary//1* (1.10m) Intermediate/2* (1.15m) Advanced/3* (1.20m) 4* (1.20m) Other
<b>Height</b>	measured in hands
<b>Horse Scale Weight</b>	
<b>Length of body</b>	point of shoulder to point of buttock
<b>Heart Girth</b>	around horse touching just at the withers to behind elbow
<b>Circumference of Neck</b>	around the middle of the horse's neck
<b>Length of Neck</b>	base of ear to center of where the neck meets shoulder
<b>Circumference of Head</b>	around head just below cheek
<b>Length of Head</b>	base of ear to tip of nose
<b>Rider Height</b>	
<b>Rider Weight</b>	
<b>Home Location</b>	(City, State, Country)

**USEA Safety Survey by the University of Kentucky**

**Metric units**

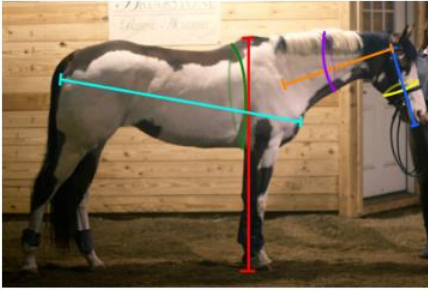
**Breed**

- Thoroughbred
- Warmblood Cross
- Warmblood - Light bodied
- Warmblood - Heavy bodied (weight above 635 kg)
- Other: \_\_\_\_\_

**At what level is the horse currently competing?**

- BN (.80 m)
- Novice (.90 m)
- Training (1.00 m)
- Preliminary/1\* (1.10 m)
- Intermediate/2\* (1.15 m)
- Advanced/3\* (1.20 m)
- 4\* (1.20 m)
- Other: \_\_\_\_\_

Please safely take the measurements of your horse as pictured below.



Height (Measured in hands)

Figure 3.7 Partial image of the USEA survey

### 3.4 Results from the USEA Survey

The survey has received inputs from various locations in the United States and throughout the world. Inputs are summarized in Table 3.10 and Figures 3.8-3.11 in this section. Along with the geometrical measurement that were provided in the USEA survey, the methods discussed earlier in this Chapter were utilized to approximate inertial properties for both the individual segments and also the overall composite-body in the standing configuration. The latest results (May 2017) although not used throughout the thesis due to their unavailability during the writing of this thesis are available in Appendix A.

A key finding from the results is that the distributions for the geometric equine measurements, rider, and segment moments of inertia were found to be normal distributions. This can be observed in the histograms plotted in Figures 3.8 – 3.11. The plots show the parameter that was measured or approximated in the horizontal axis and the frequency of occurrence in the vertical axis. Distributions observed for the various geometrical parameters and cylinder-based inertia values were used to derive random normal functions using MATLAB. The random normal functions are key to the Monte Carlo analysis conducted in the following Chapter. The random normal functions are defined by the mean and standard deviation values of the measured distributions and are provided in Table 3.10. A major difference between the measured/ approximated results and the randomly generated function for that parameter is the number of frequency of occurrence. The randomly generated functions consist of 1,000 random points while the measured results are two orders of magnitude lower.

Table 3.10 Mean and standard deviation of geometric and cylinder-based inertia approximations of USEA survey about cylinder center of mass.

<b>Parameter</b>	<b>Mean</b>	<b>Standard Deviation</b>
Body Mass (kg)	550.6	79.7
Body Length (m)	1.7719	0.1845
Body Radius (m)	0.2934	0.03845
$I_{\text{Body}}$ (kg m <sup>2</sup> )	148.5	43.4
Neck Mass (kg)	55.05	11.77
Neck Length (m)	0.7112	0.06036
Neck Radius (m)	0.1552	0.01623
$I_{\text{Neck}}$ (kg m <sup>2</sup> )	2.719	0.9113
Head Mass (kg)	20.02	6.37
Head Length (m)	0.5896	0.04507
Head Radius (m)	0.1015	0.01372
$I_{\text{Head}}$ (kg m <sup>2</sup> )	0.6599	0.3390
Horse Height to Withers (m)	1.651	0.09268
Rider Mass (kg)	63.1	8.705
Rider Height (m)	1.656	0.1628
$I_{\text{Rider}}$ (kg m <sup>2</sup> )	7.52	1.8846

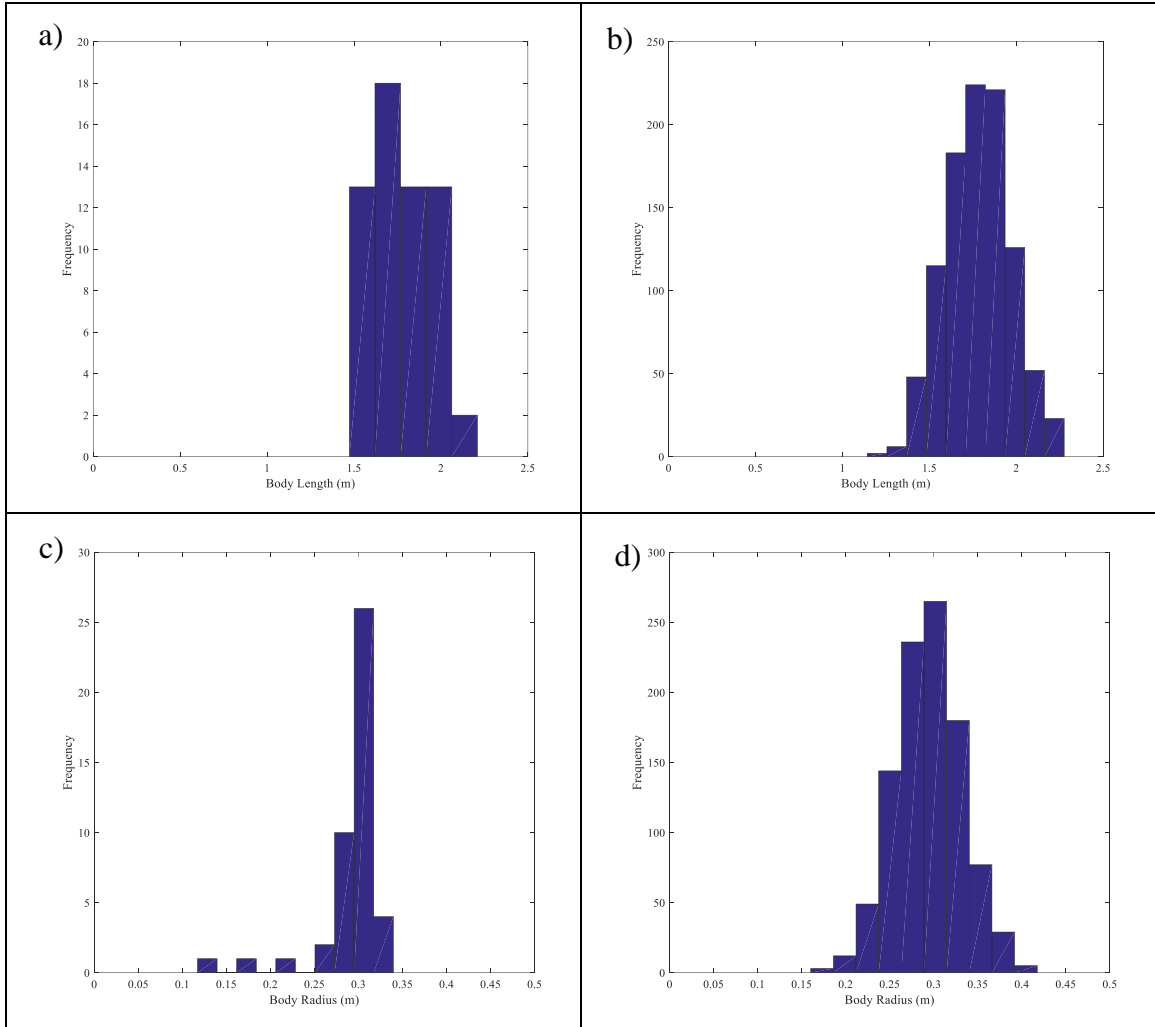


Figure 3.8 Histogram of Body Length (a) and a randomly generated distribution replicating the Body Length (b). The (c) plot the histogram of the Body Radius and the randomly generated distribution replicating the Body Radius (d)



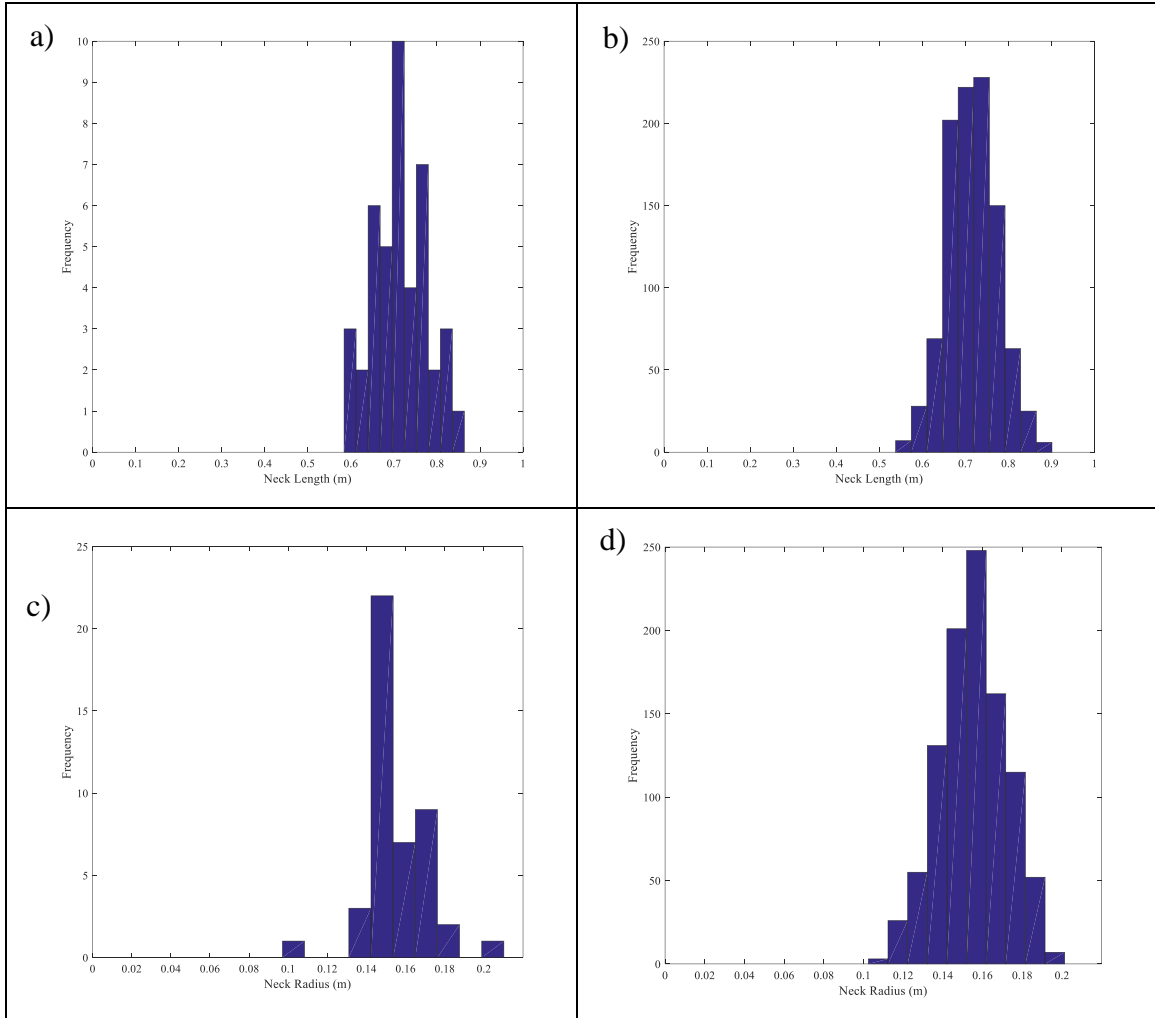


Figure 3.9 Histogram of Neck Length (a) and a randomly generated distribution replicating the Neck Length (b) The (c) plots the histogram of the Neck Radius and the randomly generated distribution replicating the Neck Radius (d)

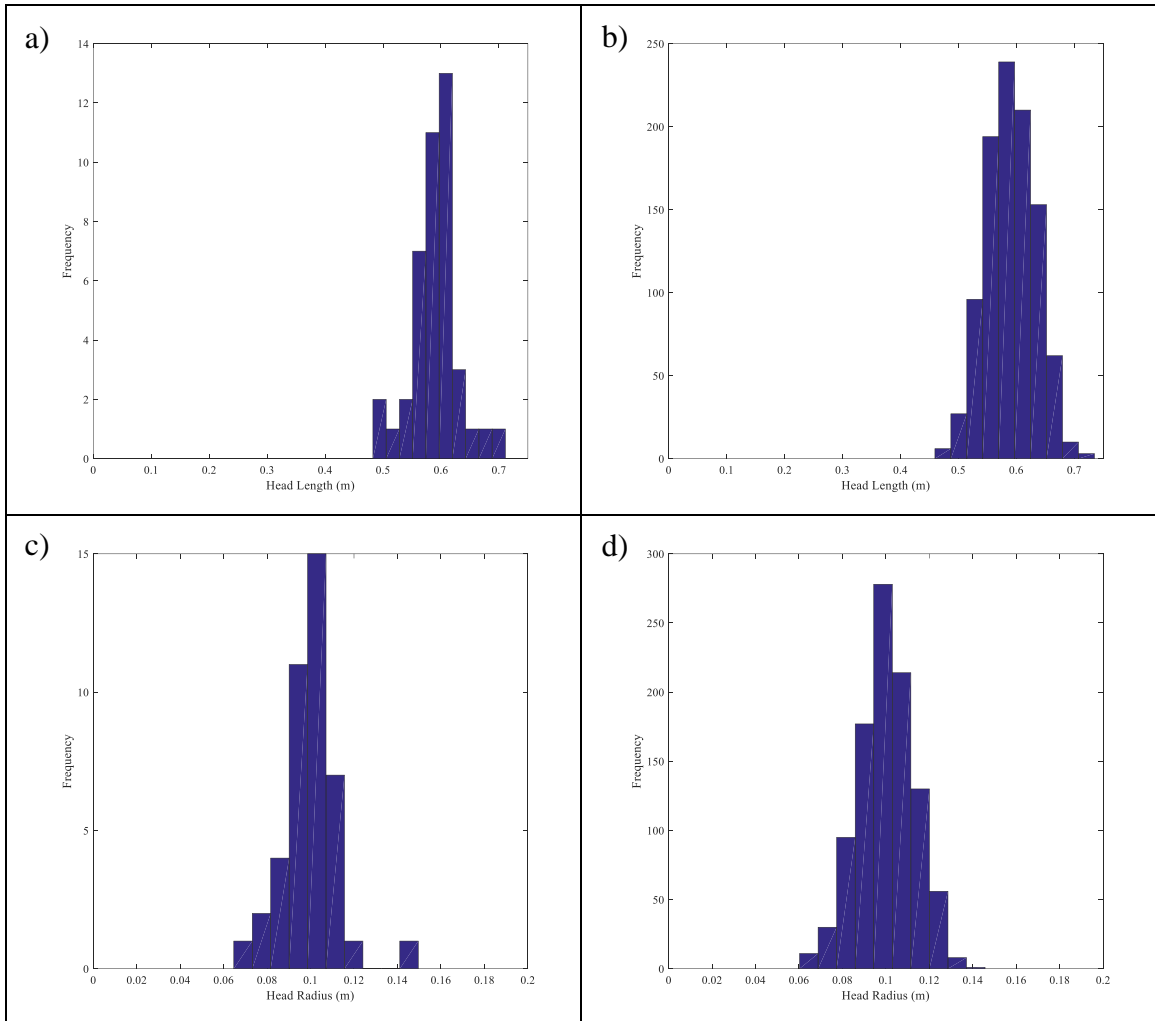


Figure 3.10 Histogram of Head Length (a) and a randomly generated distribution replicating the Head Length (b). The (c) plots the histogram of the Head Radius and the randomly generated distribution replicating the Head Radius (d)

One important Figure to note is Figure 3.13. The significance of this figure is that it highlights the difference between the standing orientation of the TCM model to that of a jumping form. In this Figure three histograms are plotted with the left plot being the moment of inertia about the COM of the TCM and rider segments in the standing orientation obtained through the use of the geometric measurement and the cylinder-based inertia approximation. The middle histogram is the randomly generated normal distribution used to create a population that imitates the measured data. The last histogram in this Figure is that of the TCM-plus-Rider segments re-oriented into the jumping position. The contact point is set at mid Antebrachium, an added length to the Body segment. A key observation is the skewness of the last histogram. The reason why it is skewed is because of the combination of the moment of inertia of the Body, Neck, and Head segments combining in the overall moment of inertia term.

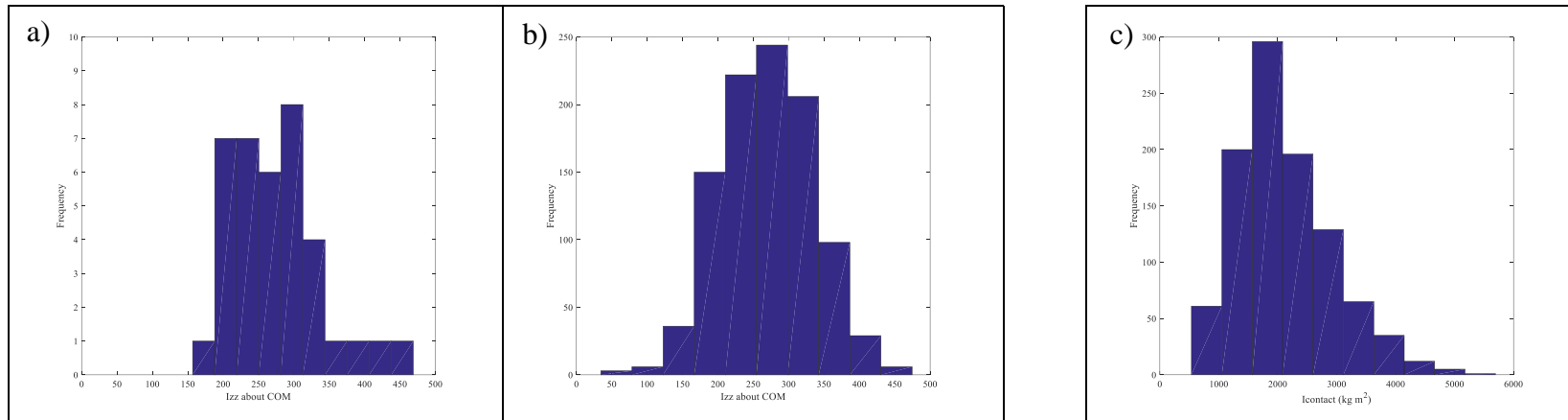


Figure 3.11 Histograms of moment of inertia about the sagittal plane of motion. Histogram (a) is the  $IZZ$  about the TCM COM calculated from USEA survey data. (b) is the approximation of the histogram on the left using normal-distribution from random generation function through the use of MATLAB<sup>TM</sup>. (c) is the translation of (b) to the contact point located at mid antibrachium

## Chapter 4: Phenomenological Study

The motion of a competitor (horse and rider) experiencing a rotational fall was understood by conducting phenomenological studies on simplified models. The essential Physics of the motion was represented so that general design guidance can be obtained from the results. To conduct such an approach the complexity of the rotational fall problem had to be simulated using current geometric and dynamic measurements on available approximations. The underlying mechanics of the motion were represented with information from various sources including the USEA survey, cylinder-based inertia approximations, literature and expert inputs.

Additionally, to fully understand and quantify the contribution of each aspect and assist in conducting a sensitivity analysis of the problem, a phased approach was used. This was achieved by first modeling a simple block overturning, then gradually increasing the complexity of the geometry and other parameters to that of the desired model of the competitor.

Furthermore, the study will be performed using a Monte Carlo simulation approach. The Monte Carlo method is a numerical method of solving mathematical problems by random sampling. The advantage of using the Monte Carlo method is that the error is reduced with increasing number of samples [36]. This method has been applied in various fields including aerospace applications. For example, the Monte Carlo method was used for launch vehicle design and requirements analysis at the NASA Marshall Space Flight Center [22], among many other applications.

## 4.1 Fundamental Mechanics of Rotational Falls

There are several key observations in regards to the foundation of the mechanics that occur during a rotational fall. The first is the dominance of key geometric elements in the motion. This observation can be seen in the cylinder-based inertia approximation where four out of 26 elements capture 71.7% of the horse and rider inertia. Therefore, the dynamic model could be simplified into the same four segments used for the cylinder-based inertia approximation.

The second key observation is the time interval of the motion. Video analysis conducted at the 1990 Stockholm World Equestrian Games revealed airborne times for competitors ranging from 0.282 seconds to 0.355 seconds [29]. As a comparison, human reaction times were tested for 94 Division 1 collegiate football players at the University of Michigan Ann Arbor using a falling meter stick. The test showed a mean reaction time of 0.203 seconds. Results were also measured with a computer and resulted in a mean reaction time of 0.268 seconds [14]. Therefore, the reaction times of a Division 1 athlete are approximately equal to the average airborne time in a jump. Since rotational falls initiate at a time during the total airborne time, it is unlikely the rider can react in time. Based on this observation, the rate of change of the orientation of the segments is ignored. This allows the angle of the competitor model segments to be fixed throughout the simulation.

The third observation that was made was in regards to the critical point after which the competitor would not be able to recover from a rotational fall. The condition that was observed to induce a non-recoverable rotational fall was found to be after the COM passed vertical (exceeded 90°). The system would experience an influx of energy after this point through conversion of potential energy to additional rotational kinetic energy.

The direction of the contact velocity vector is unknown. Due to a lack of available velocity data to quantify this property, the horse-fence contact direction obtained from the British Eventing Safety Fence was used as an initial approximation. This data did not include rotational falls. The choice will be verified with video analysis in future work.

The last fundamental property that needed to be determined was the velocity magnitude of the competitor at the contact point. Again there are currently no sources that have measured velocity magnitude at the instants before and after horse-fence contact. The most similar measurements available are of the take-off velocities at the start of the jumping arc. Therefore, the contact speed is initially approximated with the take-off velocity magnitude. All of the initial approximation will be evaluated through the phased simulations, and adjusted as indicated.

## 4.2 Mechanisms Principles

Mechanics principles used to conduct the simulations are the Principle of Impulse and Momentum and the Principle of Work and Energy. Conservation of angular momentum (2-D) is used to transition the translational motion prior to contact into a rotational motion about a fixed point as shown in Equation 4.1. This is a 2-D analysis with rotation about fixed-point axis perpendicular to the plane.

$$r_{contact-COM} \times mV = I_{contact}\omega_{contact} \quad (4.1)$$

Once the angular velocity is determined then Work/Energy is be used to determine the angular velocity at 90°. To calculate this Equation 4.5 was used.

$$\frac{1}{2}I_{contact}\omega_{contact}^2 - mg(h_2 - h_1) = \frac{1}{2}I_{contact}\omega_{90^\circ}^2 \quad (4.5)$$

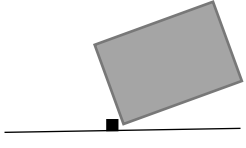
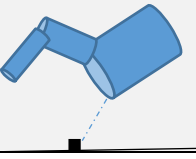
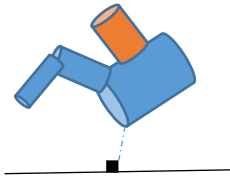
If  $\omega_{90^\circ}$  was greater than zero the system has overturned.



### 4.3 Overview of the Geometric Cases

Several geometries are used for the overturning analysis. Each consecutive geometrical case increased in complexity. The phased approach allowed for a more in-depth sensitivity study. Among the properties that were varied were the geometric shape, contact velocity, and contact angle. A list of the cases that are studied is shown on Table 4.1.

Table 4.1 Geometric illustration of the three cases explored

Case Number	Geometry
1	
2	
3	

#### 4.4 Case I

Case I is the most basic case with the geometrical shape being a rectangular prism (block). The Case is divided into three different sub-cases that varied based on the conditions for contact velocity and contact angle. The main parameters in Case I are the block length, block height, contact velocity, contact angle, and mass. Further, the contact velocity direction was aligned with the midline of the body, while the magnitude varied. Table 4.2 and Table 4.3 show the case descriptions and parameter values. Furthermore, the varying properties used uniform rather than normal distributions for only this case bounded by the values specified in Table 4.3.

Table 4.2 Description of conditions for various cases

<b>Case Name</b>	<b>Block Length (m)</b>	<b>Non-dimensionalized Geometric Parameter (Block Length/Block Height)</b>	<b>Contact Angle (°)</b>	<b>Contact Velocity (m/s)</b>
Case 1a	Varied	Varied	Fixed	Fixed
Case 1b	Varied	Varied	Fixed	Varied
Case 1c	Varied	Varied	Varied	Varied

Table 4.3 Description of parameter settings on various conditions

<b>Parameter</b>	<b>Fixed Condition</b>	<b>Varied Condition</b>
Block Mass	1 kg	-
Block Length (m)	-	(0 m-3 m)
Non-Dimensionalized Geometric Parameter (m)	-	.1-3
Contact Angle (°)	0°	(-45°- 45°)
Contact Velocity (m/s)	5 m/s	(1 m/s -10 m/s)

To further understand the various cases Figure 4.1 illustrates the three cases that were modeled at the time of contact and also at  $n$  seconds later. Also in the figure the block length is denoted by the letter  $a$  and the block height is denoted by the letter  $b$ .

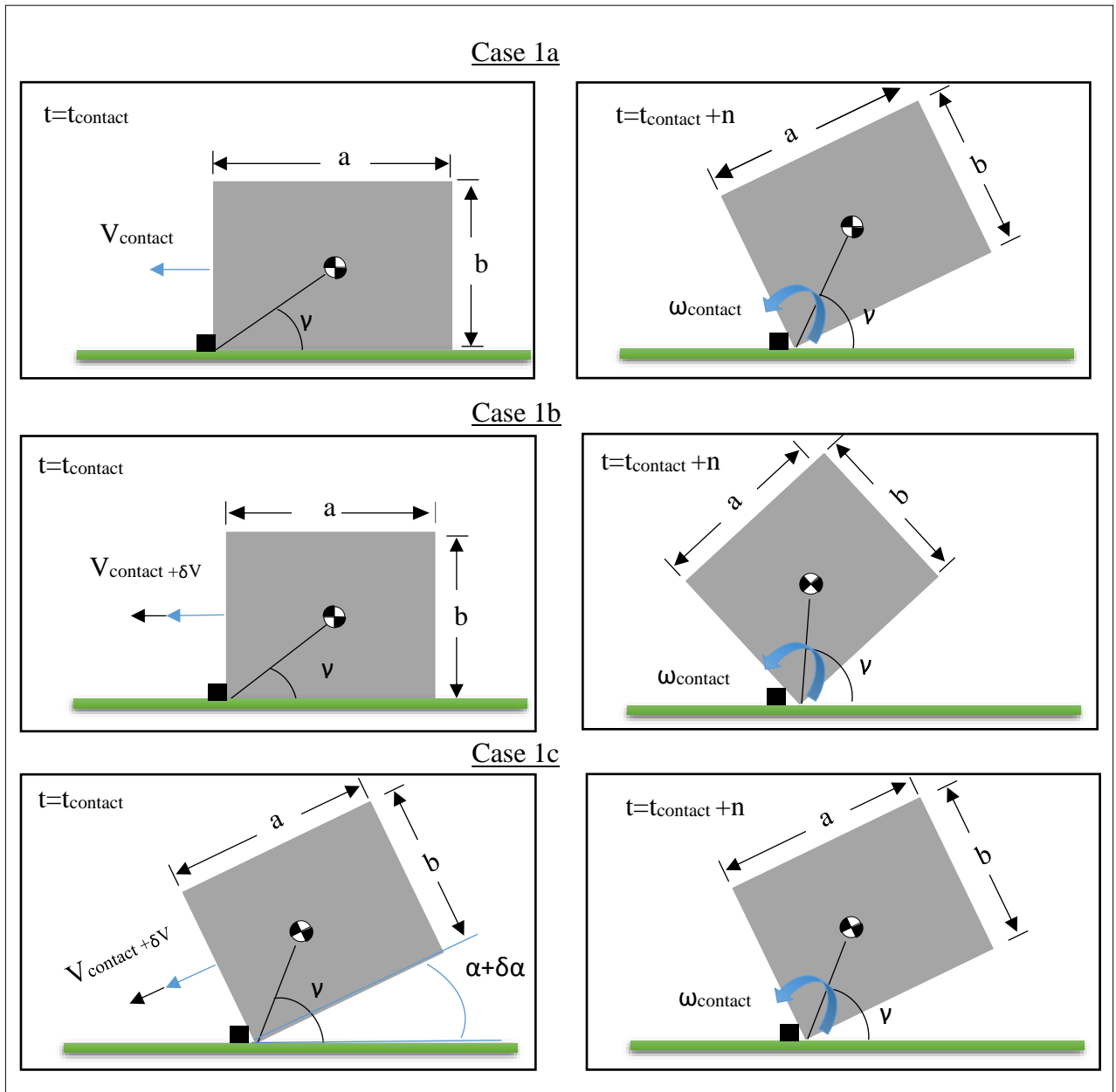


Figure 4.1 Illustration of the iterations of Case 1 at the time of contact and at a moment  $n$  seconds later

#### 4.4.1 Case 1a Results

The results of Case 1a illustrates how the geometry, as expected, has a significant effect on whether the block overturns or not. This observation can be clearly seen in Figure 4.2. In the Figure the horizontal axis plots the ratio of length over height. Parameter which was defined as block length divided by block height. The vertical axis plots  $\omega_{\text{contact}}$  which is the angular velocity at the point of contact. In the plot, the points whose  $\omega_{90^\circ}$  value were less than zero and therefore did not overturn were colored green. The points that did overturn were colored red. The black points are  $\omega_{\text{critical}}$  values for each block ratio that was found through an analytical solution. It can be seen clearly how the green and red results of the simulation are separated by the line created for the analytical solution. A key observation from this plot is the geometric aspect that as the ratio decreases the points are more susceptible to overturning. This is caused by the shape of the block being tall and slender forcing the COM to have a location farther above the contact point.

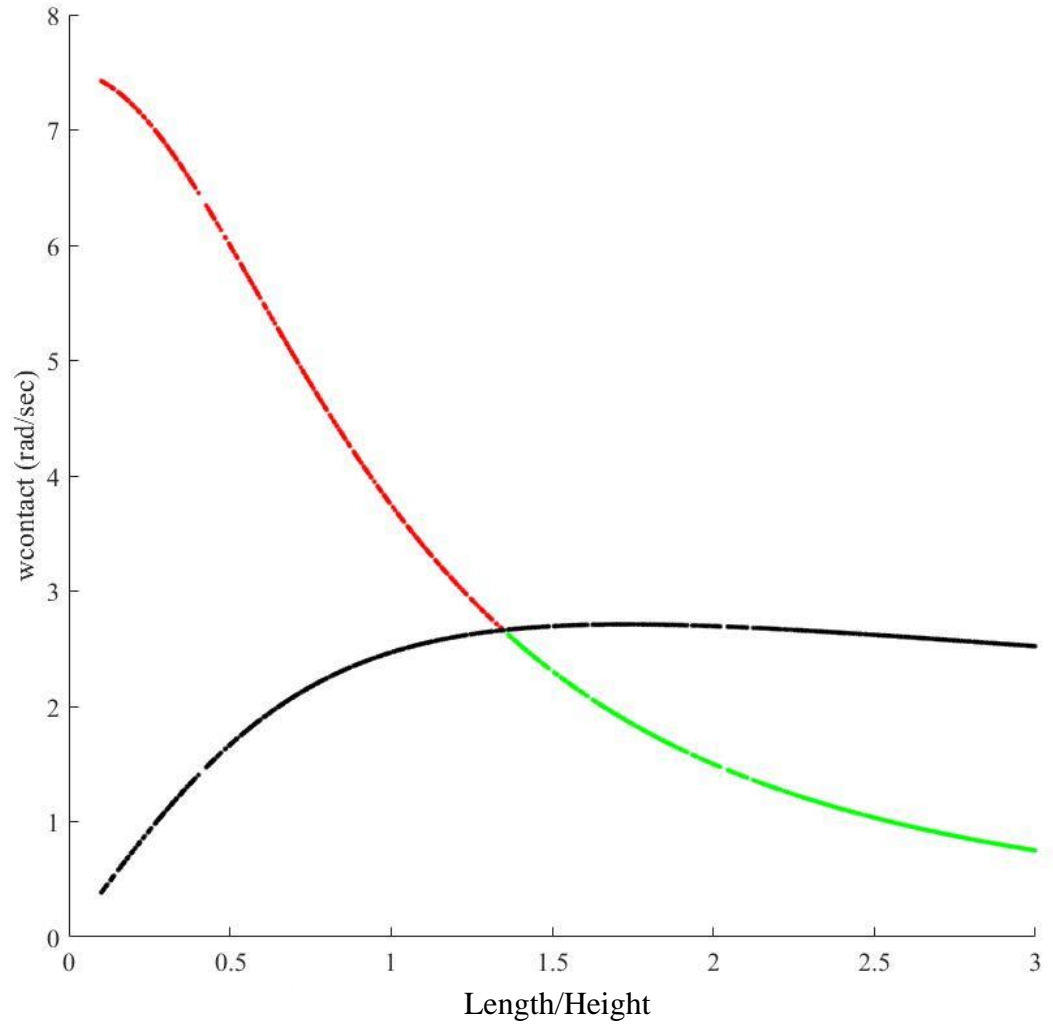


Figure 4.2 Block ratio range from 0.1 to 3 with block length held constant

#### 4.4.2 Case 1b Results

Case 1b presented further verification for the model with varying velocity magnitudes included. This can be seen in Figure 4.3 where block ratio (horizontal axis) is plotted against  $\omega_{\text{contact}}$ . The red markers are the points that failed because their  $\omega_{90^\circ}$  exceeded zero. The black solid line is the analytical solution calculated for the geometric cases. As can be seen there are no red markers below the line as the results matched the analytical solution..

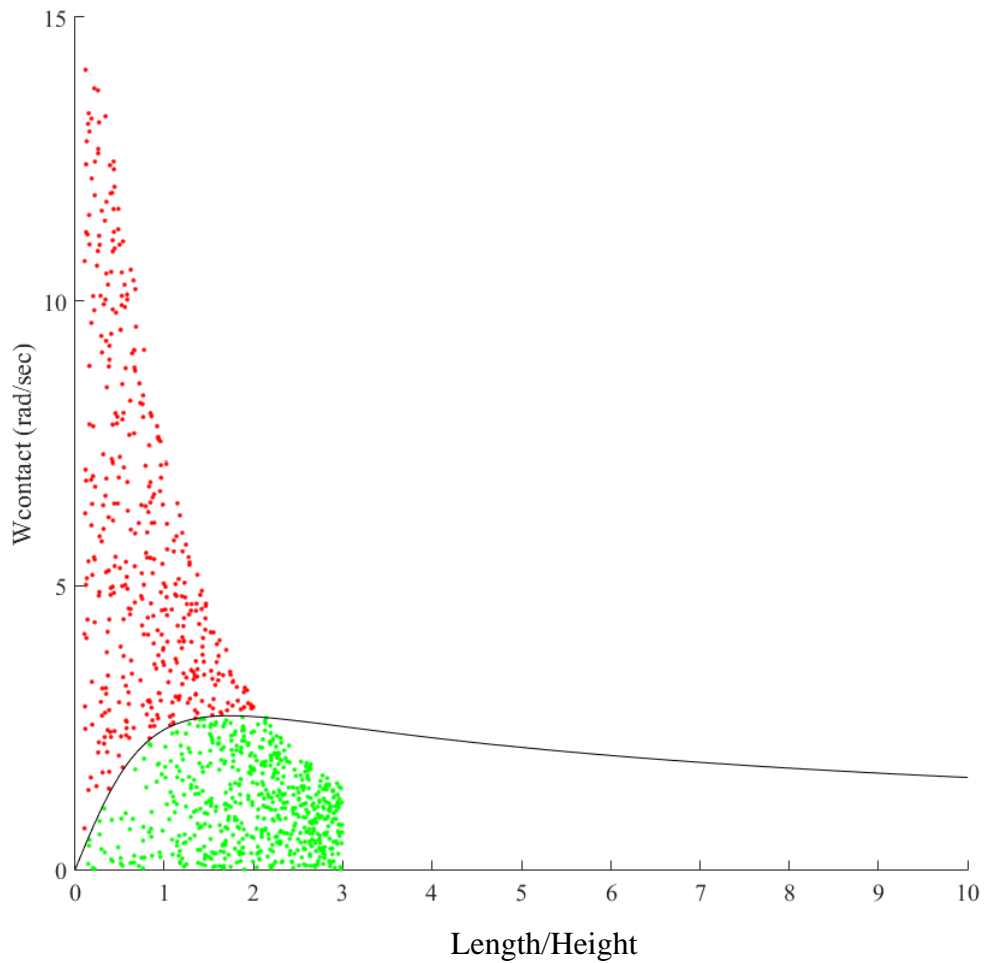


Figure 4.3 Block ratio varied from 0.1 to 3 with block length held constant. Block velocity ranged from 0 m/s to 10 m/s

Another way of looking at the results is to define Gamma as the angle from the positive x-axis to the COM of the system. In this case there is no variation for the incoming angle  $\alpha$  that is set to zero degrees, Gamma is an inherent property of the geometry. The property Gamma is plotted as the horizontal axis in Figure 4.4 plotted against  $\omega_{\text{contact}}$  in the vertical axis. It can be observed that the higher Gamma is the easier it is for the block to overturn with initial smaller angular velocity.

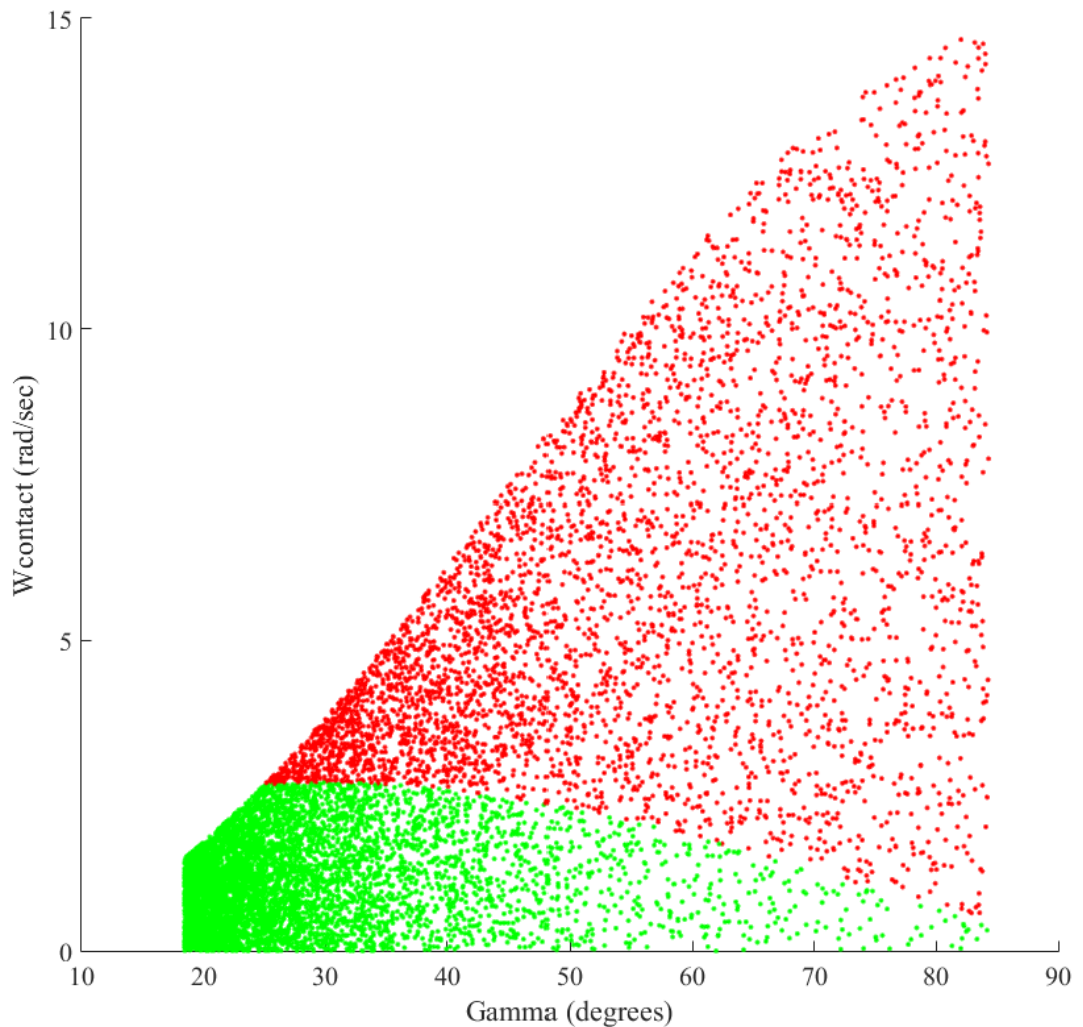


Figure 4.4 Block ratio ranged form 0 to 3 with block length held constant. Velocity varied from 0 m/s to 10 m/s

#### 4.4.3 Case 1c Results

Case 1c expanded the complexity of the results by the addition of the angle,  $\alpha$ . Figure 4.5 shows how adding a variable contact angle can affect the overturning block problem. In the figure the horizontal axis plots block ratio, the vertical axis plots  $\omega_{\text{contact}}$ , and the third axis is alpha.

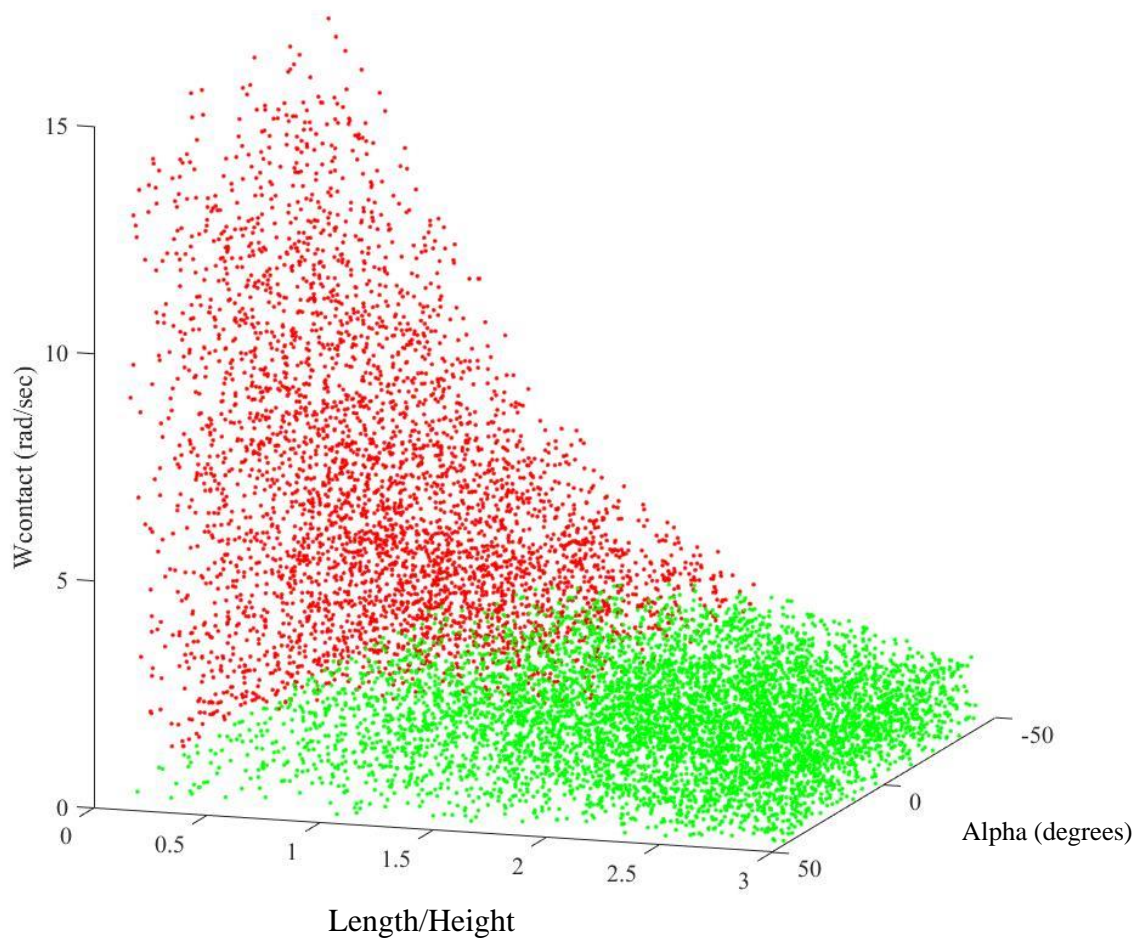


Figure 4.5 Block ratio ranged from 0 to 3 with block length held constant at 1. The velocity ranged from 0 m/s to 10 m/s. Alpha ranged from  $-45^\circ$  to  $45^\circ$



The alternate form of looking at the results of Case 1c is by looking at Gamma rather than block ratio. This plot can be seen in Figure 4.6. Three axes include Alpha, Gamma, and  $\omega_{\text{contact}}$

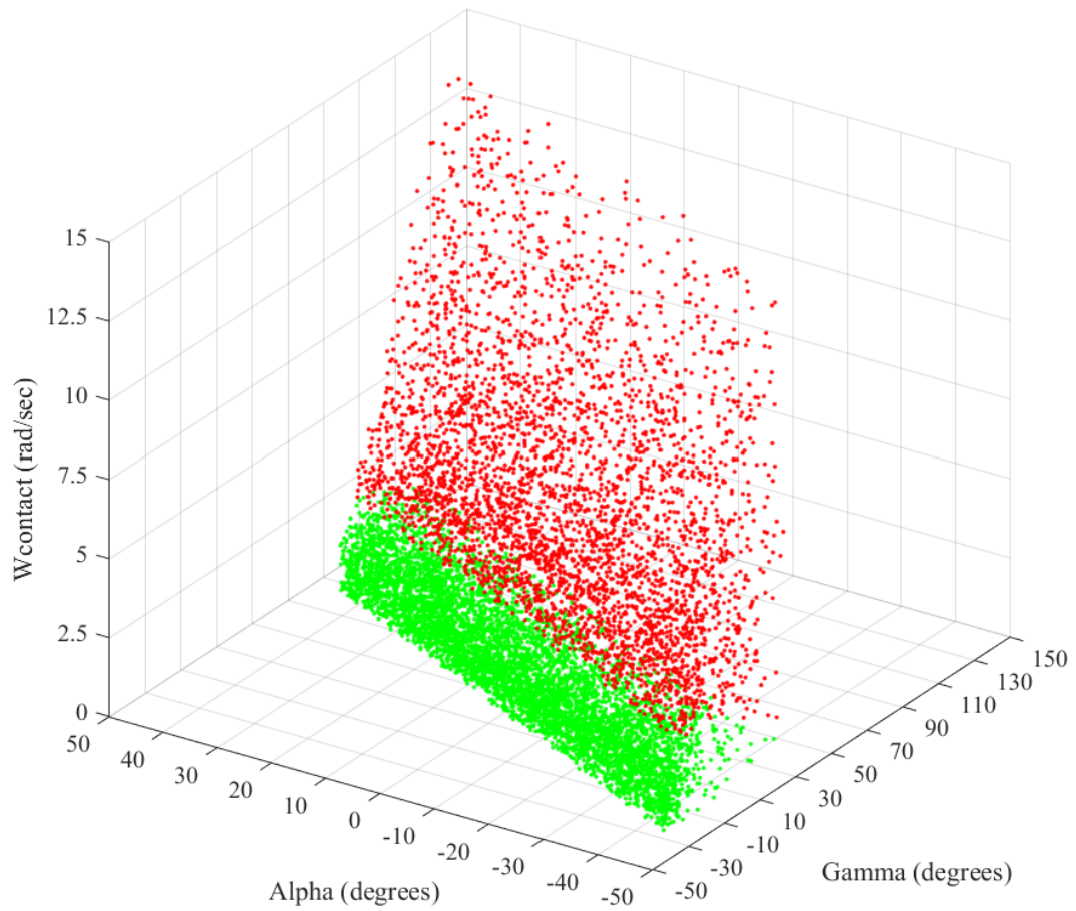


Figure 4.6 Gamma vs  $\omega_{\text{contact}}$  vs Alpha

## 4.5 Case 2

The geometrical shape explored in Case 2 is the TCM. For further details on the TCM refer to Chapter 3. The case is divided into four subcases to highlight differences between contact velocity variation and inertias. These sub-cases are further explained in Table 4.4. It should be noted that the Antebrachium length is not an element with mass, but rather a finite length and direction added to more accurately locate the point of contact for a rotational motion. Also, in Table 4.4 FLFR signifies front leg-front rail and FLRR signifies front leg-rear rail.

Table 4.4 Subcases for Case 2

Case Name	Elements	Contact Velocity (m/s)	Contact Angle (degrees)
2a	Body, Neck, Head	Varied	FLFR
2b	Body, Neck, Head, Antebrachium length	Varied	FLFR
2c	Body, Neck, Head	Varied	FLRR
2d	Body, Neck, Head, Antebrachium length	Varied	FLRR

### 4.5.1 Initial Conditions for Variables

Prior to reviewing the results, it is necessary to define the new geometric and physical parameters used in Case 2. First of all, the geometric parameters used in Case 2 are shown in Figure 4.8. The length and radius of the segments were obtained from the USEA survey discussed in Chapter 3. The mean and standard deviation of the parameters were then used to randomly generate a normal distribution of the parameters using MATLAB.

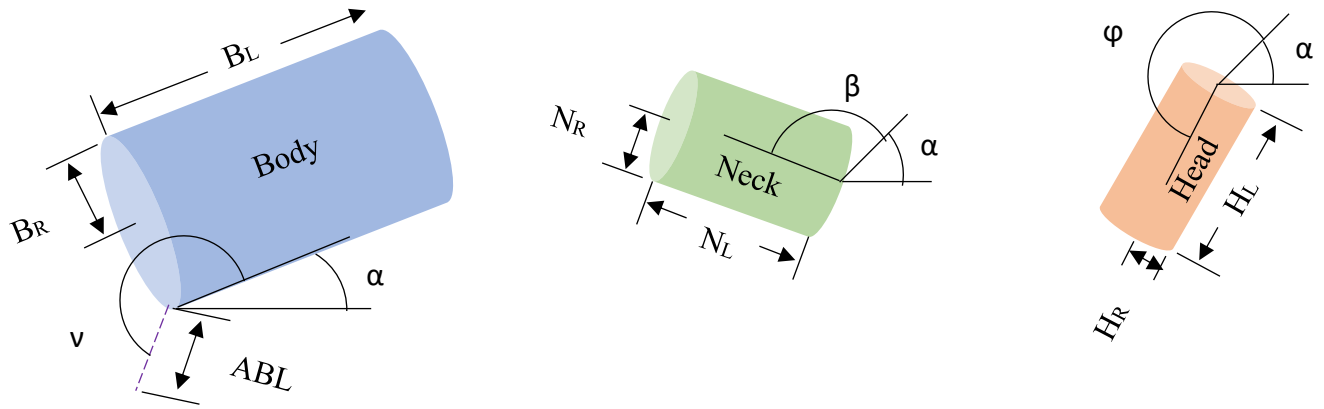


Figure 4.7 Illustration of Case 2 geometric parameters

The angles  $\beta$ ,  $\phi$ , and  $v$  were defined relative to the body angle,  $\alpha$ . The angles  $\beta$ ,  $\phi$ , and  $v$  were not defined based on publications due to the lack of available measurements. They were, however, estimated by an experienced eventer in the University of Kentucky team. Furthermore, their range was widened to encompass more possible options. The ranges for these variables will be narrowed by the use of video analysis in future work. Another variable that is used is that of  $\gamma$ .  $\gamma$  is defined as the angle from the positive x-axis to the overall (all elements in the specified subcase) center of mass. This is the same angle as that used in Case 1.

The last set of variables that need to be defined for Case 2 are the Antebrachium length, antibrachium contact percentage, and angle  $v$ . The antibrachium length can be seen illustrated in Figure 3.1 where it is defined by reference points 8-9. The antibrachium contact percentage simply stands for the percentage of the antibrachium

length at which the contact occurred. For example, 75% antebrachium contact percentage would mean the contact occurred  $\frac{3}{4}$  of the way down from the pivot point between the antebrachium length and the Body. Lastly the angle  $\nu$  (nu) is defined from the angle  $\alpha$ , counter-clockwise until reaches the antebrachium length. The angle  $\nu$  can be in both the third and fourth quadrants.

Furthermore, to define the range of antebrachium lengths the results from the USEA survey were used. The antebrachium length was defined by Equation 4.6. The variables used in this equation are defined as follows;  $H_H$  is the horse height up to the withers,  $B_D$  is the diameter of the body,  $ABL$  is the antebrachium length and the value 0.6 is derived from the average percentage contribution of the  $ABL$  to the total forelimb length ( $ABL$ , metacarpus, and digit forelimb).

$$(H_H - B_D) \cdot (0.6) = ABL \quad (4.6)$$

Another important assumption that should be restated is that of the velocity vector direction. As was stated in Section 4.1, the velocity vector direction was defined by the angle  $\psi$ . However, due to a lack of measurements angle  $\psi$  was assumed to be equal to angle  $\alpha$ . Furthermore, it should be restated that angle  $\alpha$  was defined by the force contact directions measured in the British Eventing Safety Research Fence.

In addition, a modification of the FLRR measurement from the British Eventing Safety Research Fence was performed. As can be seen in Chapter 3, the FLRR contacts

contain angles greater than  $90^\circ$ . Since such an angle would be impractical, it was decided to neglect all contact angles that are greater than that value.

Finally, an overview of the variables that were used in Case 2 are shown in Figure 4.8. In the Figure, the variables that are varied in the initial conditions are shown by shaded blocks.

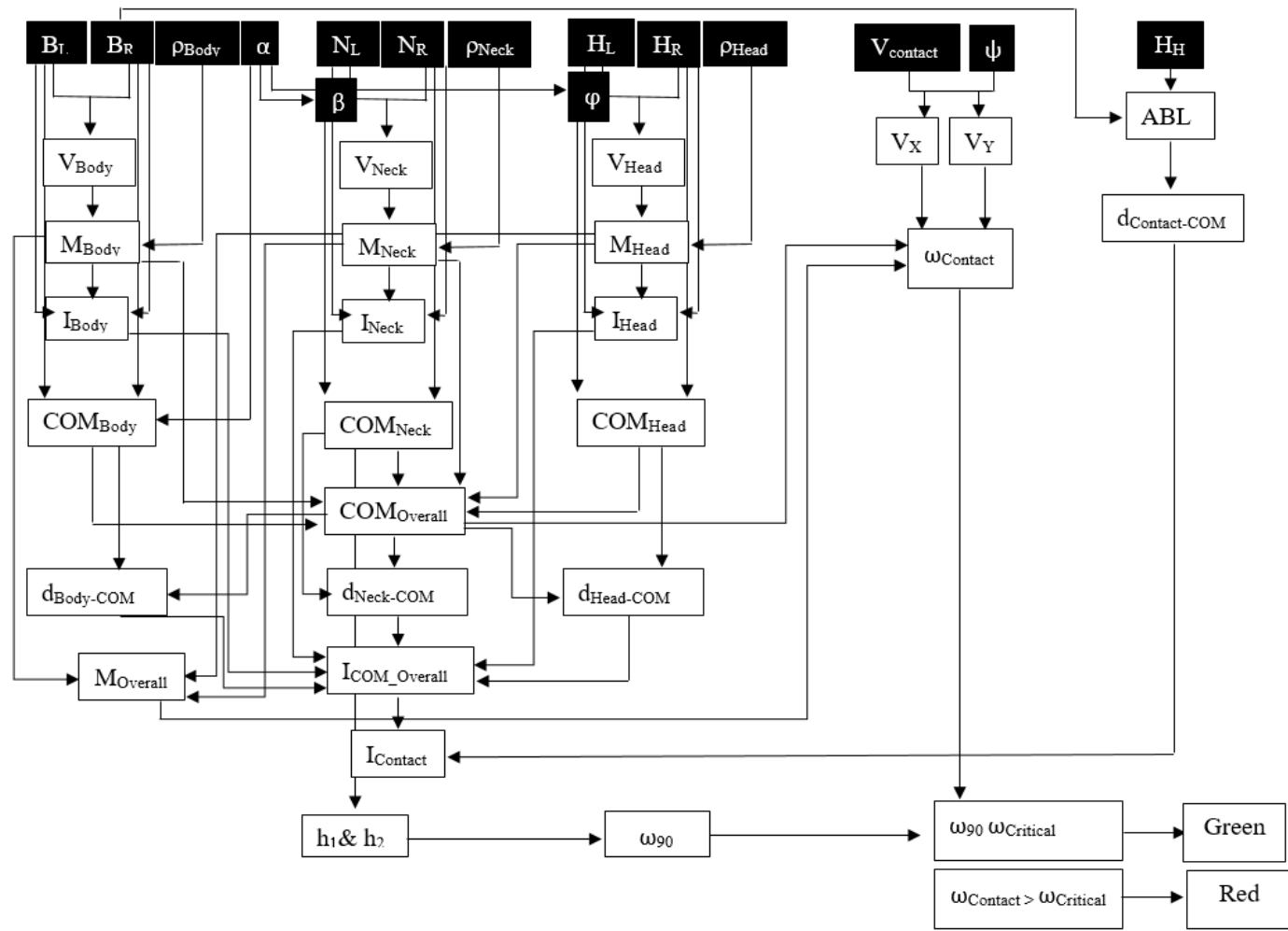


Figure 4.8 Parameter map of variables used in Case 2

#### 4.5.2 Case 2a Results

Case 2a includes the TCM with the contact angles experienced by the front leg-front rail contacts in the Goodyear Safety Research Fence. The results for this particular geometry and input conditions showed that no points overturn. This result is shown in Figure 4.9. The reason for there not being any overturning is due to the contact point being located at the bottom front of the body.

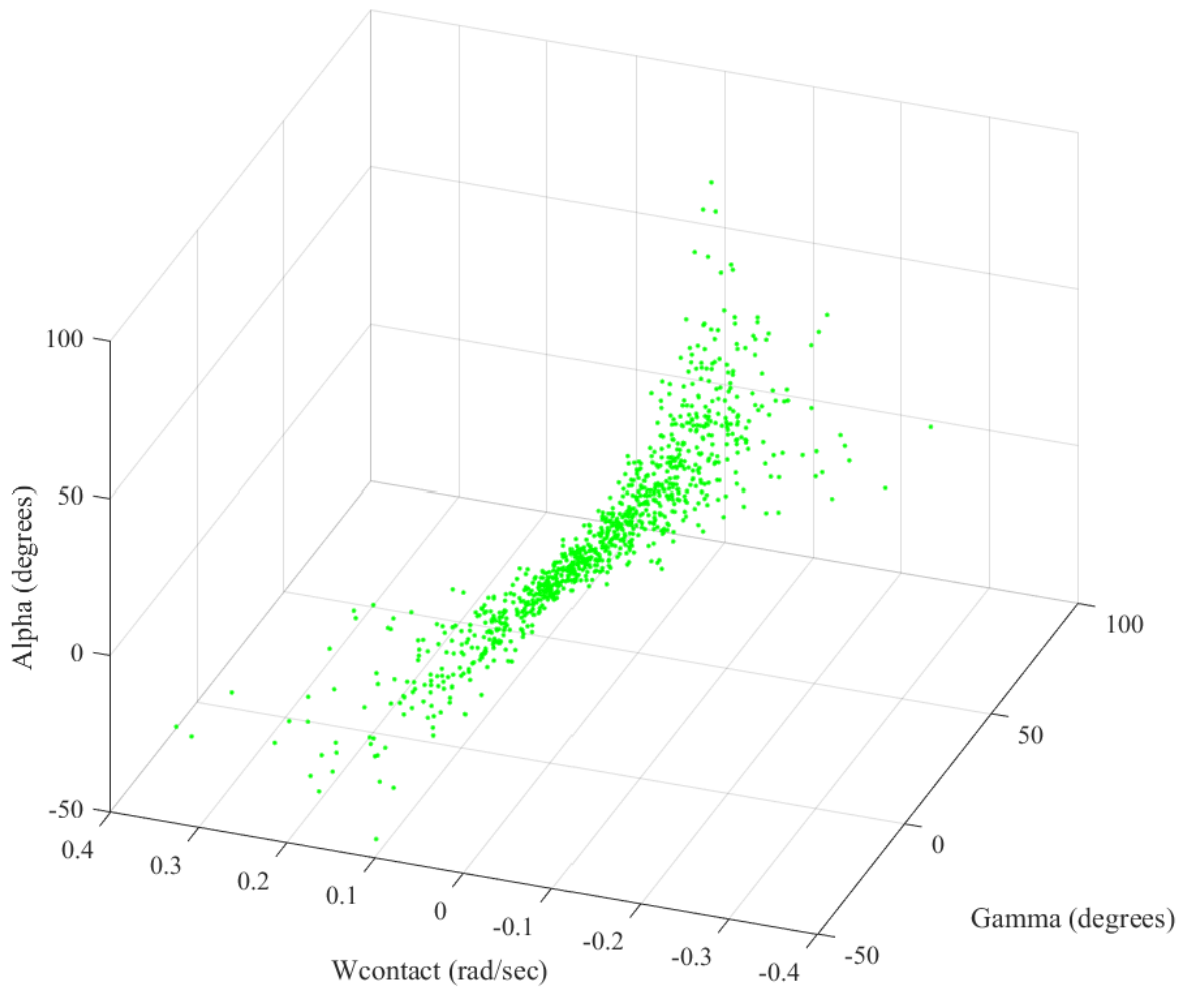


Figure 4.9 Case 2a scatter plot of Gamma (angle from x-axis to TCM COM), contact velocity, and Alpha

### 4.5.3 Case 2b Results

Case 2b is similar in geometry as Case 2a except that it has the added antebrachium length that was previously discussed. The Antebrachium Length percentage was set to 50%. Case 2b uses the contact angles obtained from the FLFR contacts in the British Eventing Safety Research Fence. The Npass for this analysis was 99.6% with 1,000 randomly generated points. These results can be seen in Figure 4.10.

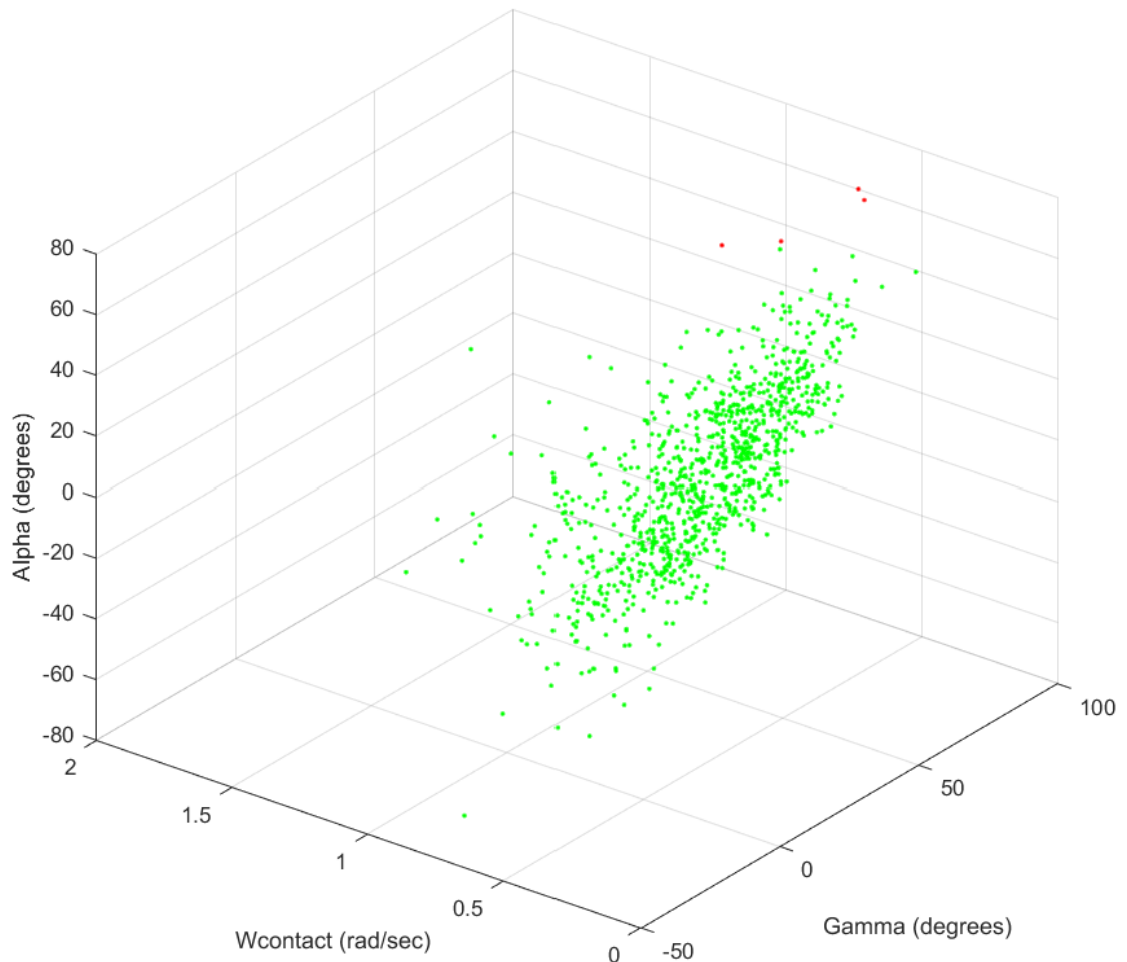


Figure 4.10 Case 2b scatter plot of Gamma, contact angular velocity, and Alpha



#### 4.5.4 Case 2c

In Case 2c the geometry is still the TCM, however, the contact angles are those recorded as FLRR in the British Eventing Safety Research Study. This case does not have the antebrachium length added. The Npass was 97.3% with the number of random points being equal to 1,000. The results are plotted in Figure 4.11.

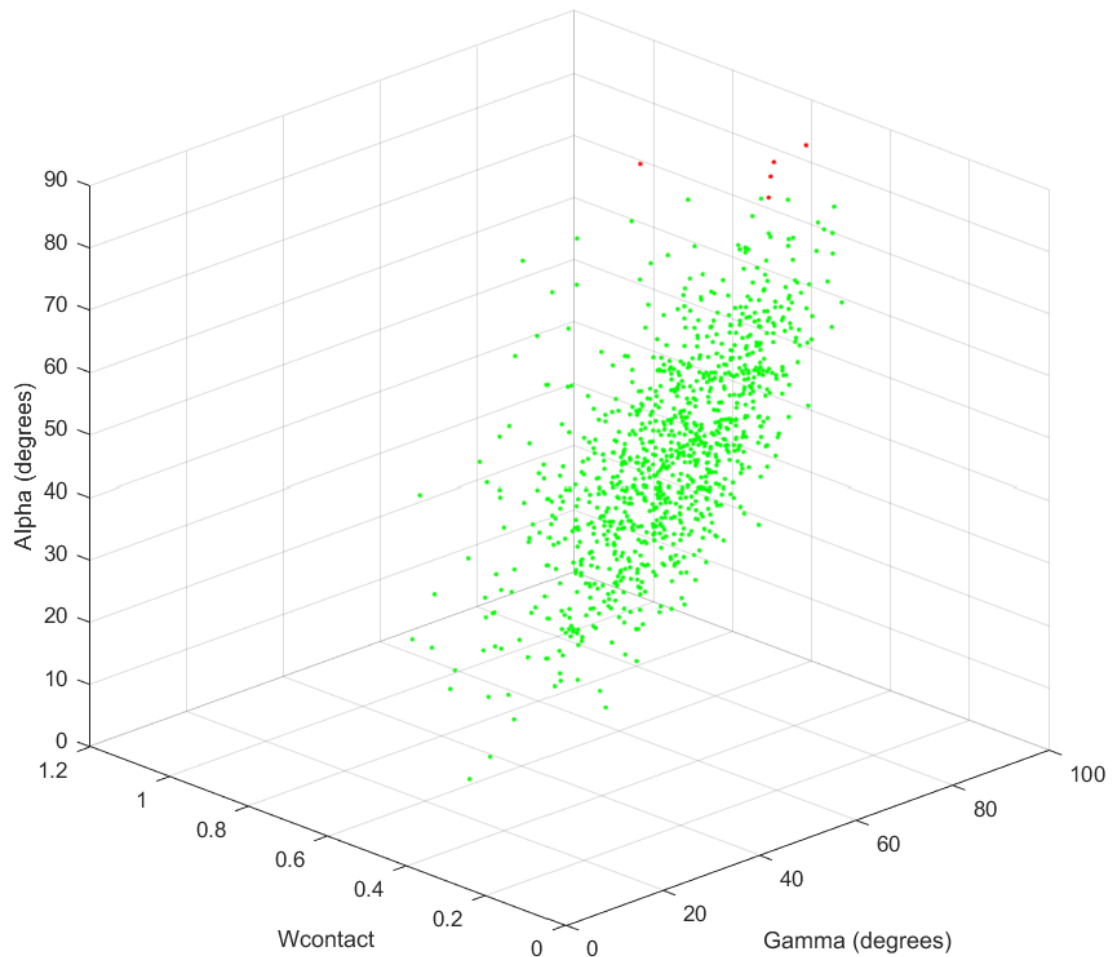


Figure 4.11 Case 2c scatter plot of Gamma, contact angular velocity, and Alpha

#### 4.5.5 Case 2d

Case 2d is similar to Case 2b, however, the contact angles were changed to simulate those experienced by FLRR contacts in the Goodyear Safety Research Fence. Similar to Case 2b this case has an added Antebrachium Length set to 50%. The Npass was equal to 92.4%. These results are illustrated in Figure 4.12.

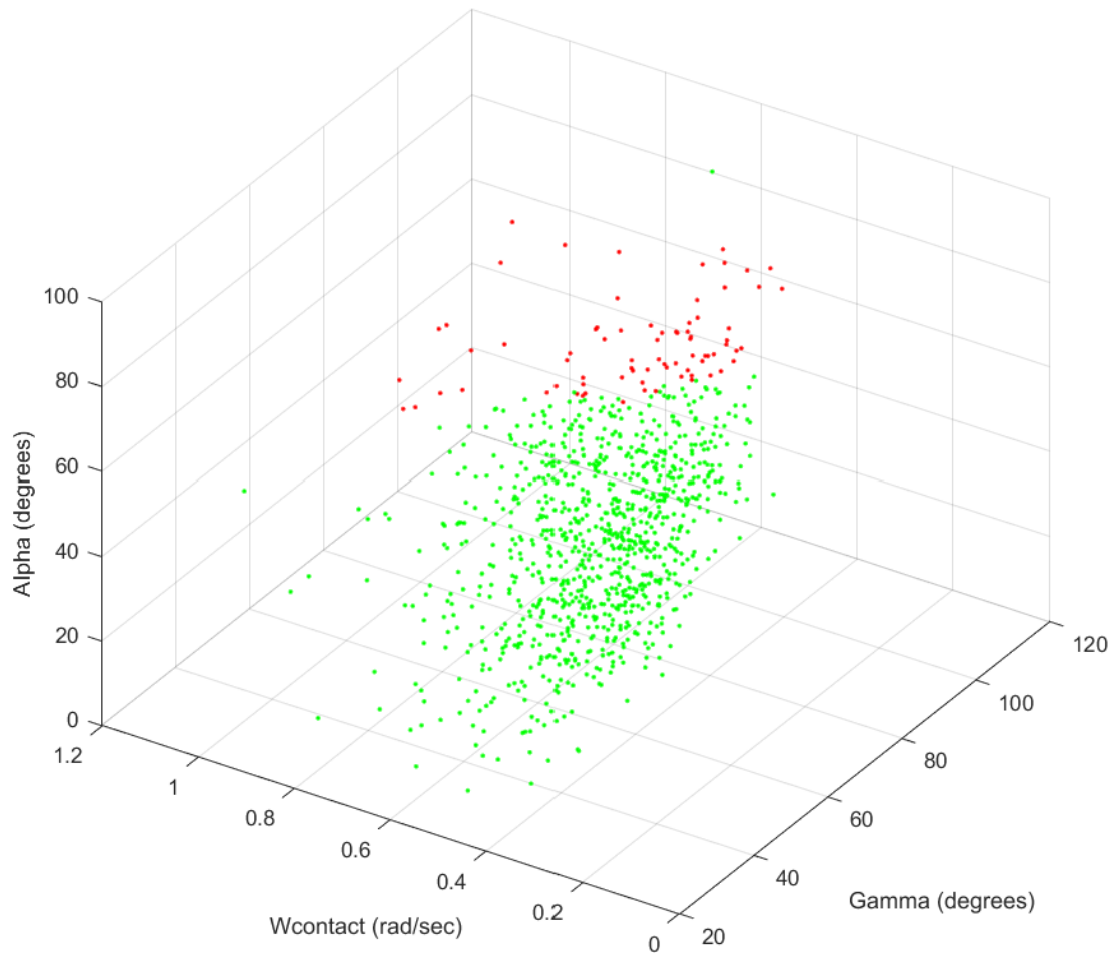


Figure 4.12 Case 2d scatter plot of Gamma, contact angular velocity, and Alpha

#### 4.6 Case 3

In Case 3 there was an additional element added to the Case 2 model. The element that was added was the rider. The variables for the rider are the Rider Height, Rider Radius, Rider Pseudo Height, and Rider Mass. For further information on how these variables are used to calculate the moment of inertia for the rider element refer to Chapter 3. Additionally, there was a new angle defined for the rider orientation. The angle was called Lambda and was defined to be relative to Alpha. Lambda was a normal distribution centered at  $90^\circ$  and with a standard deviation of  $13.4^\circ$ . Case 3 was divided into two subcases. Case3a would use the FLFR contact angle distribution. Case 3b would use the FLRR contact angle distribution. Again for Case 3 gamma is defined as the angle from the positive x-axis to the overall center of mass with the origin set at the contact point.

#### 4.6.1 Case 3a Results

The number of the 1,000 randomly generated points that did not overturn in Case 3a were 98.6%. This is 1% less than the result of Case 2a. However, the change is so small that it can be attributed to the statistical variability in the Monte Carlo analysis. This will further be explored in Chapt 5. To illustrate this result Figure 4.13 shows the scatter plot of Gamma vs contact angular velocity vs Alpha.

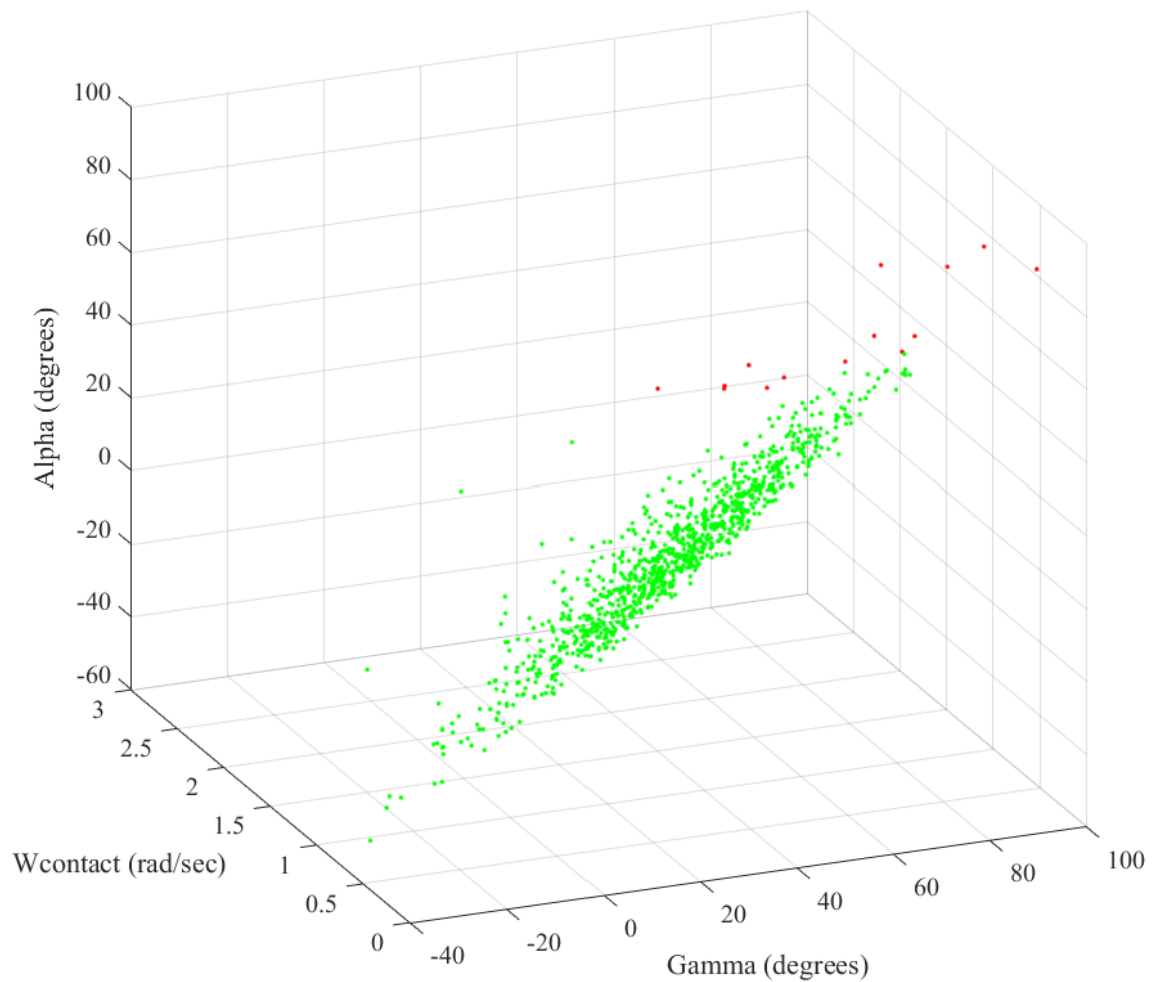


Figure 4.13 Case 3a scatter plot of Gamma, contact angular velocity, and Alpha

#### 4.6.2 Case 3b Results

As expected Case 3b performed similar to Case 2d and had a significantly higher number of points overturning. The Npass for this case was 78.1%. The results for Case 3b can be seen in Figure 4.14.

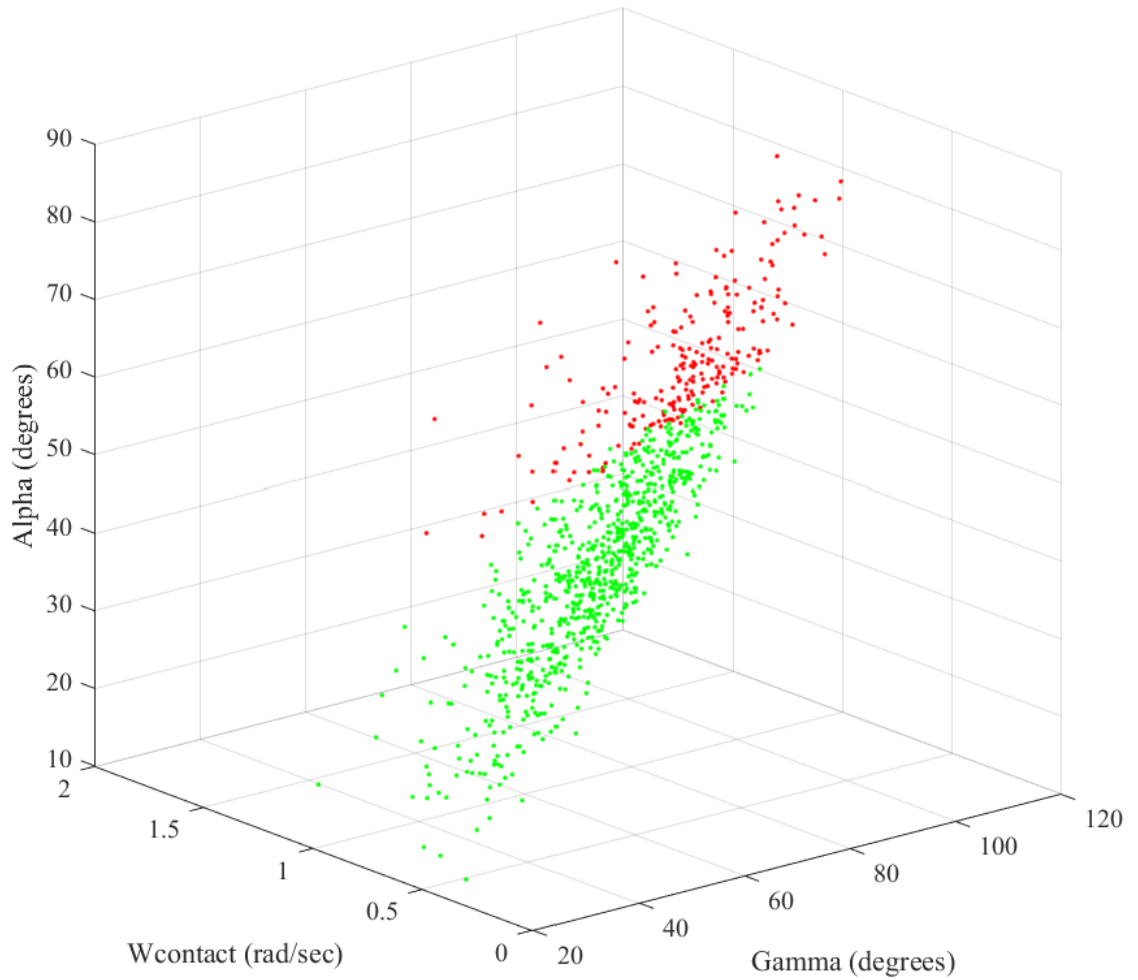


Figure 4.14 Case 3b scatter plot of Gamma, contact angular velocity, and Alpha

## Chapter 5: Sensitivity Analysis

Following the development of the three case studies discussed in Chapter 4 a subsequent study was performed to determine the dominant variables for Case 3a. Case 3a was selected since it encased the full geometry as well as the measured front-leg, front-rail contact angle distribution. Determination of the dominant variables was conducted by using the percentage of the points whose initial conditions would lead it to not overturn (Npass percentage) as the principal measure. All variables except the designated control variable were held constant. The Npass percentage was measured for all control variable settings.

Additionally, to compensate for the statistical variance of the input normal-distributions multiple test runs were performed for each individual control variable setting. It was determined that an average of five test runs was sufficient to obtain adequate results. The control variables along with the range they were iterated through are shown in Table 5.1.

Table 5.1 Control variables and ranges used in sensitivity study

Variable	Range
Convergence	100 -100,000 random points
Alpha	$290^{\circ}$ - $70^{\circ}$
Beta	$\alpha+110^{\circ}$ - $\alpha+160^{\circ}$
Phi	$\alpha+200^{\circ}$ - $\alpha+260^{\circ}$
Nu	$\alpha+200^{\circ}$ - $\alpha+340^{\circ}$
Lambda	$\alpha+160^{\circ}$ - $\alpha+90^{\circ}$
ABL pct	10%-100%
Contact Velocity pct	10%-100%
Psi	$290^{\circ}$ - $80^{\circ}$

## 5.1 Sensitivity Analysis

### 5.1.1 Convergence

The first control parameter that was explored was the number of random points. Since the accuracy of the Monte Carlo method increases with the number of random points it was necessary to see at what point the analysis would converge to a solution. Therefore, Case 3a from Chapter 4 was simulated with 100 random points, gradually increasing the number of points to 100,000 random points. The result of this analysis can be seen in Figure 5.1 where the number of random points (horizontal axis) can be seen plotted against the Npass rate for Case 3a (vertical axis). It was observed that for Case 3a 10,000 points were sufficient to obtain a converged solution.

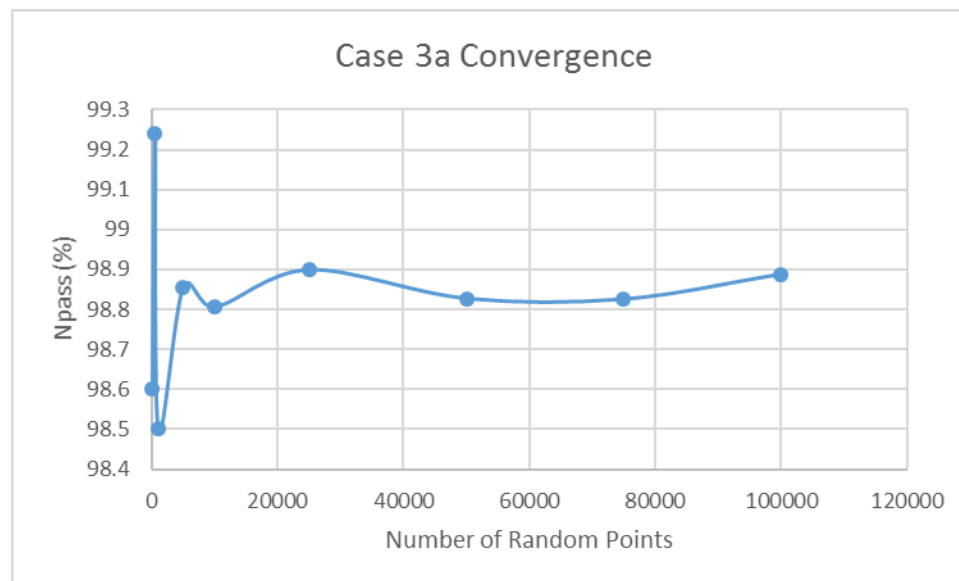


Figure 5.1 Convergence study of Case 3a

### 5.1.2 Alpha

Alpha or the contact angle of the Body was the second control variable. Alpha was varied from  $290^\circ$  to  $70^\circ$ . This range was constrained to the first and fourth quadrants since those would be the only possible ranges. Alpha was expected to be a dominant control variable since it is a key contributor to the location of Gamma. The results of this control variable can be seen plotted in Figure 5.2. The plot shows the range of settings for Alpha in the horizontal axis and the Npass percentage for each setting in the vertical axis. The results showed a drop of approximately 60% in Npass as Alpha was changed from  $0^\circ$  to  $70^\circ$ . Therefore, fence designs in which the horse would be approaching it at a high Alpha would require greater consideration.

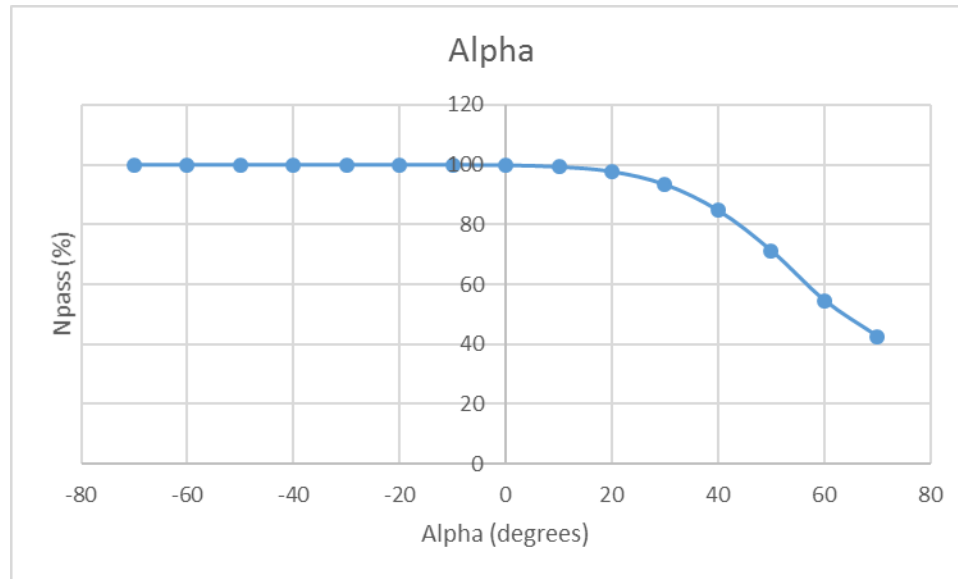


Figure 5.2 Sensitivity Analysis of Case 3a with Alpha set as the control variable



### 5.1.3 Beta

Beta or the angle of the Neck relative to Alpha at contact was the third control variable. Beta's range was set from  $\alpha+110^\circ$  to  $\alpha+160^\circ$ , with alpha being constrained to the distribution measured for a front leg-front rail contact on the British Eventing Safety Fence. The solution to this analysis can be seen in Figure 5.3. In the figure the horizontal axis plots the angle setting relative to Alpha. The vertical axis plots the Npass percentage recorded for the control setting. The results showed that the Npass percentage was not greatly affected by the variation of Beta. Over a range of 50 degrees the overall change was approximately 0.4%. Therefore, Beta was deemed not to be a dominant variable.

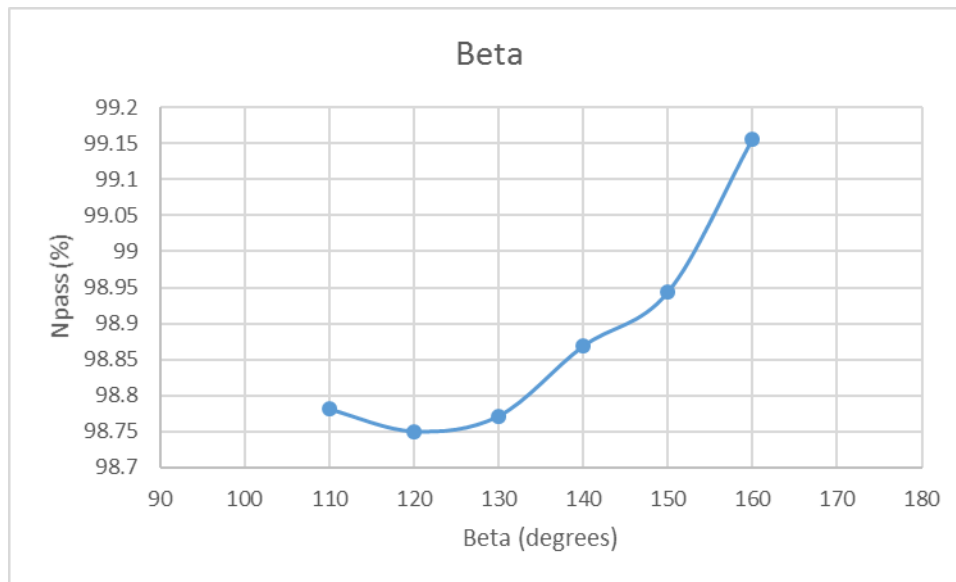


Figure 5.3 Sensitivity Analysis of Case3a with Beta set as the control variable

#### 5.1.4. Phi

Phi or the angle of the Head relative to Alpha was selected as the fourth control variable. Phi was varied through a range of  $\alpha+200$  to  $\alpha+260^\circ$ . This motion was constrained by the inherent range of motion of a horse. The results can be seen in Figure 5.4. The figure plots the relative angle of Phi to Alpha in the horizontal axis. The vertical axis of the figure shows the Npass percentage. Eventhough, Phi was ran through a range of  $60^\circ$  it only caused an improvement of 0.14%. Therefore, Phi was not deemed to be a dominant control variable.

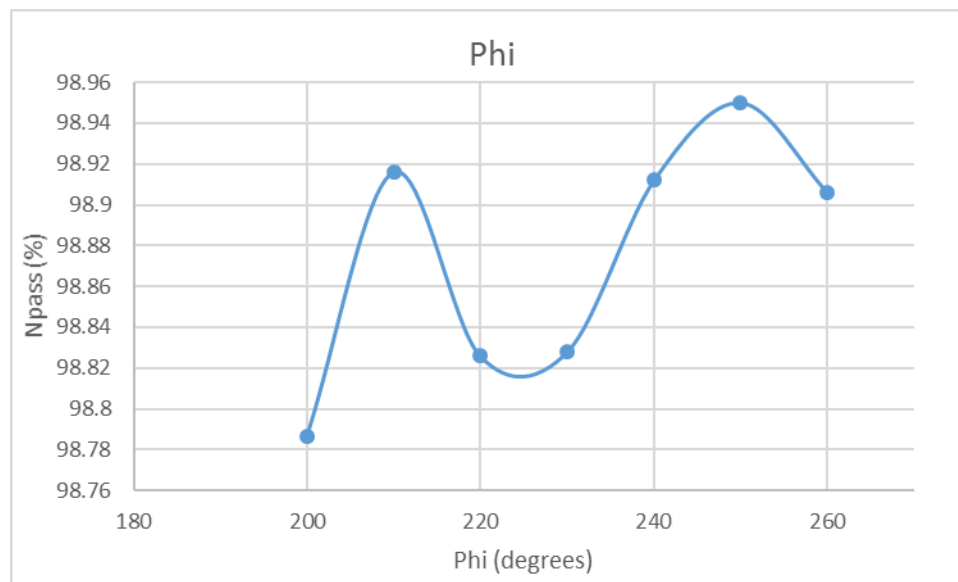


Figure 5.4 Sensitivity Analysis of Case3a with Phi set as the control variable

### 5.1.5. Nu

Nu or the angle of the Antebrachium length relative to Alpha was selected as the fifth control variable. Nu was varied through a range of  $\alpha+200^\circ$  to  $\alpha+340^\circ$ . The results of the evaluation are shown in Figure 5.5. The figure plots Nu relative Alpha in the horizontal axis. The vertical axis plots the Npass percentage. The results did show a slight dependence of Npass percentage to Nu. Although its effects are not as dominant as those observed for Alpha, the combination of this variable with a more dominant variable could lead to a significant effect on Npass.

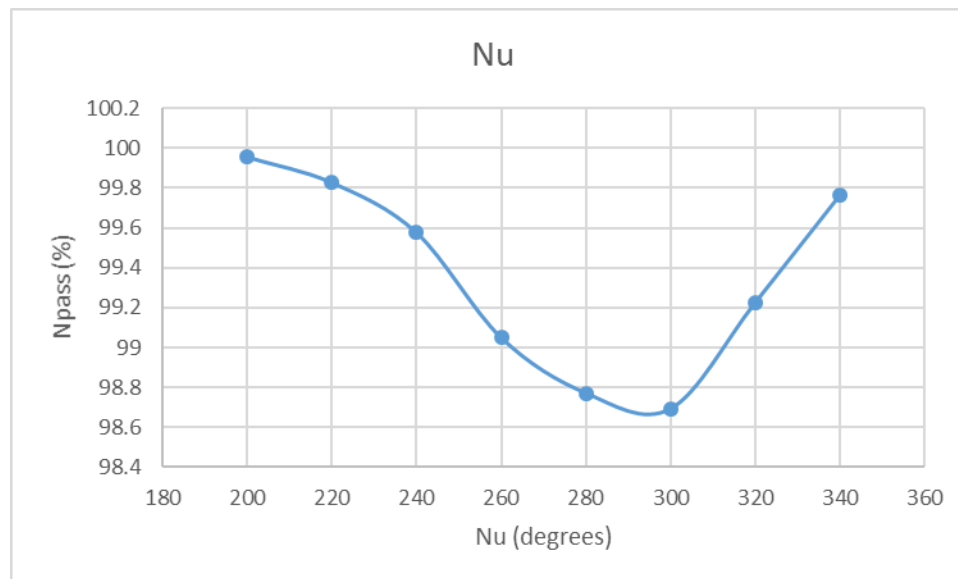


Figure 5.5 Sensitivity Analysis of Case 3a with Nu as the control variable

### 5.1.6. Lambda

Lambda or the angle of the Rider relative to Alpha was selected as the sixth control variable. Lambda was varied through the range of  $\alpha+160^\circ$  to  $\alpha+90^\circ$ . Lambda was not varied in the first quadrant as that rider position would be impractical. The results for this control variable can be seen in Figure 5.6. the figure plots the Lambda angle relative to Alpha in the horizontal axis. The vertical axis of the figure plots the Npass percentage. Lambda did not vary significantly. The variance that was observed could even be attributed to be within the statistical variation of analysis.

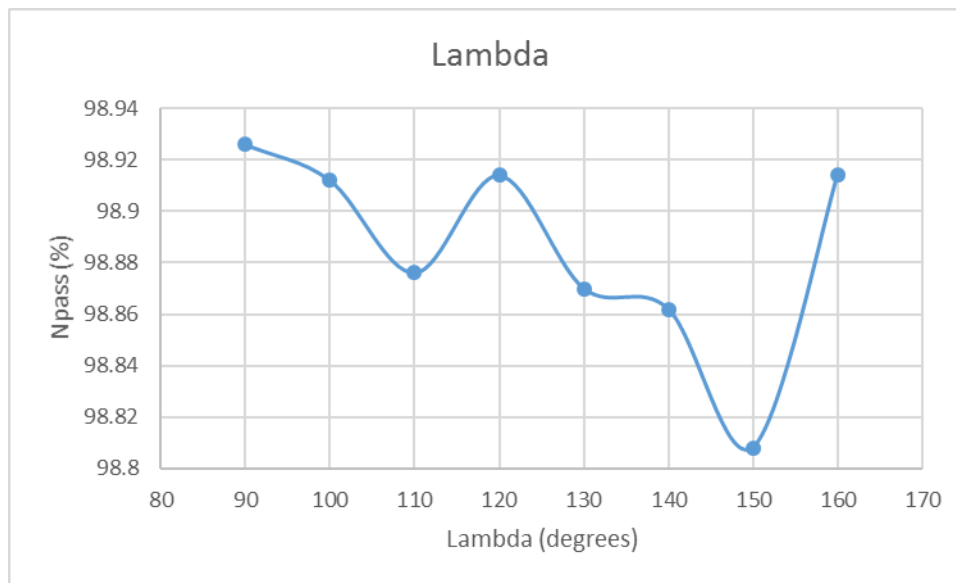


Figure 5.6 Sensitivity Study of Case 3a with Lambda as the control variable

### 5.1.7 Contact Velocity Percent

Contact Velocity percentage or the magnitude of the contact velocity at the instant before contact was selected as the seventh control variable. The contact velocity was reduced gradually from the value used in Case 3a down to 10% of its original value. The results can be seen in Figure 5.7. The figure plots the percentage of the original contact velocity distribution from Case 3a in the horizontal axis. The vertical axis plots the Npass percentage for each control variable setting. The results did show an increase in Npass as the contact velocity magnitude decrease. However since Case 3a had a high Npass to begin with the variation of the Contact Velocity magnitude only had minimal effect. Perhaps if Contact Velocity magnitude was combined with a high risk initial conditions then the effect might become more dominant.

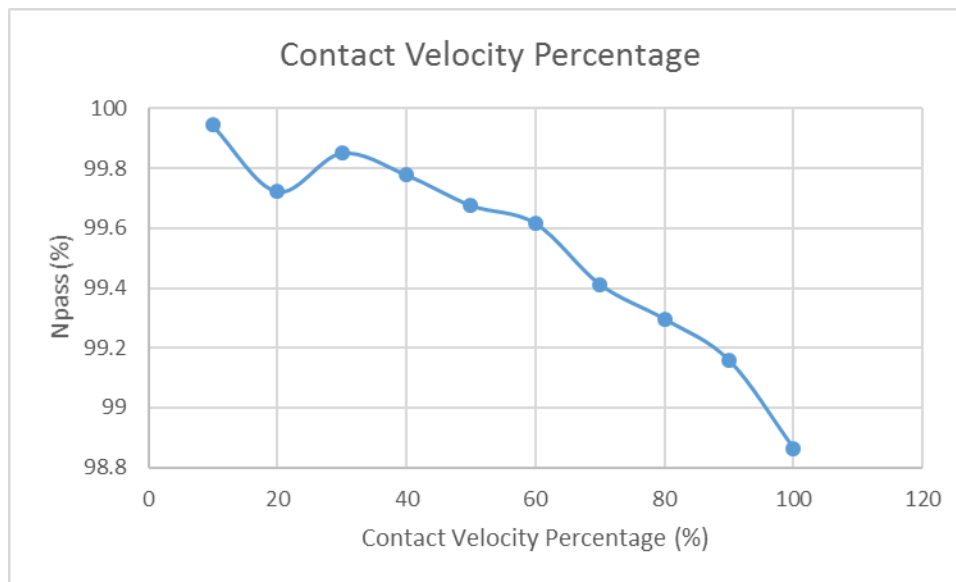


Figure 5.7 Sensitivity analysis of Case 3a with Contact Velocity Magnitude as the control variable

### 5.1.8 ABL Percentage

Antebrachium length contact percentage was defined as the location along the Antebrachium length at which the contact occurred. The contact point was varied from 0%, which was the joint between the Body and the Antebrachium length, to 100%, which was located at the knee. Another property that was not an angle that was explored was the location of the contact point on the Antebrachium length. The results can be seen in Figure 5.8. The figure plots the location of the contact point along the Antebrachium length on the horizontal axis. The vertical axis plots the Npass percentage. The results showed significant variation of Npass as the contact location was varied. A drop of Npass of 16% was found as the contact is moved from the Body-Antebrachium joint to the knee. Therefore ABL percentage was deemed to be a dominant variable.

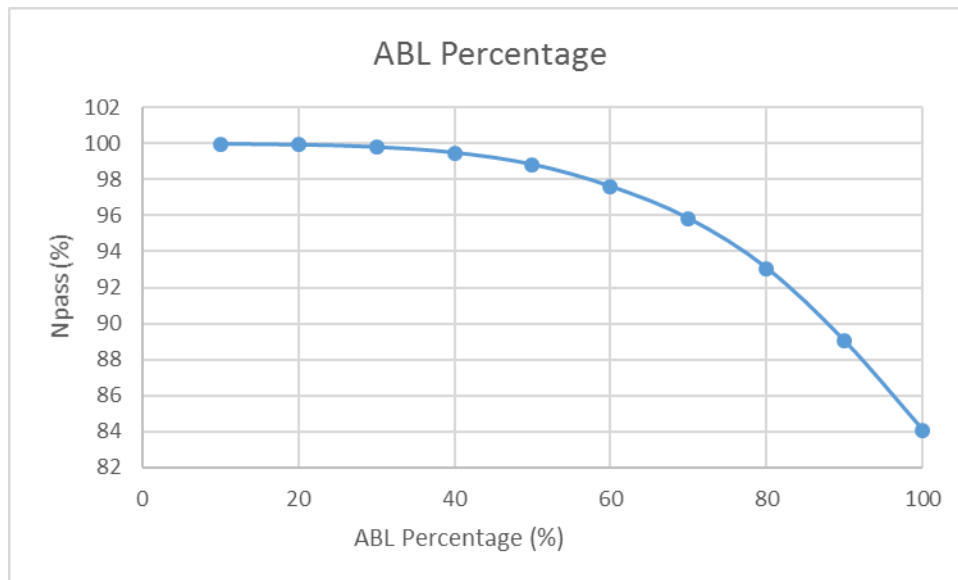


Figure 5.8 Sensitivity analysis of Case 3a with ABL percentage as the control variable

### 5.1.9 Psi

Psi of the contact velocity direction was selected as the last control variable. Psi was varied through a range of  $290^\circ$  to  $80^\circ$ . The results of the variation can be seen in Figure 5.9. The horizontal axis of the figure plots the setting of Psi and the vertical axis plots the Npass percentage. An interesting result was found since a Psi angle below  $0^\circ$  resulted in a lower Npass than that for an Psi angle above  $0^\circ$ . It was also seen that the Npass began to drop after Psi exceeded approximately  $50^\circ$ . This results was attributed as increase or decrease of the overall moment about the contact point. For example a Psi angle of  $-70^\circ$  would have a high positive velocity component in the vertical direction inducing a high positive moment, while a Psi angle of  $70^\circ$  would have a high negative velocity in the y-direction inducing a negative moment. Nevertheless Psi was deemed to be a dominant variable.

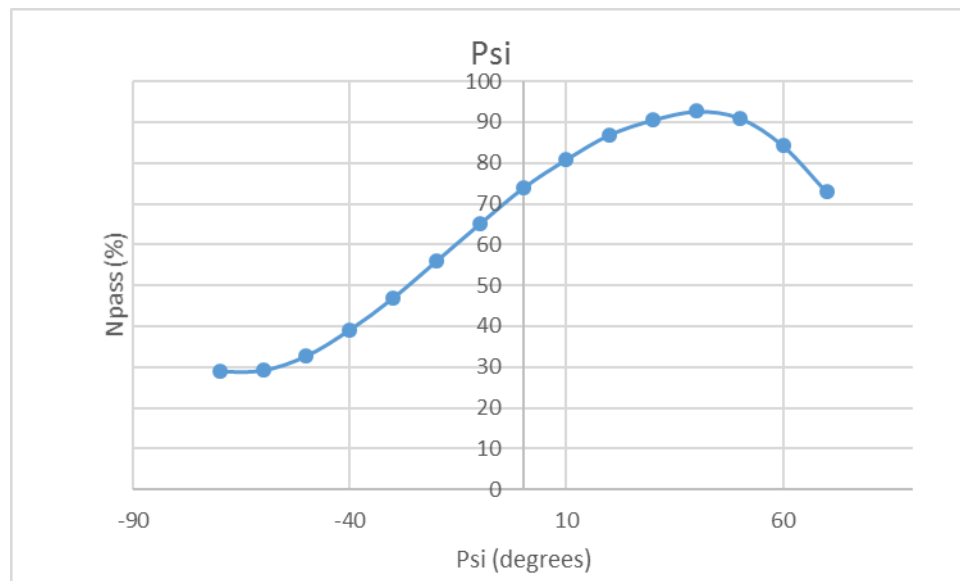


Figure 5.9 Sensitivity analysis of Case 3a with Psi as the control variable

#### 5.1.10 Npass Sensitivity Results

The sensitivity analysis of Npass showed five main parameters that have a moderate to drastic effect on Npass. The parameters are Alpha, Nu, Contact Velocity Magnitude, ABL percentage, and Psi. Even though, Nu and Contact Velocity Magnitude did not have as great an impact as the other main dominant parameters they still had a moderate effect. This moderate effect when combined with high risk combinations of the other dominant parameter would increase in significance. The identification of these dominant variables allows the researchers to evaluate their effect when modeling several deformable fence mechanisms. Ultimately allowing for design guidance for Eventing fence designers.



## Chapter 6: Conclusion and Future Work

### 6.1 Conclusion

Several outcomes were achieved in the efforts outlined in this thesis. The first of these outcomes was the determination of the underlying mechanics of the motion that occurs during rotational falls. These properties, when available, were defined by previous studies or estimated using the data that was available at the time of this effort. Several of the fundamental properties will have to be verified in future studies. Nevertheless, the foundational understanding of the motion is believed to capture a large percentage of the overall dynamics that occurs in rotational falls.

One fundamental property of the analysis that was missing was a large data set of moments of inertia for the horse and rider. The key moment of inertia was the inertia about an axis perpendicular to the sagittal plane of motion. To compensate for the lack of measured data a cylinder-based inertia approximation was developed that captured 71.7 % of the overall moment of inertia of the horse and rider. Furthermore, the cylinder-based model was applied in conjuncture with a citizen science survey effort distributed through the USEA to collect a wide data set of horse and rider geometric properties. Using the wide range of geometric results the inertias were determined for the population of geometric values that were recorded.

Following the collection of a database for the geometric measurements and inertia approximation MATLAB<sup>TM</sup> random generation function was used to generate normal-distribution functions of the input values for a rotational fall analysis. The analysis broke

down the problem into simple components in order to gain a higher understanding of the dominant factors in causing the rotational fall. The Monte Carlo method, a numerical method used for solving mathematical problems using random sampling, was used to widen the analysis to a large sample size that could more accurately model the various horses and riders that compete in the sport.

The results from the Monte Carlo analysis resulted in five dominant variables that increase the risk of rotational falls. The variables are Alpha, Nu, Contact Velocity Magnitude, ABL percentage, and Psi. These variables were tested by holding all other variables constant while the control parameter was varied through a range of values. The measure for the performance of the control parameter was the number of random points that passed relative to the original condition.

## 6.2 Future Work

Future aspects of the project can be divided into two main efforts: high-speed video analysis and design validation of cross-country fences. The first effort is set to take place at the Rolex Eventing 2017 competition. High-speed cameras will be used to identify the fundamental mechanics that were observed for rotational falls. Even though actual video of a rotational fall is extremely rare, the results from typical jumping attempts can help reveal/verify several key underlying parameters.

The second main aspect is to apply the Monte Carlo analysis towards various fence design. Also part of this effort is the evaluation of several deformable safety devices. As part of this effort the impulse between the at the point of contact and the resultant force from the fence will be explored. The results of these efforts in conjunction to the ones discussed in this thesis will provide a platform to optimize fence designs.

## APPENDIX A

### USEA Survey Results (May 2017)

	Breed	Withers Height	Horse Height (cm)	Horse weight	Calculated weight	Length of Body	Heart Girth	Circumference of neck	Length of neck	Length of head	Circumference of head	Rider height	Rider Weight	Level	Location
1	Thoroughbred	16.2	168	0	484	163	188	91	71	61	64			0	0
2	Thoroughbred	16	163	476	486	155	193	94	66	58	61			0	0
3	Warmblood - Light bodied	17	173	0	551	163	201	97	81	64	66			0	0
4	Thoroughbred	16.1	165	0	450	147	191	97	76	61	64			0	0
5	Thoroughbred	17.1	175	0	546	165	198	99	74	58	64	173	50	BN	0
6	Thoroughbred	16.1	165	0	463	160	185	91	69	56	66	188	73	Novice	0
7	Warmblood - Heavy bodied (weight above 1,400 lbs)	17.2	178	0	627	180	203	104	81	61	71	168	68	Training, Preliminary	0
8	Thoroughbred	16	163	0	456	157	185	94	69	58	61	180	74	Novice	0
9	Thoroughbred	16.3	170	499	506	170	188	91	71	58	66	170	73	Advanced/3*	0
10	Thoroughbred	16.1	165	0	461	155	188	89	81	56	66	155	54	Starter	0
11	Other	15.2	157	499	449	155	185	104	66	61	69	163	48	BN	0
12	Thoroughbred	16	163	482	484	163	188	99	71	61	61	160	64	Dressage	0
13	Thoroughbred	16	163	482	484	163	188	99	71	61	61	160	64	Dressage	0
14	Other	15.1	155	499	429	152	183	94	66	58	66	155	52	Hunters	0
15	Thoroughbred	16.1	165	544	544	183	188	102	71	61	74	160	54	Hunter	0
16	Thoroughbred	17.1	175	590	680	196	203	107	76	61	69	170	68	Novice	0
17	Other	14.3	150	0	537	191	183	91	64	48	48	165	52	0	0



39	Warmblood - Light bodied	16.2	168	0	0							163	54	Training	0
40	Warmblood Cross	16	163	0	0								60	Intermediate/2* (1.15 m)	0
41	Warmblood - Light bodied	16	163	540	562	170	198	94	76	56	64	163	50	BN	0
42	Thoroughbred	16.1	165	0	550	175	193	91	66	56	64	168	59	BN	0
43	Thoroughbred	15.2	157	480	0	180						155	55	Novice (.90 m)	0
44	Thoroughbred	15.2	157	499	0	188								Novice	0
45	Thoroughbred	15.2	157	513	0							155	58	Novice (.90 m)	0
46	Arabian	0	0	354	361	152	168	84	66	53	58	160	58	Training	0
47	Haflinger	13.25	138	0	486	188	175	104	61	64	69	170	85	BN	0
48	Warmblood Cross	16	163	499	0	198						163	54	Novice, Training	0
49	Thoroughbred	17.2	178	499	0	198						173	73	Novice	0
50	Thoroughbred	16.1	165	0	0							165	61	BN	0
51	Arabian welsh cross	13.1875	137	0	0							165	61	BN	0
52	Thoroughbred	0	0	0	0								61	0	0
53	Warmblood Cross	16.1	165	0	596	180	198	109	66	61	69	173	61	Training	0
54	Thoroughbred	16.2	168	454	0							173	66	Novice	0
55	Quarter Horse	15	152	340	0	193						147	73	BN	0
56	Warmblood Cross	17.2	178	680	740	193	213	112	79	66	66	178	73	Training	0
57	Warmblood - Light bodied	15.2	157	476	0	183						163	59	Novice	0
58	Irish draught x	16.1	165	590	0	206						180		Novice (.90 m)	Aberdeen
59	Thoroughbred	17.1	175	0	0							170	59	Preliminary/1*	virginia Beach Va
60	Thoroughbred	15.1	155	495	558	178	193			69	56	170	52	Preliminary/1*	Mullica Hill, NJ

61	Warmblood - Light bodied	15	152	431	345	155	163	107	61	56	61	165	70	Novice	greencastle,In
62	Thoroughbred	16.3	170	499	0		132					170	75	Preliminary/1*	Unionville, PA
63	Thoroughbred	18	183	658	0	213						173	68	Novice	New Hampshire
64	Thoroughbred	16.2	168	0	556	173	196	102	74	58	66	175	58	Training	Gleneig, Maryland
65	Warmblood - Light bodied	14	142	0	0							163	57	BN	Troy, Mi
66	Warmblood - Light bodied	16	163	499	456	157	185	99	76	58	61	168	68	Intermediate/2*	Denver, Colorado
67	Warmblood - Light bodied	16.1	165	472	474	155	191	91	64	58		64	61	Preliminary/1*	Ocala, FL
68	Thoroughbred	16	163	497	498	168	188	94	69	58	58	173	68	Preliminary/1*	Ocala, Florida
69	Warmblood - Heavy bodied (weight above 1,400 lbs)	17	173	546	548	170	196	114	79	58	64	173	68	Preliminary/1*	Ocala, Florida
70	Thoroughbred cross	16.1	165	0	446	150	188		74	56	56	180	77	Advanced/3*	Ocala, Florida
71	Warmblood - Light bodied	16.3	170	544	556	173	196	104	76	58	61	180	77	Intermediate/2*	Ocala, Florida
72	0	16.2	168	522	532	165	196	107	76	61	71	180	77	Preliminary/1*	Ocala, Florida
73	Warmblood - Light bodied	16.1	165	513	523	163	196	109	74	56	69	180	77	Intermediate/2*	Ocala, Florida
74	Thoroughbred	17	173	530	529	183	185					173	60	BN (.80 m)	Melbourne, Victoria, Australia
75	Warmblood Cross	0	0	567	0	198								Training	0
76	Warmblood Cross	16.1	165	567	0	191		107	71	51		173	82	Novice	Orlando, fl, usa
77	Thoroughbred	16.3	170	0	0							152	47	BN	Medford, NJ, United States
78	Thoroughbred	17	173	548	0			112	99	69	56	163	58	Training	Temecula, California, US
79	Warmblood - Light bodied	16.3	170	544	0							173	61	4*	Temecula CA 92593
80	Warmblood Cross	16	163	567	0	208						173	64	Novice	Portland,Oregon

81	Qh welsh	14.1	145	408	0	175				61	51	170	57	BN	0
82	Thoroughbred	16.3	170	590	0							168	91	BN	Crestwood, IL, US
83	Warmblood - Light bodied	16.2	168	531	0	208						170	57	BN	Springfield, Missouri, USA
84	Connemara/Thoroughbred	16.2	168	567	444	206	160	104	91	76	61	165	66	Training	Aiken, SC USA
85	Thoroughbred	17	173	547	0	203						163	61	Training	canaan nh usa
86	Thoroughbred	15.2	157	579	780	185	224	97		51	66	165	57	Novice	Lexington ky USA
87	Warmblood Cross	15.1	155	499	0							155	50	BN	Lopez island, wa, usa
88	Thoroughbred	16.3	170	671	629	206	191			41	56		82	BN	Aumsville, oregon, Marion county
89	Warmblood - Light bodied	0	0	0	0							170	59	Preliminary/1*	Dekalb, IL, USA
90	Thoroughbred	16	163	567	367	165	163	109	71	53	64	168	60	Novice, Training	REDDICK, FL, USA
91	0	14	142	408	0	183						157	66	BN	Kearneysville, West Virginia USA
92	Thoroughbred	18.1	185	0	579	206	183	97		91	56	175	84	Training	Southern Pines NC USA
93	Thoroughbred	17	173	544	0	198						175	68	Novice, Training	Stevensville MI USA
94	Thoroughbred	16	163	454	0							163	57	Training	Arnold, Md US
95	Warmblood - Light bodied	15	152	419	0							168	53	BN	Sudbury, Massachusetts US
96	Thoroughbred	17	173	658	0	198		76	76	51		168	83	Training	Usa
97	Thoroughbred	16.1	165	499	0	193						157	79	BN	northeast ohio,ohio,usa
98	Morgan Standardbred cross	15.3	160	522	0	193			97	61	61	168	59	Intermediate/2*	Florida
99	0	16.1	165	544	0	206						160	57	Novice	warrensburg, il, usa



100	Thoroughbred	16.1	165	499	0							170	68	Training	Lakebay Washington, USA
101	Quarter horse/ throughbreed	15	152	454	0		132					157	45	Just stated her under saddle	Highland Maryland Howard
102	Warmblood Cross	17.1	175	635	0	213						178	73	Training	Sheboygan, WI, US
103	Warmblood Cross	17.1	175	635	0	213						178	73	Training	Sheboygan, WI, US
104	Warmblood - Light bodied	17.1	175	590	568	213	178		102	76		178	77	Training	Santa Cruz, CA USA
105	Warmblood - Light bodied	16.2	168	567	0	206						175	61	Novice	Ewing, Virginia, United States
106	Thoroughbred	16.4	173	0	0							168	64	BN	Rochester MI USA
107	Thoroughbred	15.3	160	454	0							140	82	Training	USA
108	Thoroughbred	16.1	165	454	0	193						160	64	Intermediate/2*	Strafford, VT, USA
109	Warmblood - Light bodied	17	173	590	1352	213	274	86	69	61		157	76	Training	Amarillo, Texas, United States
110	Thoroughbred	16.1	165	499	0	198						168	59	Training	Fort Collins, CO, USA
111	Appendix	15	152	0	0							157	50	BN	Pittsburgh, PA USA
112	Quarter Horse	17	173	635	760	213	206	91	84	61	53	185	75	Novice	Oregon, USA
113	Thoroughbred	16.3	170	567	0	206						168	54	Intermediate/2*	Rye, ny
114	Thoroughbred	16.1	165	544	0	198						178	75	BN	Ocala FL USA
115	Warmblood - Heavy bodied (weight above 1,400 lbs)	16.3	170	714	756	229	198	107	76	66	61	170	67	Novice	Ruffin NC USA
116	Mustang	15.1	155	386	0							163	45	BN	Spokane, WA, USA
117	Warmblood Cross	15	152	442	0							168	66	Novice	Connecticut
118	Thoroughbred	16.1	165	431	0	198						160	54	Starter	Lexington, KY, USA

119	Warmblood Cross	16.3	170	499	0	173						165	59	BN	Dover, NH
120	Warmblood - Light bodied	15.2	157	544	0							175	66	Novice	Woodbury,MN,USA
121	Saddlebred	15	152	363	0	157						180	82	BN	0
122	Paint	14.2	147	680	0								59	BN, Novice	Lexington Ky
123	Thoroughbred	16.2	168	0	0	203			84	66	64	157	51	Preliminary/1*	Louisville KY USA
124	Quarter/Mustang	14.2	147	445	420	163	175					160	59	BN	Victorville CA United States
125	Thoroughbred	15.3	160	363	0	183						168	54	BN	Girard, Pennsylvania, USA
126	Thoroughbred	17	173	635	0							163	54	BN, Novice	Avon, oh, united states
127	Warmblood - Light bodied	16.2	168	680	0							157	50	Preliminary/1*	Gig Harbor, WA, USA
128	Thoroughbred	15.3	160	499	0	191	244					163	77	Preliminary/1*	Aiken, SC, USA
129	Warmblood Cross	17.2	178	635	0							163	66	Preliminary/1*	Newark, Ohio, USA
130	Irish Sport Horse	0	0	0	0									Intermediate/2*	0
131	Thoroughbred	15.1	155	635	0									Training	0
132	Thoroughbred	16.1	165	544	0							168	67	BN, Novice	Slingerlands, NY, USA
133	Thoroughbred	15.3	160	0	0							173		BN (.80 m)	Cocoa fl brevard
134	0	0	0	0	0										
135	Quarter Horse	15.2	157	567	0							163	45	BN	Versailles, KY, USA
136	Thoroughbred	16.3	170	585	587	178	198	102	71	58	64	170	79	Novice	Rochester, NH.
137	Warmblood Cross	15.2	157	522	543	178	191	102	69	58	66	145	59	Training	Spring City, UT, USA
138	Thoroughbred	16.2	168	567	548	170	196	104	74	56	61	170	59	Intermediate/2*	Spring City, UT, USA
139	Quarter horse not	16	163	0	571	173	198	114	74	61	66	163	61	Novice	Lehi, It, USA

140	Warmblood - Light bodied	16.2	168	590	526	168	193	94	89	48	56	157	54	Preliminary/1*	Round Hill, VA
141	Thoroughbred	18.1	185	0	735	183	218	122	94	81	74	168	77	BN	Round Hill, VA, USA
142	Percheron TB cross	15.1	155	0	594	175	201	114	94	71	58	168	73	Training	Round Hill, VA
143	Warmblood - Heavy bodied (weight above 1,400 lbs)	17.1	175	0	827	188	229	112	86	76	66	170	52	Novice	Round Hill, VA
144	Thoroughbred	16	163	544	0	198						165	77	BN, Novice	Lexington, KY
145	Warmblood Cross	16.3	170	624	679	191	206	104	81	66	66	188	70	Preliminary/1*, About to make the move up to Intermediate this coming season	Medina, Ohio, United States
146	Warmblood Cross	17	173	624	629	185	201	112	79	61	69	188	70	Novice, Retired recently. Competed Novice recognized and Training level at unrecognized	Medina, Ohio, United States
147	Appendix	15.2	157	544	551	180	191	107	69	56	66	168	54	BN, Novice	Westerville, Ohio
148	Warmblood Cross	17.1	175	610	687	188	208	109	74	58	66	185	85	BN	Westerville, Ohio, United States
149	Warmblood Cross	17.1	175	590	598	191	193	102	74	56	61	170	59	Preliminary/1*, Moving up to intermediate this year	Westerville, Ohio, United States
150	Thoroughbred	16.2	168	499	0	203						168	59	Novice	Dorset, Vt

## REFERENCES

- [1] Allott, John, et al. "An Investigation Sponsored by British Eventing into the Safety of Cross Country Obstacles." 2007.
- [2] Barnett, Charles. "An Audit into Eventing Incorporating an Analysis of Risk Factors for Cross Country Horse Falls at FEI Eventing Competitions." 2016.
- [3] Bobbert, Maarten F. and Susana Santamaria. "Contribution of the Forelimbs and Hindlimbs of the Horse to Mechanical Energy Changes in Jumping." *The Journal of Experimental Biology* (2005): 249-260.
- [4] Buchner, Florian. Interview. Gregorio Robles Vega. 05 July 2016.
- [5] Buchner, H. H. F., et al. "Inertial Properties of Dutch Warmblood Horses." *Journal of Biomechanics* (1997): 653-658.
- [6] Chandler, R. F., et al. "Investigation of Inertial Properties of the Human Body." 1975.
- [7] Chapman, Meredith and Kirrilly Thompson. "Preventing and Investigating Horse-Related Human Injury and Fatality in Work and Non-Work Equestrian Environments: A Consideration of the Workplace Health and Safety Framework." *Animals* (2016).
- [8] Clayton, Hilary M. "Time-Motion Analysis of Show Jumping Competitions." *Journal of Equine Veterinary Science* (1996).
- [9] Competitive Measure Ltd. "Goodyear Safety Research Project 2008 Initial Report." 2008.
- [10] Competitive Measure Sports Engineering. "Field Data Acquisition Goodyear Safety Research Fence 2008 Season." 2008.
- [11] Competitive Measure Sports Engineering. "Top 20 Impacts Goodyear Safety Research Fence 2008 Season." 2008.
- [12] Dutto, Darren J., et al. "Moments and Power Generated by the Horse (Equus Caballus) Hind Limb During Jumping." *The Journal of Experimental Biology* (2004): 667-674.
- [13] Dutton, Phillip, et al. *Modern Eventing with Phillip Dutton: The Complete Resource-Training, Conditioning, and Competing in All Three Phases*. Trafalgar Square Books, 2013.
- [14] Eckner, James T., Jeffrey S. Kutcher and James K. Richardson. "Pilot Evaluation of a Novel Clinical Test of Reaction Time in National Collegiate Athletic Association Division I Football Players." *Journal of Athletic Training* (2010): 327-332.

- [15] Erdmann, Wlodzimierz Stefan. "Geometry and Inertia of the Human Body - Review of Research." *Acta of Bioengineering and Biomechanics* (1999).
- [16] Fédération Equestre Internationale . "2015 FEI EVENTING RISK MANAGEMENT SEMINAR - MADRID (ESP) REPORT." 2015.
- [17] Fédération Equestre Internationale. "Eventing Risk Management Programme Statistics 2005-2015." 2016.
- [18] Fédération Equestre Internationale. "inside.fei.org." 12 April 2013. *Deformable & Frangible Devices*. 23 March 2017.
- [19] Fédération Equestre Internationale. "Standard for the Minimum Strength of Frangible/Deformable Cross Country Fences." 2012.
- [20] Ginsberg, Jerry H. *Advanced Engineering Dynamics*. Cambridge University Press, 1995.
- [21] Greenwood, Donald T. *Advanced Dynamics*. Cambridge University Press, 2003.
- [22] Hanson, J. M. and B. B. Beard. "Applying Monte Carlo Simulation to Launch Vehicle Design and Requirements Analysis." Technical Publication. 2010.
- [23] Hibbeler, R. C. *Engineering Mechanics Dynamics*. New Jersey: Pearson Education, 2010.
- [24] Hurst, Thomas, et al. "Measuring the Force in a Horse and Cross-Country Fence Collision." 2008.
- [25] International Olympic Committee. "Equestrian Eventing." 26 January 2017. *Olympic*. <<https://www.olympic.org/equestrian-eventing>>.
- [26] Jurga, Fran. "FEI Eventing Safety Committee Prioritizes Issues." *EQUUS*. 21 June 2007.
- [27] Kahmann, Katherine M. "Engineering Sport Safety: A Study of Equestrian Cross Country Eventing." 2010.
- [28] KUBO, Katsuyoshi, et al. "Segmental Body Weight, Volume and Mass Center in Thoroughbred Horses." *Japanese Journal of Equine Science* (1992): 149-155.
- [29] Moore, D. P., et al. "Kinematic Analysis of World Championship Three-Day Event Horses Jumping a Cross-Country Drop Fence." *Journal of Equine Veterinary Science* (1995).
- [30] Murray, Jane Katherine. "An Epidemiological Study of the Risk Factors Associated with Falls of Horses and Riders in the Sport of Eventing." 2004.
- [31] Nauwelaerts, Sandra, et al. "Inertial Properties of Equine Limb Segments." *Journal of Anatomy* (2011): 500-509.

- [32] O'Brien, Denzil and Raymond Cripps. "Safety for Horses and Riders in Eventing: The SHARE database." 2008.
- [33] Powers, P. "Linear Kinematics at Take-Off in Horses Jumping the Wall in an International Puissance Competition." *Sports Biomechanics* (2005): 149-162.
- [34] Powers, P. N. R. and A. J. Harrison. "A Study of the Techniques used by Untrained Horses During Loose Jumping." *Journal of Equine Veterinary Science* (2000).
- [35] Powers, P. N. R. and A. J. Harrison. "Influences of a Rider on the Rotation of the Horse-Rider System During Jumping." *Equine and Comparative Exercise Physiology* (2003): 33-40.
- [36] Sobol', Ilya M. *A Primer for the Monte Carlo Method*. CRC Press, 1994.
- [37] Starck, Dan. "An Introduction to Frangible Fences." 2009.
- [38] Swearingen, John J. "Determination of Centers of Gravity of Man." 1962.
- [39] The International Eventing Safety Committee . *The International Eventing Safety Committee Report April 2000*. London, 2000.
- [40] Transport Research Laboratory. "Transport Research Laboratory: Synopsis of Frangible Fence Project." 2000.
- [41] Ugural, Ansel C. and Saul K. Fenster. *Advanced Mechanics of Materials and Applied Elasticity*. Pearson Education, 2012.
- [42] United States Eventing Association. "Discover Eventing." 22 March 2017. *History of Eventing*. <<http://www.discovereventing.com/?q=node/67>>.
- [43] van den Bogert, A. J. "Computer Simulation of Locomotion in the Horse." PhD Thesis. 1989.
- [44] Wood, Shannon. "Citizen Science Survey for Inertial Parameters of Live Horses and Riders for Rotational Fall Problems." 2017.

## VITA

Gregorio Robles Vega was born in Nayarit, Mexico in 1993. He immigrated to the United States of America at the age of six and graduated from Mayfield High School in 2011. He attended the University of Kentucky Paducah Campus and obtained a B.S. in Mechanical Engineering and Aerospace Certificate in 2015. While in his undergraduate studies, Gregorio had the opportunity to conduct research focused on gas turbine engines under the guidance of Dr. Vincent Capece. He then had the opportunity to begin his Masters of Science in Mechanical Engineering in 2015 under the guidance of Dr. Suzanne Smith at the University of Kentucky. Funding for Gregorio's project was provided by the United States Eventing Association and the University of Kentucky Graduate School. After graduating with his M.S. degree Gregorio is pursuing service as a Peace Corps Volunteer in Guinea. After his service in the Peace Corps, Gregorio hopes to pursue a career in the aerospace or power generation fields and undertake in efforts to help undeveloped communities throughout the world.